Thrombotic Fingerprints for the Enhanced Prediction of Thrombosis

by

Javier Jacobo Echenique

B.S. Mechanical Engineering
Massachusetts Institute of Technology, 2005

SUBMITTED TO THE DEPARTMENT OF MECHANICAL ENGINEERING IN PARTIAL FULFILLMENT OF THE REQUIREMENTS FOR THE DEGREE OF MASTER OF SCIENCE IN MECHANICAL ENGINEERING

AT THE

MASSACHUSETTS INSTITUTE OF TECHNOLOGY

JUNE 2007

Signature of Author: _____
Department of Mechanical Engineering
May 7, 2007

Certified by: _____
Elazer R. Edelman
Thomas D. and Virginia W. Cabot Professor
Division of Health Sciences and Technology
Thesis Supervisor

Read by: _____
Germeshau
Associate Direc

_____
Roger D. Kamm
: Biological Engineering
Biomedical Engineering

Accepted by: _____
Lallit Anand
Chairman, Graduate Thesis Committee

THROMBOTIC FINGERPRINTS FOR THE ENHANCED PREDICTION OF THROMBOSIS

by Javier Echenique

Submitted to the Department of Mechanical Engineering on May 7, 2007 in Partial Fulfillment of the Requirements for the degree of Master of Science in Mechanical Engineering.

Abstract

Controlled thrombosis initiates and regulates tissue repair and remodeling in the vessel wall. Processes from heart attack to stroke, and deep vein thrombosis to pulmonary embolism, are all derived from unrestricted clotting. The frustrating aspects of these diseases lie not only in the difficulty of their timely diagnosis, but in the selection of appropriate therapy, titration of intervention, and identification of patients at risk. Assays like the INR, PTT, and ACT can follow the course of specific pathways that govern activation of specific coagulation factors or platelet function, but they do not provide the insight into mechanism, risk and potential therapeutic benefit.

We posit that elucidation of the complex dynamics of clot generation requires an integrated assessment that takes into account all of the factors driving thrombosis simultaneously. Virchow's Triad, has for years been identified as the three critical parameters of clot formation. We propose to examine an individual's clot propensity and response to therapy on minute blood samples, in virtual real time, across a range of flow rates, blood state, and wall conditions with the use of our newly developed *in vitro* high-throughput testing device. In this manner we will generate a unique *thrombotic fingerprint* that defines an individual's risk of clotting at a specific point in time over a range of stresses. This fingerprint can aid in tailoring therapeutic clinical treatments, determining the duration and dose of therapy, and assist in clinical trial management and establishment of clinical norms.

Thesis Supervisor: Elazer R. Edelman

Thomas D. and Virginia W. Cabot Professor of Health Sciences and Technology

TABLE OF CONTENTS

TABLE OF FIGURES

CHAPTER 1: INTRODUCTION

The past decade has brought along rapid evolution of the pathophysiological understanding of coronary artery disease (CAD). Initially considered a cholesterol storage disease, the current body of knowledge indicates that a more complex interaction between risk factors such as endothelial cells of the artery wall, the blood and its components, and the messages exchanged between the two, are at the center of atherogenesis.

1.1 CORONARY ARTERY DISEASE

The formation of a CAD lesion begins with an interaction between the arterial endothelium and bacterial products, or any number of a variety of risk factors, including dyslipidemia, vasoconstrictor hormones due to hypertension, glycoxidation products present during hyperglycemia, or proinflammatory cytokines derived from excess adipose tissue [1]. During this interaction, the endothelial cells increase the production of adhesion molecules, known as chemoattractant cytokines, which attract blood leukocytes to the interior artery wall surface. At this point, leukocytes, which are mainly composed of mononuclear phagocytes and T lymphocytes, begin communication with the endothelial and smooth muscle cells of the intima. An inflammatory response is initiated, and during the early atheroma, smooth muscle cells migrate from the tunica media into the intima, proliferate, and compose a complex extracellular matrix. To maintain the inflammatory response, a number of metalloproteinases (MMPs) are released to modulate a variety of functions of the vascular cells, including activation, proliferation, migration, new vessel formation, remodeling, healing, and cell death. Calcification may occur by mechanisms similar to those which form bone [2]. In addition, cell death, especially the death of lipid-laden macrophages, soon becomes a

common occurrence. This accumulation of extra-cellular lipid eventually grows to form the lipid-rich necrotic core of the atherosclerotic plaque [1].

During the process of plaque formation and growth, the geometry of the plaque contributes to remodeling of the vasculature. For a number of decades, the narrowing of the artery (stenosis) due to the formation of a plaque was considered the main threat of this condition. More recently, it was found that an atherosclerotic lesion actually grows outwardly for the majority of its life, instead of into the lumen [3, 4]. (Lesions of the stenotic and non-stenotic variety are shown in Figure 1.)

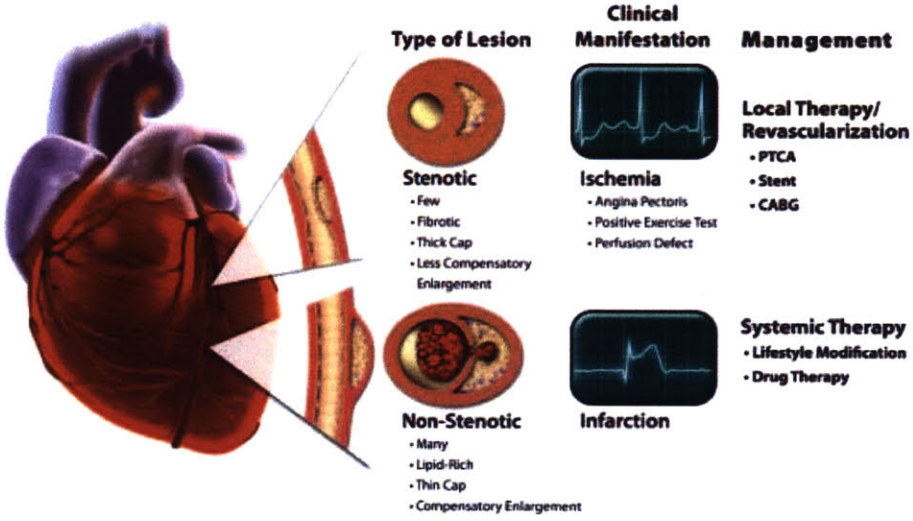

Figure 1: Stenotic and non-stenotic lesions [1].

These findings indicated an understanding of the process of lesion formation unable to encompass the large number of atherosclerotic lesions that could exist without producing stenosis [3, 4]. In addition, it was found that by the time lesions had developed to the point of causing stenoses, intimal atherosclerosis could be found widespread through the vasculature of the patient [5].

The growth of stenoses has been found to transpire through a series of sudden spurts, rather than smoothly and continuously [6, 7]. This effect may be due to acute disruptive episodes of the atherosclerotic lesion, followed by thrombosis at the site, and a healing process that may actually further exasperate the obstruction of blood flow. The process by which a plaque is disrupted and healed by the body is

an area of great interest, and requires a closer look at the interaction between the lesion and the components of the blood around it.

1.2 THE PLATELET AND THE COAGULATION CASCADE

The platelet is a small anucleate cell produced in the bone marrow by megakaryocyte cells, and in the absence of vessel wall injury, can circulate in the blood for 8-11 days. A normal platelet count varies from 150,000 to 300,000 platelets/mm^3 blood. Platelets in their quiescent state are generally unreactive to their environment but can easily be activated by interaction with endothelial subcomponents and external membrane glycoproteins. During this activated state, the platelets can perform several functions [8]:

1) Adhere to injuries in blood vessels to form the primary hemostatic plug that prevents the loss of blood.

2) Provide a surface on which soluble coagulation factors can react.

3) Promote the integrity of the endothelium by sharing metabolic products with it.

4) Release a variety of chemical regulators that can control vascular tone, regulate inflammatory reactions, and initiate the repair of damage in vessels.

The clotting mechanism in mammals begins with damage to the vascular system, which simultaneously initiates two pathways – one is the aggregation of blood platelets at the site of injury, the other is the activation of the enzymes of the coagulation cascade.

Platelet activation begins with the blood exposure of subendothelial components of the vascular wall due to vessel injury. The platelet adheres to exposed collagen and other components, conformationally changes, and undergoes a primary release of regulators by means of dense and alpha granules. There are normally about ten

dense granules in each platelet, which contain ADP, ATP, calcium, serotonin, and vasopressin. There are about ten times as many alpha granules, which contain a large variety of coagulation proteins including fibrinogen, fibronectin, factor V, and vWF [8]. The release of the products contained in the granules initiates the coagulation cascade (Figure 2).

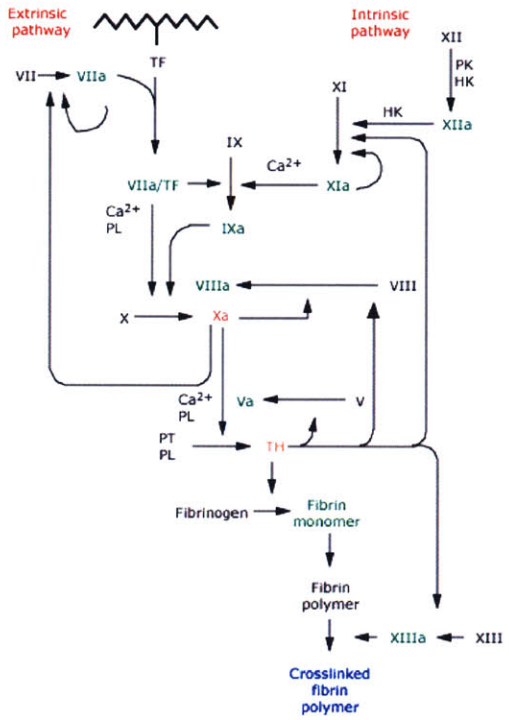

Figure 2: Schematic representation of the coagulation cascade [9].

VWF interacts with subendothelial structures in a calcium dependent process, leading to an alteration of the structure, such that it will recognize specific receptors on the platelets' surface. The release of ADP from the adherent platelets stimulates even more platelets to aggregate together to generate thrombin on the platelet surface, and form the primary hemostatic plug. Finally, conversion of fibrinogen to fibrin strands by the high concentrations of thrombin in the plasma, links one platelet to another to solidify the platelet plug, forming the secondary hemostatic plug [10].

During the coagulation cascade, several aspects of the vascular environment serve to control the reaction and limit the extent of blood coagulation. First, the continued flow of blood past the growing platelet plug washes away loosely adhered platelets and helps to dilute the concentrations of soluble regulators in the plasma. The plasma also provides ADPases which help degrade ADP to adenosine, a competitive inhibitor of platelet aggregation. Finally, the endothelial cells around the injury produce prostacyclin (PGI_2), which serves as an additional platelet inhibitor [8].

1.3 ARTERIAL THROMBOSIS

Thrombosis is the formation of a blood clot in the vasculature by means of the coagulation cascade and platelet interactions. As explained earlier, atherosclerotic plaques contain a fibrous cap that keeps separate the highly reactive components of the plaque and subendothelium from the platelets and soluble regulators found in blood. Thus, it would be expected that a physical disruption of the plaque accounts for the majority of acute coronary thromboses. These disruptions are resultant from a variety of events (Figure 3).

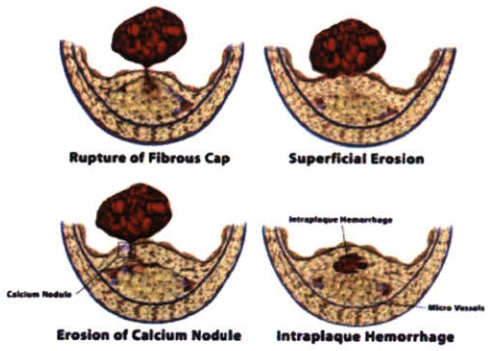

Figure 3: Disruptions of the atherosclerotic fibrous cap [1]. The cases are explained in the text.

The case in which the fibrous cap is ruptured accounts for about 66-75% of fatal coronary thromboses [1]. In this scenario, rupture may occur due to two factors. First, chemical factors released from inflammatory cells within the lipid-laden core of the plaque can compromise the integrity of the fibrous cap. For example, cells within lesions produce enzymes that act upon the interstitial matrix, degrading the cap's strength. Secondly, physical stresses applied to the plaque may aid in its rupture. A fibrous cap weakened by chemical means is especially subject to stresses caused by blood pressure and blood flow in the "shoulder" region of the plaque, where the plaque borders the normal arterial wall. These types of events are most likely to occur during moments of strenuous physical activity or emotional upset [11]. In certain populations, such as diabetic individuals and women, superficial erosion of the plaque by way of exterior hydrodynamic stresses are actually more common causes of fibrous cap disruption. Also, microvessels in the base of the plaque may rupture, causing intraplaque hemorrhage. The combination of hemorrhage and local generation of coagulation regulators in the plaque can cause sudden lesion expansion into the vessel lumen (Figure 4).

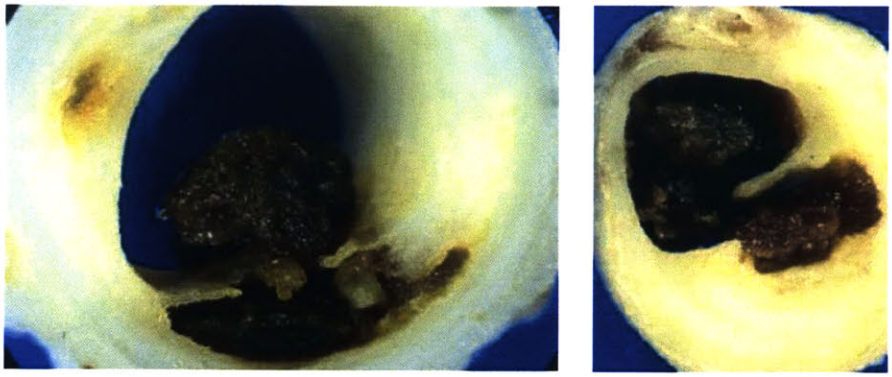

Figure 4: Partial lumen area reduction by thrombosis caused by plaque disruption (left). Complete blocking of the lumen by thrombosis caused by plaque disruption (right) [12].

The condition of the blood surrounding the plaque can also play a large role in its disruption. Subjects with diabetes, obesity, or hypertension experience heightened levels of circulating plasminogen activator inhibitor-1 (PAI-1), which helps to decrease the body's natural fibrinolytic mechanism – the mechanism that

combats the persistence and accumulation of thrombi. This type of blood condition has led to patients being diagnosed as "vulnerable patients" due to their predisposition toward coronary thrombosis [1, 13].

Following the disruption of the plaque, the blood coagulation pathway is begun by exposure to tissue factor originating from the lesion's atheromatous core, while exposure to subendothelial collagen fibrils activates platelets. In addition, regulators cause narrowing of the blood vessel, which in turn creates turbulence, increases blood shear rate at the vessel wall, and activates more platelets. As an additional positive feedback measure, the resulting reduction in coronary blood flow decreases the washout of coagulation proteins, further enhancing thrombogenicity [13].

1.4 THERAPY FOR ACUTE CORONARY SYNDROMES (ACS)

The concept of the "vulnerable patient" has brought about a new look at acute coronary syndromes, where the search for plaques at high risk of causing thrombotic complications has become a high priority. As the majority of lesions grow outwardly and do not encroach on the artery's lumen, searching for vulnerable plaques by traditional angiographic means has proven to be difficult. It has become necessary to monitor the plaque morphology, and not simply the degree of luminal obstruction. Other means of studying these plaques, such as ultrasound, have shown multiple disrupted lesions in patients, challenging the traditional view that ACS is a localized disease that deserves localized therapies such as bypass surgery [1]. Analysis of these plaques has resulted in a set of characteristics of a vulnerable plaque:

- Lipid core comprises 50% of plaque volume
- High density of macrophages
- Low density of SMCs in the cap

- High tissue factor content
- Thin plaque cap in which the collagen structure is disorganized

The chance a patient with CAD may encounter an ACS depends upon the number of vulnerable plaques present in their vasculature, rather than simply on the number of plaques. This relationship can be noted in variations in frequency of infarcts in particular patients. Some patients may experience them relatively frequently, while others may go ten to twenty years after an infarct with no reoccurrences [12].

Currently, therapy for ACS includes two phases. Early on, the acute phase of the treatment is instituted whereby death of cardiomyocytes is reduced by addressing the features of a thrombotic event that reduce flow to areas of the heart through embolization. The second phase of therapy involves management of the patient's condition by means of a combination of drugs to inhibit platelet activity and thrombin generation. In addition, percutaneous or surgical revascularization to stabilize the culprit lesions may help greatly in high-risk patients. The drug cocktail during this portion of the therapy includes oral aspirin, clopidogrel, and an intravenous glycoprotein IIb/IIIa during the angioplasty [1].

This revision on the classic views of atherosclerosis has left a great impact on patient care. The need to systemically prevent episodes of ACS in individuals at risk has been highlighted. A more individualized therapy based on specific patient characteristics, may be an efficient and cost-effective solution for preventative therapy in the future.

1.5 VIRCHOW'S TRIAD

Rudolf Virchow (1821-1902) is recognized as the discoverer and originator of a number of advances in medicine that continue to influence physicians today. One theory that has been somewhat incorrectly attributed to him (the ideas were

neither original to Virchow, nor did he synthesize them in the manner currently understood by physicians [14]) for over 150 years has been a theory which explains the pathogenesis of venous thrombosis, Virchow's Triad. The theory suggests that three criteria must be met to begin thrombogenesis: abnormalities of the vessel wall, altered blood states, and altered blood flow conditions [15].

1.5.1 VESSEL WALL CONDITIONS

Under normal healthy conditions, the endothelium of the vessel wall prevents blood coagulation and platelet activity by means of glycoproteins on the endothelial cell surfaces as well as the release of a variety of molecules. Glycoproteins such as ectonucleotidase, reduce the coagulant activity of blood by minimizing the pro-thrombotic effects of nucleotides like ADP [16].

In the acute time frame of endothelial damage, a highly reactive set of subendothelial components are exposed to a great deal of blood full of components ready to initiate the coagulation cascade. In the chronic time frame of abnormal vessel wall conditions, where the endothelium may be damaged or dysfunctional, a number of molecules normally held within the cell are present in elevated amounts in the plasma [15, 16]. This change in the particulate composition of plasma can be interpreted as the endothelium's response to injurious stimuli, which brings about a change in the function of the endothelial cells. Specifically, measurements of the plasma concentration of certain molecules are often used as markers of endothelial disruption and dysfunction. Variations in these plasma concentrations have been found to accurately predict cardiovascular events, mortality, and morbidity [17]. Increased levels of von Willebrand's Factor (vWF) is a common marker of atherosclerosis, and unless the atherosclerotic condition is dealt with, the high levels of plasma vWF may actually increase the risk of thrombus formation in patients with atherosclerotic lesions, further reinforcing the diseased condition [17]. Another marker used to indicate vascular disease states is thrombomodulin, an important regulator of thrombin. When functioning correctly, thrombomodulin is a

cell membrane protein that converts thrombin from a procoagulant to an anticoagulant. Release of the protein from the cell into the plasma tips the hemostatic balance of the blood to a more pro-coagulant state [16]. The endothelium is considered the largest complex functional organ, and from these serological methods (measurement of plasma composition), it can easily be seen that it has a great influence on disease states of the cardiovascular system.

1.5.2 BLOOD STATE

The next component of Virchow's Triad refers to the condition of the blood and any abnormalities in its constituents, such as the increased presence of clotting or hemostatic factors or activated platelets [15]. The process of thrombogenesis is a balance between the fibrinolytic system and the platelets. The fibrinolytic system is first influenced by plasminogen activators and inhibitors. A plasminogen activator such as tissue plasminogen activator (tPA) helps to promote fibrinolysis, while an inhibitor such as plasminogen activator inhibitor-1 (PAI-1), helps to modulate the fibrinolytic process. Maintaining a correct balance between these two factors is highly important in avoiding a pro-thrombotic blood state. For example, normally a male patient has a 1:8 ratio of active tPA to active PAI, but atherosclerotic men experiencing a more pro-thrombotic blood state may show a severe disturbance in this ratio, approaching 1:50 [15].

Other soluble coagulation factors have been found in increased levels during disease states. High concentrations of fibrinogen, an essential component of the coagulation cascade, have been found in conjunction with many forms of cardiovascular and inflammatory diseases, as well as smoking, physical inactivity, and obesity. In addition, increased fibrinogen has a number of prognostic implications for cardiovascular death and nonfatal myocardial infarction, raising the risk cardiovascular events in a patient [17].

The other half of the blood state balance involves the activation of platelets. Platelet activation occurs as a result of cell interaction with any one of a number of

soluble factors or subendothelial wall components. Activation of the platelet causes its integrin receptors to change from the low to high affinity state, supporting the firm adhesion of the platelets onto fibrinogen, collagen, and fibronectin surfaces [18]. The steps following activation and adhesion of the platelet include spreading of the cell onto the surface and aggregation of other platelets to the site, forming the primary hemostatic plug.

1.5.3 THE LOCAL HEMODYNAMIC SETTING

Altered hemodynamic states forms the last leg of Virchow's Triad. Of interest in this realm is the rheology of blood, especially the viscosity of the blood and the shear force with which it impinges on the vessel walls. As a non-Newtonian fluid, the viscosity of blood is not a constant, but variable according to the shear rate experienced by the blood. In conditions of low shear rates, or stasis, hyperviscosity of blood may occur, initiating coagulation, causing atherogenesis, endothelial cell dysfunction, thrombogenesis, and ischemia [15]. On the other hand, elevated shear rates have a hand in platelet activation, initiating the coagulation cascade from another pathway.

The local flow state inside a vessel greatly influences the biological interactions, be them on the molecular, microscopic, or macroscopic scales. On the molecular level, the transportation of substances from a source, like the blood, to an activating locus, like a receptor, by means of diffusion or convection, plays an important role [18]. Microscopic interactions also play a role in the hemostatic environment. As blood flows through the vasculature, the Fåhræus-Lindqvist effect causes the hematocrit, composed of red blood cells, to migrate towards the center of the vessel lumen, displacing the platelets to the flow periphery. Due to this, fluid shear at the wall combined with cellular transport mechanisms and endothelial wall activity become an important factor in the process of thrombosis [19, 20]. Finally, in the macroscopic realm, high shear forces or pressure fluctuations can have a significant impact on the spread and

progression of disease states such as acute thrombotic events. These types of events involve the sudden rupture of atherosclerotic plaques due to the fact that the plaque fibrous cap strength is too weak in relation to the local fluidic forces [21-24].

As the local flow field yields a great amount of influence over the biological response of the area, physiological attributes of the vasculature that affect the flow also play a large role by association. Simple profiles are to be found in purely axial flows where dimensional symmetry abounds in the vessel. On the other hand, curved flow streams cause additional axial and orthogonal pressure gradients, which in turn bring about secondary and recirculant flows [25, 26]. These complex flows, in turn, bring about changes in the shear stresses applied to the vessel walls by the fluid. These effects are normally essential in the remodeling and maintenance of healthy vessels, but at times can prove detrimental to the vessel health, and actually help progress vascular disease. This effect can be noted in the substantially higher rate of atherosclerosis at sites of vessel curvature and branching, as compared to areas of little to no curvature [27, 28].

The three main vascular environmental parameters that affect the thrombotic process have been briefly described. The goal of the following study is to encompass these three thrombotic controls in a testing mechanism and allow them to be manipulated and studied in a controlled fashion. The result will be a highly individualized body of data consisting of a given patient's potential for thrombosis across a vast range of physiological and iatrogenic conditions, from here on known as a "thrombotic fingerprint". We posit that the generation, study, and refinement of the thrombotic fingerprint will help to gain further insight into the nature of thrombosis and the clinical response to the disease state, as well as aid in tailoring therapeutic clinical treatments, determine the duration and dose of therapy, and assist in clinical trial management and establishment of clinical norms.

CHAPTER 2: METHODS OF STUDYING THROMBOSIS

2.1 TRADITIONAL MODELS

A number of methods to study the process of thrombosis under controlled conditions are currently available to researchers and clinicians. This group of models can be split between the *in vitro*, *in vivo*, and *ex vivo* varieties. Each one of the tests offers a unique and useful insight into thrombogenesis, while providing a particular set of constraints due to the nature of the testing. These constraints may be realized in the parametric conditions tested, or in the types and extent of information derived from test results. Over time, the combination of these tests has greatly helped to further the body of knowledge regarding vascular biology. Briefly, the current set of tests used to study thrombosis, as well as the particular insights and advances they have provided, will be described.

2.1.1 *IN VIVO* MODELS

The main advantage of *in vivo* models is their high degree of realism and physiological relevance that is in most cases, unattainable in the realm of *in vitro* testing. *In vivo* models include clinical trials and animal studies. These two types of tests allow for monitoring of the complex biological interactions occurring inside a subject for long periods of time. These enhanced observational aspects improve disease characterization, patient risk stratification, and the efficacy of therapeutic options [18]. In general, mechanistic and pathological insights have been acquired by observing the human condition, especially during moments of overt system failure. By these means, several important processes related to thrombosis have been initially discovered, such as GPVI deficiency, Glanzmann's thrombasthenia, Bernard-Soulier, GPIb deficiency, and vWF disease [29]. Among the variety of tests,

clinical trials are the most relevant to the human condition, and due to the fact that the primary goal of the trial is to help the patient, making progress on the scientific front generally proves difficult. The long time scales of these projects, as well as the lack of ideal condition controls and the inherent patient variability, can frequently lead to increasingly complicated results which may yield unclear conclusions.

The next step away from the human model is the animal study. In these cases a detailed observation of the physiologic environment can be obtained with the added benefit a tighter control over the experimental conditions. A wide variety of animals are used in the study of thrombosis and vascular biology. The decision on what animal to use in a model is based on the balance of testing condition requirements. Large animals may better represent the architecture of the human vasculature to apply results more directly to the human model, while small animals are more easily manipulable and cost less, allowing for fundamental questions to be probed. The animal study is still limited, although less so than the human clinical study, by the list of parameters that may reasonably be manipulated [30-33].

2.1.2 *IN VITRO* MODELS

In vitro models give researchers the added benefit of a much tighter parametric control over the variables governing thrombosis. Powerful manipulations may be performed on isolated biological components, while under a highly consistent set of hemodynamic and physical conditions. In general, these systems may be categorized into models that either maintain physical geometric properties, or those that maintain the physiological flow properties [18].

2.1.2.1 MODELS THAT MAINTAIN PHYSIOLOGICAL GEOMETRY

The group of *in vitro* models that focus on maintaining physical geometric properties, such as realistic vascular dimensions, have been utilized in a variety of studies, ranging from endovascular device thrombogenicity to cellular adhesion in

vascular deformities. Of great importance in all of these models is the method by which the blood flow is actuated and maintained. A variety of solutions have been formulated by researchers, such as gravitationally powered one-pass flows and flow loops. Systems powered by gravity feature the benefits of a high predictability and control, low noise, and simple set up, but encounter issues with large static volumes of blood which limit the experimental flow rates and run times [33]. Some flow loop systems feature a tubing loop partially filled with blood, mounted on a tilted turntable, and spun about the center of the loop to induce motion of the blood relative to the walls of the loop. These systems improve upon the gravitationally actuated flow systems by utilizing small blood volumes, but suffer from problems stemming from the recirculation of blood and the inbuilt air-fluid interface [34-36].

The next iteration in flow system design was the use of pumps (such as peristaltic pumps) to actuate and control the flow through a circuit. Unfortunately these systems generate excessive background noise from unwanted mechanical or electro-magnetic activation of blood components, resulting in a system whose environment is too traumatic to correctly replicate arterial-like flow conditions [37, 38].

2.1.2.2 MODELS THAT MAINTAIN PHYSIOLOGICAL FLOW CHARACTERISTICS

The second category of *in vitro* thrombosis models seek to reproduce the vascular flow conditions. The models that replicate the geometry of the vasculature are typically constrained by the range of shear rates they can elicit. Models that forgo the need to model the exact geometry of the vasculature, but instead focus on the flow conditions, make use of small circuit geometries that allow the development of high shear rates with low volumetric flow rates, such as parallel-plate flow chambers [39-43]. In addition to maintaining physiological flow conditions, these systems have been extremely useful due to their tight biological

environment control and their ability to offer microscopic visualization of surface-cellular interactions in real time.

Other techniques that maintain physiological flow conditions include cone-plate and annular ring devices. These systems create a relative motion between a fluid and two of the surfaces which contact it, creating a Cuvette-type flow. Although these models take great liberties with the physical flow shape, they are capable of establishing well-described and controlled surface and volumetric shear profiles. Using suitable scaling and careful experimental design, these systems have been able to answer geometrically relevant questions, and have greatly enhanced our fundamental understanding of shear-dependent, thrombotic surface reactions [18, 44, 45].

2.2 THROMBOTIC FINGERPRINTS

As explained earlier, a variety of anti-thrombotic agents and strategies have become the standard of care in the treatment and prophylaxis of thrombotic events. At the basis of these strategies is balancing the risk of blood clot and the equally important risk of major bleed. Due to this, decision-making trees, developed from the outcomes of numerous studies and professional opinions, have been employed in clinical scenarios. These empirically-based strategies have been traditionally based on lumped populations, and only more recently has focus switched to the interaction of a multitude of genetic and environmental factors which determine an integrated outcome, generating a highly individualistic record of a patient's propensity to clot. The need to break down these groups into smaller sub-populations and individuals has become increasingly recognized.

Many clinical decision are based upon the findings of *in vitro* models, whose problems are highlighted by their general inability to represent clinically relevant, complex *in vivo* thrombotic scenarios. These current tests are capable of producing a single output which is then related back to *in vivo* information, forming a one-to-one

mapping of data. At the basis of these *in vitro* tests, though, is powerful factor isolation, assay activators, and system standardization which skew the outcomes of these tests, reducing the foresight and ability to predict clinical outcomes that the experimenters may derive from the test results. Rather than relying on such single potentially biased values, our approach will ascertain a larger portion of this map from parametric considerations of qualitative biological factors. We propose that such an *in vitro* mapping of relevant parametric space will yield an individual Thrombotic Fingerprint that should contain novel information of *in vivo* clinical relevance that could otherwise not be gained from single-value correlations.

2.3 FLOW SYSTEM EVALUATION

The current list of model flow systems available to researchers and clinicians to study the process of thrombogenesis and the hemodynamics with respect to it and to the human condition, was compared against a variety of criteria (Table 1).

Table 1: Comparison of flow system attributes. (Subjective scale that ranges from +++ → ---, which is equal to Excellent → Poor.)

Experimental Systems		System Performance Attributes												
		Complex Interactions	Physiological Shear	Physiological Geometry	Parametric Analysis (Biological)	Parametric Analysis (Physical)	Signal / Noise	Cost	Range of flow conditions	# of flow conditions	Blood Volume	Visual Observation	Indirect measures of platelet reaction	Ease of loading
In Vitro	Gravity Driven Systems	--	-	++	+	-	+	+	-	-	--	+	++	++
	Peristaltic Systems	--	--	++	++	-	-	++	+	+	-	+	++	++
	Parallel Plate Chambers	--	++	--	++	-	++	++	++	+++	++	+++	++	++
	Cuvette Systems	--	++	-	++	-	+	++	++	++	+	+	++	++
	Rotational Systems	--	++	++	++	+	++	+	++	++	-	-	++	+
In Vivo	Clinical Trials	+++	+++	+++	---	---	---	---	---	---	NA	---	--	--
	Large Animal Studies	++	++	++	--	--	--	--	--	--	NA	-	-	-
	Small Animal Studies	+	+	-	+	--	-	-	--	--	NA	-	-	-
Ex Vivo	*Ex Vivo* Circuits	-	++	++	-	+	+	--	+	-	NA	+	-	-

The tests listed in this table have brought scientists and clinicians great advancements in the understanding of acute thrombosis. The third major type of experimental system, the *ex vivo* model, has provided the bridge necessary to relate results derived from *in vitro* and *in vivo* models [19].

Even with all the models available, inherent problems still remain with the models' ability to encompass all aspects of the thrombotic process. Newer testing methods, such as the *in vitro* accelerating loop system developed by Kumaran Kolandaivelu [18], have successfully improved upon the weak points of the previous systems. His system is capable of maintaining a strong control over the *in vitro* biological environment, while creating well defined and physiologically relevant blood flows, as well as maximizing the biological signal output and reducing noise in the results. Having studied and tested with the rotating loop device, the advantages and shortcomings of the machine became apparent. The testing system described in this thesis project solved several of the rotating loop device's problems through the key criteria of our new machine design. These criteria include:

1) The ability to tightly control and concurrently test a wide number of test conditions dictated by Virchow's Triad.

2) Utilize small blood sample volumes to perform these tests.

3) Allow for the high volume of test conditions to be run quickly and easily, while outputting accurate and consistent data.

Briefly, a variety of routes for improvement upon Kolandaivelu's rotating loop machine design were initially considered. This was followed by the decision to leave the constraints of the loop design and develop a 384 channel device capable of varying flow, blood, and vessel wall conditions across all of the blood channels. The device would allow for simple and safe manipulation of the blood, and would feature

a reliable and ubiquitous assay method to produce strong and reliable biological signals. Finally, the device allows for the use of small blood sample volumes per test, and is cost effective in terms of both capitol and time costs.

2.4 MULTIPLE-PARAMETER *IN VITRO* MODELS OF THROMBOSIS

2.4.1 PULSATILE LOOP MODEL OF THROMBOSIS

The *in vitro* pulsatile loop model of coronary lesion thrombosis (by Kumaran Kolandaivelu) [18], served as the inspiratory and investigatory starting point for our new *in vitro* model. At the basis of the thrombotic model is a fluid filled torus which is rotated about its axis (Figure 5).

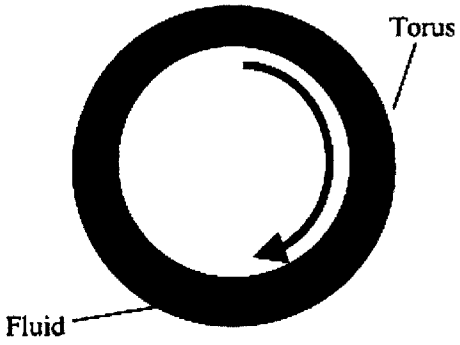

Figure 5: Fluid filled torus. A clockwise motion of the torus about its axis causes clockwise fluid motion relative to the torus wall [18].

When the torus is impulsively moved an inertial fluid motion results in the opposite direction. Assuming that the torus is quickly spun up from rest to a constant angular velocity, with time the fluid inside the torus will accelerate to match the speed of the rotating torus due to a bulk momentum transfer into the fluid via shear forces. This sort of fluid flow has been analyzed by Lyne, who likened

the flow in the torus to that of a pressure driven flow, where the acceleration of the fluid takes on the driving character of a body force [46]. In the case of flow-dependent thrombotic reactions, the important characteristic of the flow is the velocity gradient or shear rate, which characterizes the velocity profile of the fluid when looking at a tube flow from a longitudinal cross-section view [29, 47, 48]. Using this technique, the model would create time-varying flows whose characteristics would match the flow qualities found in the coronary arteries, specifically the mean Reynolds, Womersley, and peak Dean parameters (Figure 6). In addition, the model also took into account the Newtonian approximation for the kinematic viscosity of blood (a non-Newtonian fluid) which has been shown to be valid for high shear conditions (>100 s^{-1}) and is often applied when considering coronary flow [25, 28, 49, 50].

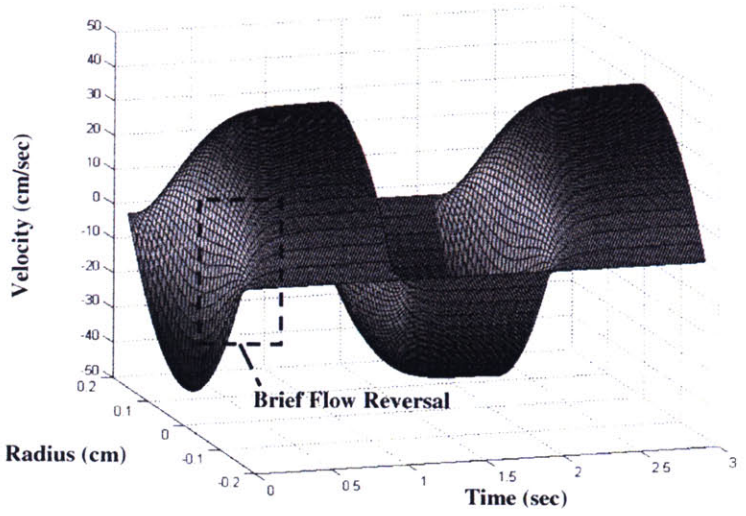

Figure 6: The meshed plot surface depicts the axial fluid velocity distributed radially in the flow tube, as a function of time given a square wave angular velocity input [18].

The full embodiment of the system includes (Figure 7) a fluid loop, rotor-stage on which the loops are mounted, driving motor, motor controller, and a measurement system.

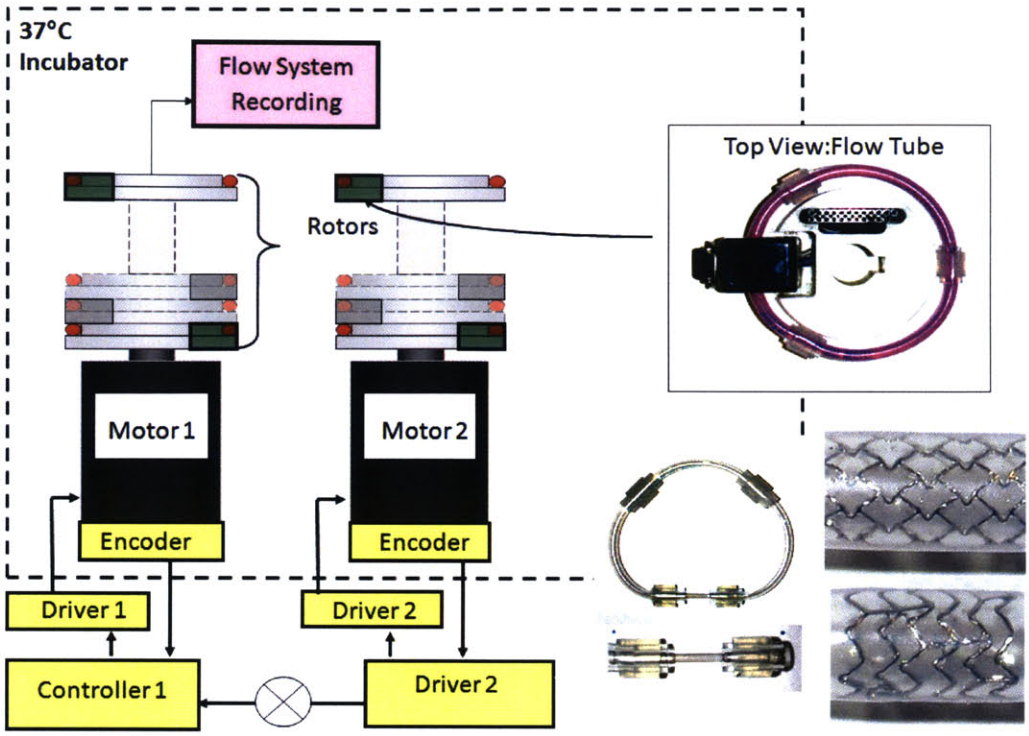

Figure 7: Schematic of multi-rotor i*n vitro* flow loop model of thrombosis. (Left) Two rotors with attached flow tubes, mounted upon two motors conencted to supporting hardware. (Upper right) Photograph of a flow tube with dyed water. Note the blue flow transducer that returns instantaneous flow data. (Bottom right) Photograph of flow loop with a reactive section containing a stent. [18]

This embodiment of the rotating loop flow system allows simultaneous testing of six blood samples via six modular rotor platforms per axis. The blood samples would be loaded into the flow loops which were coated with a blood-unreactive protein, such as albumin. A small section of the tubing, labeled the reactive section, was coated with a reactive species such as one of the constituents of the subendothelium, and could also contain an expanded and implanted stent. The rotors set up on the motors were then driven through a desired angular motion profile by means of a control system on a computer linked to the motor. This bi-directional spinning motion would create internal flows which were then measured via onboard flow transducers built into the rotor stage. These transducers would instantaneously provide information about the flow profile and the rheometry of the blood.

2.4.1.1 PARAMETER VARIATION AND OUTPUT DATA

One of the greatest advantages of this apparatus was its ability to experiment with a wide span over any of the Virchow's triad derived parameters. Specifically, a large number of permutations of physiological shear rates, vessel wall coatings, and hyper/hypocoagulable blood states could be tested. The single output variable derived from the three input variables was an indication of the amount of thrombotic burden captured by the reactive section of the flow tube. Assays would characterize the amount of thrombosis in the test loop by the concentration of platelets and other bound cells to the reactive segment. This data would be directly correlated with the thrombogenicity of the particular set of blood and wall states, and flow conditions experienced in the tube during the test run. This enhanced experimental resolution would greatly improve upon the limited perspective that current testing systems have given us about the hemodynamic nature of thrombosis.

2.4.1.2 LIMITATIONS OF THE PULSATILE LOOP MODEL OF THROMBOSIS

The pulsatile loop model of thrombosis provides a great number of improvements upon previous assay systems and extended knowledge, for example, by comparing the thrombogenicities of gold coated versus bare metal stents. This model also featured some process and mechanical limitations discovered over the course of building, validating, and testing with the model. Primarily, it was found that greater use of the data derived from this machine would be derived from a larger number of tests featuring a wide variation of parameters. Due to the sensitive nature of blood, tests on blood samples drawn on two different days may not provide accurate or relevant data, as a variety of environmental or physiological conditions could affect the thrombogenicity of the blood from one blood draw to another. Because of this, tests would have to concurrently examine parametric variations on a single blood draw, necessitating the ability of the thrombosis model to accept a number of blood, wall, and flow conditions in parallel. The physical embodiment of the rotating loop model was hindered by its ability to test blood

samples at a single flow condition, making it very difficult to compare the thrombotic signal due to variations in flow across tests on different blood samples.

In addition, the machine featured a large amount of user involvement during the preparation, testing, and assaying steps. To properly and safely prepare the machine for a run, a team of at least two individuals would have to carefully load the blood into the tubes, while removing all entrapped air. Each flow loop required at least a full minute to fill with blood and ensure the escape of air. This process alone injected a considerable degree of error into the testing process due to the inability to fill all the tubes at the same time, such that a staggered order of tube filling would have to be compensated for. The human factor concerning the interaction with needles, syringes, and blood made the situation impossible to speed up, and greatly increased the biological hazard of blood contact.

Finally, from a point of view of future expansion, the machine lacked the ability to grow with the increasing test volume needs as investigations developed. Each flow loop required a 3mL blood sample, requiring large samples of blood to be drawn from volunteers or animals when testing a variety of conditions with several repeats. Also, the design of the machine required increased user interaction with each increase in test volume. Adding more rotors to accept more blood samples would quickly reach a limit defined by the users' abilities to quickly and properly load the samples into the tubes, test, and assay the results. As an investigation on the nature of thrombosis develops, an increased number of tests covering a wider parametric scale would be required. Eventually, a solution would be needed that greatly reduces the blood volume per test while increasing the parametric variation and resolution featured in concurrent tests.

2.4.2 RATIONALE FOR NEW FLOW MODEL PURSUIT

Consideration of the process and design limitations of the rotating loop flow model led to a list of the basic constraints and goal parameters to guide us in developing an improved flow model. In reaction to the previous design, it was

determined that the number one priority of this design was to concurrently test one or more variables, while also performing repeats of each testing condition to ensure precision. Secondly, the sample of human or animal blood required for each test needed to be decreased considerably. It was understood that the nature of this thrombotic testing would eventually lead to high volumes of tests brought about by exponential test number growth from parametric variation along three axes. The final major design goal was to integrate a commonly found and easy to use lab and clinical blood collection and assay system into the design from the outset. This element would ensure a minimum of noise from preparatory processes and human error, while maintaining hygienic conditions and adaptability to the clinical environment.

Two high-throughput flow models were proposed: a rotating well flow model and a linear flow model. The rotational flow model was the most directly derived from the pulsatile loop model, incorporating the principle of utilizing the inertia of a stagnant fluid as a means of developing motion relative to the container walls by imparting a spinning force on the container. Briefly, a container resembling a 96-well or 384-well plate would be pre-treated, then filled with blood samples and covered with a lid. The plate would then be centered on a turntable. Combinations of well dimensions and turntable spinning programs would be used to develop well controlled fluid shears in each well.

The linear flow model involved a one-pass system whereby 384 glass capillaries would allow blood to flow down a pressure gradient from one blood collection receptacle to another. All of the flow routes would feature a section of identical dimensions, followed up by a section featuring custom dimensions that would allow flow rate variation. The glass capillaries of the flow system would also be designed to mate with a standard 384-well plate to incorporate standard assaying systems into the protocol.

The initial determination of the feasibility of these concepts was based on the theoretical fluid mechanical models that would inform us about the rotation rates, pressures, dimensions, and sample sizes necessary to create the desired model flow profiles.

CHAPTER 3: FLOW MODEL DESIGN

3.1 ROTATING WELL FLOW MODEL

3.1.1 DESCRIPTION OF SITUATION

The rotating well flow model was a high throughput evolution of the flow model developed by Kolandaivelu [18]. A fluid filled container was accelerated about its axis of symmetry to create wall motion in relation to the fluid, whose angular speed lagged behind that of the wall because of its own inertia. The relation between the wall and fluid's rotational velocity became the wall shear rate, which is of interest to us in our flow model. With the use of periodic accelerations and decelerations, one could ideally maintain a particular shear rate in a fluid filled container. In this particular model, the containers that held the fluid were of dimensions equal to the wells of a 96-well plate and were arranged radially on a circular disk that was spun from its center. The advantage of this configuration was that it potentially allowed for the easy loading and testing of many samples of blood, as well as it would allow for an easier assay of the samples to obtain a great deal of data per test run.

3.1.2 ROTATING BUCKET EXAMPLE

The rotating bucket is a classic name given to the situation where a closed cylindrical fluid filled cavity is spun up from a standstill. The analysis of this type of system is much easier when assumptions such as the fluid being in rigid body rotation or an infinitely long cylinder, can be made. This approximation, though, must be carefully applied to a finite length situation (especially if the aspect ratio is low), as experimental results may vary greatly from the theoretical results. For a

liquid of low viscosity, a relatively long time is required for the liquid to rotate as a solid body, and even during this transitional period, the fluid flow may become unstable [51]. The reason that an assumption that the cylinder is infinitely long is difficult to make is because it has been found that the effects of cylinder ends on the fluid motion can actually dominate the flow, even in very slender cylinders. This fluid motion is affected by a secondary flow caused by the cylinder ends in a region called the Ekman layer, which convects the fluid from the walls to the interior of the cylinder. As a result, the fluid attains rotational velocity much more quickly than without these secondary flows (Figure 8).

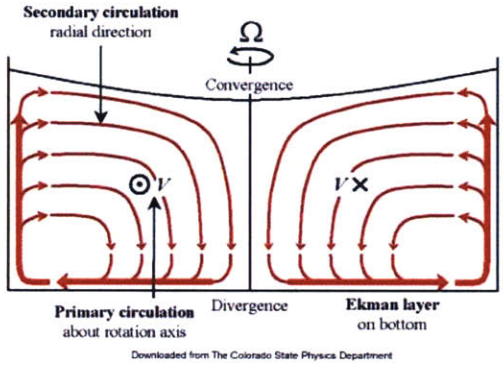

Figure 8: Rotating bucket flow profile. Note the secondary circulation caused by the Ekman layer.

3.1.3 EQUATIONS AND SOLUTIONS

In the particular case of rotationally symmetric flow, with small radial and axial secondary flow in the interior, Greenspan [52] explains that the azimuthal fluid spin-up is governed by:

$$\frac{\partial v}{\partial t} + u\left(\frac{\partial v}{\partial r} + \frac{v}{r}\right) = \nu\left[\frac{\partial^2 v}{\partial r^2} + \frac{\partial}{\partial r}\left(\frac{v}{r}\right)\right], \qquad \textbf{Eq. 1}$$

where u is the radial velocity, v is the azimuthal velocity, and r is the well radius. This can then be solved by

$$u = -K\left(\frac{\nu}{\Omega h^2}\right)^{\frac{1}{2}}(r\Omega - v), \qquad \textbf{Eq. 2}$$

where Ω is the angular velocity and h is the height of the cylindrical well. Greenspan explained that when K=1, Equation 2 becomes identical to the corresponding equation for linear spin up. In addition, he made several substitutions into the resulting equation:

$$R = \frac{r}{a}, V = \frac{v}{a\Omega}, T = \frac{t(\nu\Omega)^{1/2}}{h}, A = \frac{a}{h}, E = \frac{\nu}{\Omega h^2}$$
$$\frac{\partial v}{\partial t} + (V - R)\left(\frac{\partial V}{\partial R} + \frac{V}{R}\right) = A^{-2}E^{\frac{1}{2}}\left[\frac{\partial^2 V}{\partial R^2} + \frac{\partial}{\partial R}\left(\frac{V}{R}\right)\right] \qquad \textbf{Eq. 3}$$

In the previous equation, a is the radial distance from the center of the well, A is the aspect ratio, E is the Ekman number, and the portion $A^{-2}E^{1/2}$ can be substituted with α_0. In their paper, Watkins and Hussey [53] explained that depending on the size of α_0, the equation can be solved in different manners. A small α_0 indicates that the system response to the rotation of the cylinder is very much dependent on the Ekman layer. On the other hand, if α_0 is large, it indicates that the response of the fluid to the acceleration of its container is mostly, to completely, dependent on viscous effects from the cylinder wall. There is also the regime of α_0 that falls in between both extremes and considers a combination of the two effects. Unfortunately, of the three regimes only the small α_0 has been studied extensively, while only very rough solutions have been found for the rest. In this model we only want to deal with viscous effects, to avoid secondary flows in the well. In the case that α_0 is large, its solution is found in the form:

$$V = R + 2\sum_{n=1}^{\infty}\left[\frac{J_1(j_n R)}{j_n J_0(j_n)}\right]\exp\left(\frac{-j_n{}^2 \nu t}{a^2}\right), \qquad \textbf{Eq. 4}$$

where J_i is the Bessel function of the first kind of order I and j_n is the n^{th} zero of J_1. This equation was solved with the use of the program Excel for a variety of conditions. The extreme conditions, especially the maximum shear rates that we wanted to test, were focused on to determine the feasibility of this type of apparatus. While determining the parameters necessary to create the maximum

shear rates, it was necessary to take note of the well radius, the maximum rotational speed reached by the spinning platform, α_0, the centrifugal acceleration experienced by the fluid in the well, the volume of blood in the well, and the time for the fluid to reach a state of solid body rotation. The results of experimenting with the upper limit conditions revealed the results presented in Table 2.

Table 2: Results of solving Equation 4 for extreme parameters.

Shear Rate [s^{-1}]	R_{well} [cm]	$T_{solid\ body\ rotation}$	Max Well RPM	α_0	Centrifugal Acceleration (@ r=1cm) [G]	Blood Volume [mL]
3980.47	0.5	0.15	9300.00	0.012	968.69	0.98
4007.53	2	10.0	3780.00	0.001	160.03	15.0

We expound the conditions necessary to produce the upper shear rate design limit, which was $4000s^{-1}$ (Table 2); as confirming whether the apparatus is capable of these limits determines the feasibility of the device. The largest difference between the two cases presented in the table is found in the radius of the well (R_{well}), where one well is about the size of a well in a 96 well plate, while the other is much larger to provide a good contrast. The advantages of a small well can be seen in this table. The small well requires a much smaller blood volume, allowing for nearly 60 experiments to be run from a typical blood sample, which is generally about 60mL. The larger volume would only allow about 4 tests to be taken. Also, the smaller well requires much less time for the fluid in the well to achieve a state of solid body rotation, because of viscous effects and its greater surface area to volume ratio. This ratio is important when considering that the cylinder would have to cycle through acceleration and deceleration phases in order to continually create the shear rates required by the test. The dependent variable, $T_{solid\ body\ rotation}$, indicates the time delay between the moment that the well achieves its final rotational speed, and the moment that the fluid in the well reaches the rotational speed of its container's walls. A $T_{solid\ body\ rotation}$ of 0.15s is much easier to work with than one of 10.0s, which would take up a great amount of time considering that each test would only run between 1-2 minutes. Advantages to using a larger well volume include the

need to accelerate the cylinder to a considerably lower final rotation rate to achieve comparable shear rates, and therefore lower centrifugal accelerations on the samples are also expected. In theory, this system should reach its maximum rotational speed in less than 0.1s.

Outside of the advantages of one well size over another, the table provides information that indicates this testing method would not be feasible. To meet the goal shear rates of around 4000 s^{-1}, high rotation rates must be reached by the motors running the experiment. These rotation rates will then cause great centrifugal accelerations in each well, which quickly approach blood separation values as one increases the distance between the center of the plate and the well. As a rule of thumb, blood centrifuged at rates between 300-500 G's begins to separate between plasma and cells after only a few minutes. The generation of this effect would be very detrimental to the results of this experiment. In addition, the value of α_0 becomes very small at these rotational rates, which indicates that this system should actually be solved using the small α_0 approximations of Equation 3. Moreover, the fact that this system has a small α_0 denotes that the rotation of the fluid is very dependent on the Ekman layer, which in turn means that the fluid rotation is greatly influenced by secondary flows present. These secondary flows would be very detrimental in the simulation of the simplified physiological environment that this model is aiming to create, and needs to be avoided as much as possible.

Finally, during the research that was completed for this model, it was found that "spin down" or the deceleration of the fluid inside a sealed cylinder, was not symmetric to "spin up," or the acceleration of the fluid [54]. Spin down can occur in an impulsive or finite manner. During an impulsive spin down the fluid particles near the cylindrical wall will rapidly experience a centrifugal instability. This centrifugal instability can lead to the creation of "Taylor Görtler" vortices along the side wall [55]. As spin down proceeds, the smaller vortices coalesce into larger ones, generating a much more rapid spin down than what would be predicted by nonlinear theoretical arguments. This problem can be delayed by conducting spin down over a finite period of time. The problem may even be completely avoided in

the slowest deceleration conditions, but the problem with this solution is clear in this test. The time needed to decelerate, and/or change the rotation direction of the fluid is of great importance, and a great deal of time cannot be applied towards deceleration of the fluid.

The combination of all of these technical difficulties led to the decision to explore the feasibility and design of a high throughput, one-pass linear flow device.

3.2 LINEAR FLOW MODEL

3.2.1 DESCRIPTION OF SITUATION

To create the desired flow profiles, and therefore, the desired wall shear rates, a fluid flow was generated down the length of the flow tube by a pressure drop, creating a Poiseuille flow (Figure 9). The difference between the pressures at the entrance and exit of the tube allowed for fluid to be moved from its initial container to a final collection reservoir. The wall shear rate in the tube was determined by the profile of the flow, which in turn was a factor of the tube dimensions as well as the fluid flow rate. Given a particular pressure drop and volumetric flow rate, the flow's velocity was controlled by varying the cross-sectional area inside a tube. In the case of flow-dependent thrombotic reactions, the maintenance of velocity gradients or shear rates was the important flow factor.

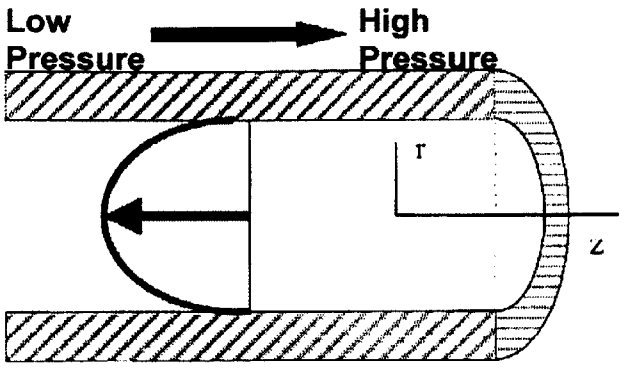

Figure 9: Parabolic flow profile generated by Poiseuille flow conditions (pressure gradient down flow channel) [18].

Using this technique, we hope to initially create time-invariant flows, whose flow characteristics such as the dimensionless flow parameter Reynolds (Re) and wall-fluid shear rate were typical of physiological blood flows found in arteries. The theoretical model developed for this apparatus represents a straight pipe composed of three sections: the test section, the contraction, and the resistance section. (Figure 10).

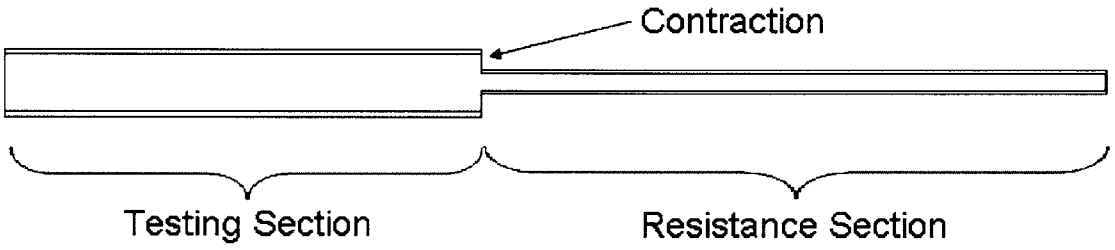

Figure 10: Cross-sectional sketch of the theoretical straight pipe model.

The test length section of the model has constant parameters across all testing conditions. The contraction and resistance sections will vary to modulate the shear rate conditions of a test.

3.2.2 EQUATIONS

The most important parameter of the fluid flow in this model was the shear rate experienced between the fluid and the wall. This information could be found by

solving only the axial (z) component of velocity of the cylindrical form of the Navier-Stokes equations (Equation 5)

$$\rho\left(\frac{\partial v_z}{\partial t}+v_r\frac{\partial v_z}{\partial r}+\frac{v_\theta}{r}\frac{\partial v_z}{\partial \theta}+v_z\frac{\partial v_z}{\partial z}\right)=-\frac{\partial P}{\partial z}+\mu\left[\frac{1}{r}\frac{\partial}{\partial r}\left(r\frac{\partial v_z}{\partial r}\right)+\frac{1}{r^2}\frac{\partial^2 v_z}{\partial \theta^2}+\frac{\partial^2 v_z}{\partial z^2}\right] \quad \textbf{Eq. 5}$$

where V_z, V_r, and V_θ are the velocity components in the axial (z), radial (r), and tangential (θ) directions, respectively. Also, t is time, ρ is the fluid density, and $\delta P/\delta z$ is the axial pressure gradient. In the case of our specific model with its circumferential and axial symmetry, Equation 5 was simplified through the elimination of several dependencies. This was then integrated to give

$$V_z=\frac{1}{2\mu}\left(\frac{dP}{dz}\right)r^2+\frac{A_1}{\mu}r+\frac{A_2}{\mu} \quad \textbf{Eq. 6}$$

Equation 6 provided the velocity profile of the flow. Inputting the boundary conditions of this system (at $r = R_{tube}$, $V_z = 0$, and at $r = 0$, $dV_z/dr = 0$) gave us

$$V_z=\frac{1}{2\mu}\left(\frac{dP}{dz}\right)r^2-\frac{1}{2\mu}\left(\frac{dP}{dz}\right)R^2 \quad \textbf{Eq. 7}$$

Taking the derivative of this function with respect to radial distance yielded a function for the shear rate of the flow.

$$\frac{\partial V_z}{\partial r}=\frac{1}{\mu}\left(\frac{dP}{dz}\right)r \quad \textbf{Eq. 8}$$

Finally, inputting a radial distance of half the tube diameter into this formula gave us the fluid's shear rate against the wall.

$$\frac{\partial V_z}{\partial r}=\frac{1}{\mu}\left(\frac{dP}{dz}\right)R \quad \textbf{Eq. 9}$$

To determine the flow profile and the wall shear rate, it was necessary to calculate the pressure head loss across a certain piping distance (major head loss), which was found with the use of the Darcy-Weisbach equation:

$$\Delta P=\frac{64}{\mathrm{Re}}\left(\frac{L}{D}\right)\left(\frac{\rho v^2}{2}\right) \quad \textbf{Eq. 10}$$

Equation 10 was used to determine the head loss across the testing and resistance lengths of the tubing. The head loss associated with the tube contraction could then be found with

$$\Delta P = \frac{1}{4}\rho V^2\left[1-\frac{D_2}{D_1}\right], \qquad \textbf{Eq. 11.}$$

where V is the linear velocity of the fluid, and D_1 and D_2 are the diameters of the tubing before and after the contraction, respectively.

Finally, the total head loss was equated to the sum of the losses incurred by each of the tubing sections. The length or diameter measurements of each resistance section were then modified until the head loss equaled the difference between the input and exit pressures of the tube. The difference between the input and exit pressures of the tube were set by using Equation 10 to determine the pressure drop necessary to move blood through a simplified model of the tubing at a shear rate of 4000 s^{-1} (the maximum shear rate to be tested). The parameters for the tubing included a diameter equal to that of the test section and a total length equal to the test and resistance sections combined.

3.2.3 SOLUTIONS

Using the linear straight tube approximation, the necessary pressure drop to move blood at a shear rate of 4000 s^{-1}, was equal to 56.5 KPa. Using this figure, it was then possible to determine the dimensions of the tube sections. All the calculations involved the test sections of one size, which were chosen such that we could meet our targeted volumetric flow rate goals while allowing for a large enough volume for a good assay signal, which was 7.5 µL. Only the dimensions of the resistance section changed according to the different shear rates. The dimensions of the test section are found in Table 3.

Table 3: Dimensions of the test section of the tubing.

Attribute	Measurement
Length	**10.00 cm**
Internal Diameter	**0.03 cm**
Cross-sectional Area	**7.06×10^{-4} cm^2**

To ensure that the thrombotic signal from the test portion of the tubing was purely due to the predictable shears of a laminar flow, the Reynolds number in the test section had to be examined (Figure 11).

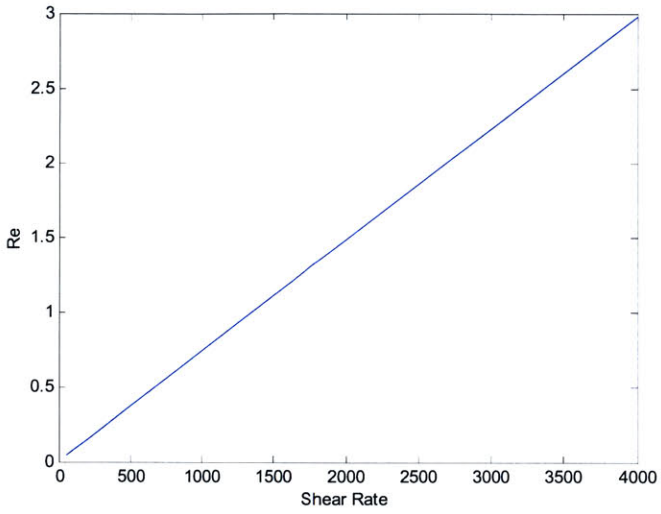

Figure 11: Reynolds number of the flow in the testing section as a function of the shear rate.

The very low Reynolds numbers experienced at our planned shear rates ensure that the flow conditions will be dominated by viscous fluid interactions and not inertial interactions. This guarantees that the flow will be laminar and therefore the mechanical interactions between the blood and wall will be predictable.

For the dimensions of the resistance section tubing, a choice had to be made about whether to modulate the flow resistance by varying the lengths or the diameters of the resistance sections. Variation of length was first investigated, but it was quickly found that the length of the longest tube would be over 80 times the length of the shortest tube which would bring about problems with the actual manufacture and design of the apparatus. Variation of the tube's inner diameter would require variation between 90 microns and 300 microns, which are well within the capabilities of modern glass capillary tube manufacturing.

Before determining the final dimensions of the resistance pieces, it was also necessary to compensate for the Fåhræus-Lindqvist effect experienced by blood, a

non-Newtonian fluid. This property of blood causes it to send most of its red blood cell content to the center of a flow tube as a means of exposing a greater part of its platelets to the periphery. As a result, the true fluid viscosity experienced at the conduit wall becomes a function of the inner diameter of the channel (Figure 12).

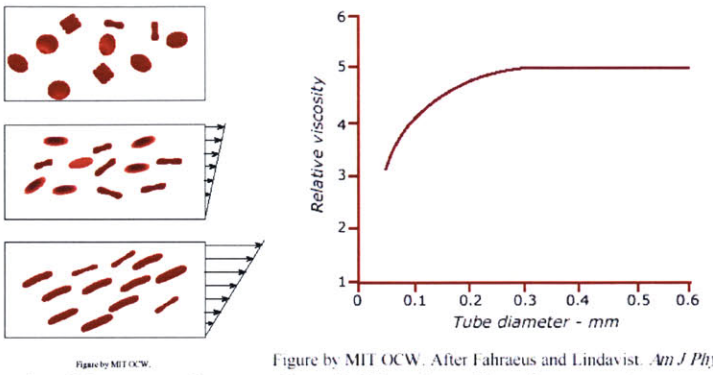

Figure by MIT OCW. After Fahraeus and Lindqvist. *Am J Physiol* 96: 562, 1931.

Figure 12: (Left) Stretching of red blood cells due to increased flow shear rate. (Right) Plot of the relative viscosity of blood as a function of tube diameter.

Due to this effect, the resulting viscosity of the blood due to the Fåhræus-Lindqvist effect had to be accounted for in calculations (Figure 13).

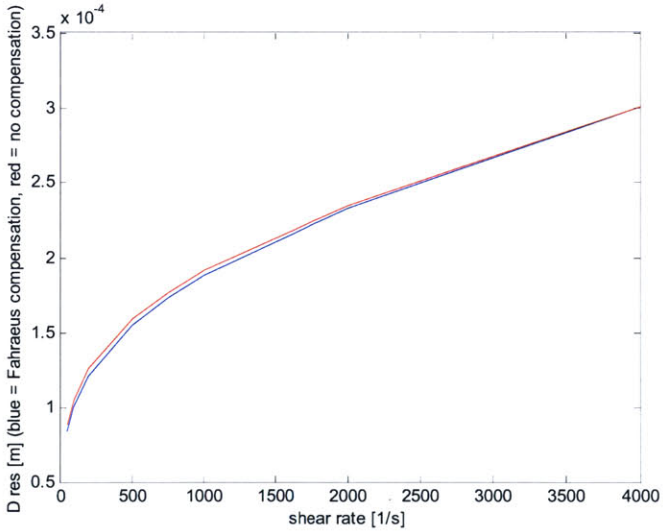

Figure 13: Inner diameter of resistance section of the tubing as a function of the intended shear rate for the channel. Note the small size difference between the calculations that compensate for the Fåhræus-Lindqvist effect, and those that do not.

The dimensions of the resistance section tubing are found in Table 4 (the Matlab code written to calculate these results is found in Appendix A).

Table 4: Dimensions of the resistance section of the tubing.

Rated Shear Rate [s^{-1}]	Length [cm]	Internal Diameter [cm]	Cross-sectional Area [cm^2]
50	17	0.0083	5.41061E-05
100	17	0.0101	8.01185E-05
200	17	0.0121	0.00011499
500	17	0.0155	0.000188692
750	17	0.0174	0.000237787
1000	17	0.0188	0.000277591
2000	17	0.0233	0.000426385
4000	17	0.0300	0.000706858

In addition, it was found that the head loss due to the tubing contraction (minor head loss) was very small in comparison to the major head loss, so that the manner in which the tubing contracts (gradual vs. sudden) matters little in this case. With the application of a specific pressure drop, we could then control the volumetric flow rate, and therefore, the wall shear rate in the tubing.

3.2.4 TESTING PROTOCOL

Once the means by which blood flow control through our thrombosis model with minimal disturbance was established, the testing protocol, and more specifically, the assay process had to be determined. The linear flow one-pass framework of the model allowed it to readily adopt a very systematic assay method, where the operator of the machine would interfere little with the concurrent processing of a large number of test samples. Borrowing much of the assay method utilized in the rotating loop model of thrombosis, the hardware and processes necessary to support the linear flow system were evolutions of the systems used in the past model.

The testing protocol involves five steps:

Step 1 – Coating of the system's reactive section with one or more subendothelial components, such as collagen, fibrinogen, or von Willebrand

Factor. This constitutes the wall condition axis of Virchow's Triad. The reactive section of the linear flow system is the testing segment of the channel (Figure 10).

Step 2 – Treatment of the blood pre/post drawing from the patient, prior to loading into the flow machine. The blood may be treated with pro/anti-platelet or pro/anti-coagulation drugs. This constitutes the pro/anti-thrombotic blood condition axis of Virchow's Triad.

Step 3 – The blood is then channeled through the reactive section (test section) at the prescribed shear rate for a specific amount of time. This step represents the last axis of Virchow's Triad, flow conditions.

Step 4 – After the blood is run, is it cleared from the tubing and any loosely bound blood components are washed away by a buffer solution (Tyrodes buffer with added MgCl and HEPES).

Step 5 – The blood components that remain bound to the test section must be quantified. This is done by lysing the bound platelets to release their internal components, specifically lactose dehydrogenase (LDH), a substance commonly assayed for when searching for signs of cell damage. The LDH released from the bound cells are contained in solution, which is then colorimetrically assayed by means of a spectrophotometer, to directly quantify the bound cell density of the test section.

The next steps involved incorporating the steps of the test protocol and the means of creating the low-disturbance Poiseuille blood flow, into a machine that bridge the ideas of biological testing and assaying with high-throughput mechanical advantages to develop the Thrombotic Fingerprint.

3.3 EMBODIMENT

The linear flow model was developed directly from the tubing schematic (Figure 10). Initially, it was understood that a means of securing a matrix of glass capillary tubes composed of a uniform testing segment and a variable size resistance section, was the foundation of this machine. After the design of these components was finalized, the supporting hardware which would help load and dispose of blood samples as well as assist with the signal assay steps, was developed. The embodiment of all these concepts kept in mind the need to maintain hygienic conditions, ease of use, protection of fragile components, repeatability, and low usage costs. The following sections describe the evolution of the major system components and their final revisions.

3.3.1 TEST BLOCK

The test block serves as a means of fixing flow channels containing the reactive section of the tubing in a fixed and specific matrix conformation, so that they may be tested upon and controlled in unison and so that the fragile glass channels may be kept safe. In the first iteration of the test block's design (Figure 14) a 3×8 matrix of capillary tubes was encapsulated in a rectangular block along with 4 hollow plastic tubes that allowed the block to be aligned on a platform.

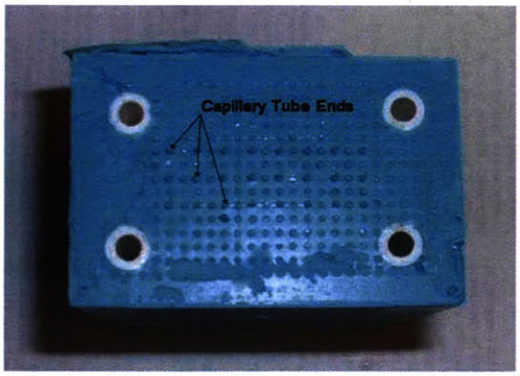

Figure 14: Photograph of the top of the first test block design iteration.

The creation of the first test block brought into mind several considerations into the block's design. First, it was found that a transparent silicone rubber would prove useful to view whether liquid was entering a particular tube, as well as inform the user about any defects or damages to the glass capillaries. Next, the elastic used to form the block was sufficiently protective for the tubes, but perhaps of too low a stiffness to provide proper alignment when mating the tube ends to another set of tubes. A different material or an internal structure to form a more rigid block was necessary. Third, any manipulations near the protruding male ends of the tubing were potentially dangerous, in that they could easily be broken. Therefore, any part in contact with this face of the block needed to have accuracy and clearance to account for these protrusions, to allow for any procedures involving this area to ensue without hitch. Finally, it was observed that as a product of the sheer number of connections between the testing and resistance blocks, it may be difficult to separate the connected blocks without possibly harming the tubes.

The first two problems were solved by finding a suitable silicone rubber. The Sylgard 184 silicone rubber was chosen due to its combination of long working time, high transparency, and a stiff enough constitution to provide proper protection for the glass while allowing for accurate positioning of the glass tubing. In addition, the material was also suitable for biological experiments where it would come into contact with blood, and had to be able to withstand several autoclave cycles.

The tube alignment problem was partially solved with the use of the new silicone material. Initially, a set of rigid metal rods spanning the length of the block was suggested as a means of increasing the stiffness of the block and the alignment of the tubes. Later, it was determined that a mold properly designed for the block that would carefully secure the glass tubes in the material at the proper matrix spacing, would ensure correct tube alignment. The final design issue dealt with the difficulty one may have disjoining a number of test blocks mated with a set of resistance blocks. A solution to this situation involved linking the various test blocks by means of metal rods threaded through them (Figure 16).

The current iteration of the test block (Figure 15) features an 8×3 matrix of glass capillary tubing. The borosilicate glass tubing is manufactured by Vitrocom

Inc. and features a 10cm length, 1.27±0.005mm OD, and a 0.300±0.005mm ID. The spacing between the tubes is specifically measured to mate directly to a 384-well plate. The layout of the block is intended to perform concurrent testing of 3 repeats of 8 different shear rate conditions. The ends of the tubes extend from the bottom surface of the block to reach into the 384-well where it deposits the biological solution to be assayed. The tubes also extend from the top surface to mate with the resistance block which will sit atop the test block. The test block also features two holes in the center of the block, that cross its thickness and are used to mount a 8×2 set of the test blocks on metal rods, in the final machine design (Figure 16, Appendix B).

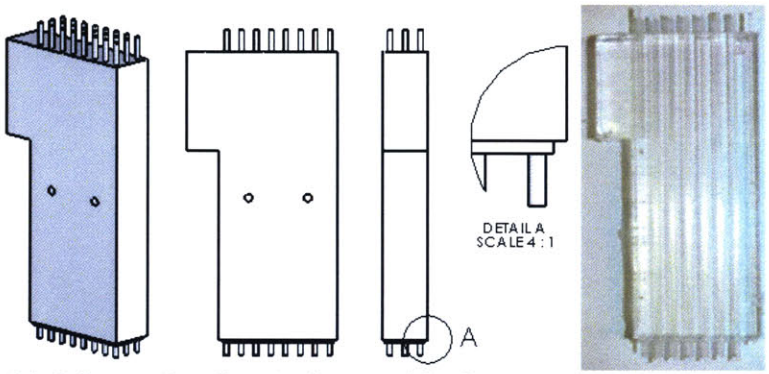

Figure 15: (Left) Schematic of a single test block viewed from various angles. Note detail A shows a step used to create a vacuum sealing lip against the supporting hardware. (Right) Photograph of a completed test block.

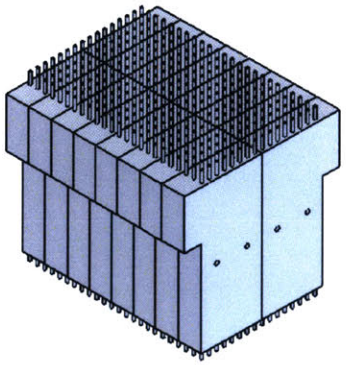

Figure 16: 8x2 array of test blocks. The footprint of this array can mate directly to a standard 384-well plate.

The mold developed to cast the test block is pictured in Figure 17. A drawing of the test block mold annotated with measurements is available in Appendix B.

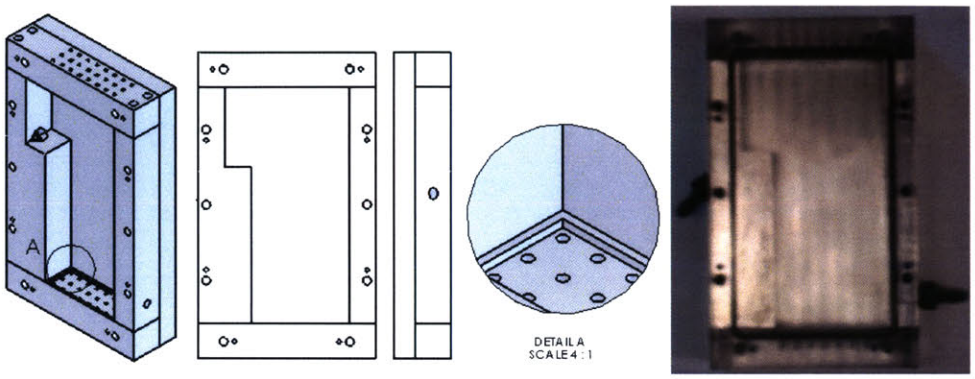

Figure 17: Schematic of the test block mold viewed from several angles. Note that the front cover of the mold is not shown in order to show the mold interior. (Right) Photograph of the completed test mold.

The test block mold allows the capillary tubes to span the length of the block while properly spaced out. The tubes are first installed into the mold, then the mold is closed and silicone rubber is injected through one of the port holes using positive pressure. Next the port holes are closed, and the block is cured in an incubator at 50-60°C for a period of 4 hours. Finally, the block is carefully removed from the mold, and any debris that may have settled in the tubes is cleared out.

3.2.2 RESISTANCE BLOCK

The resistance block (Figure 18, Appendix B) was designed very similar to the test block. The block consists of a 24×16 matrix of tubing encapsulated in silicone rubber. Unlike the capillary tubing in the test block, the resistance block contains two concentric tubes. The outer tube which is encapsulated in the silicone rubber in a mold is made of PTFE and has the dimensions of 17cm length, 3mm OD, and 1.27mm ID. Inside resides a borosilicate glass capillary tube with the dimensions of 17cm length, 1.27mm OD, and an ID specific to the shear rate desired in the channel (Table 4, pg. 44).

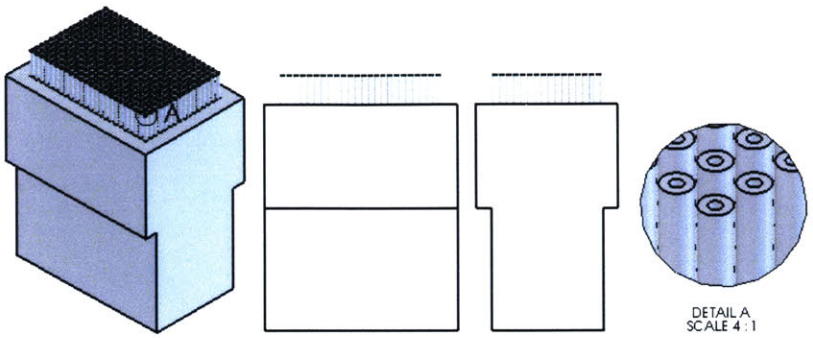

Figure 18: Schematic of the resistance block shown from several angles.

The resistance block sits atop the array of test blocks, and the glass tubes that extend from the top surface of the test block mate with the resistance tubes at the bottom surface of the resistance block. The means by which the tubes mate has undergone evolution. Initially the female end of the resistance tube was designed to have a conical entrance to assist the male ends of the test tubes to mate more easily. It was next decided that the guiding mechanism would be built into the rubber of the block instead of the glass/plastic tubing, due to the difficulty of working with these materials on such small proportions (Figure 19).

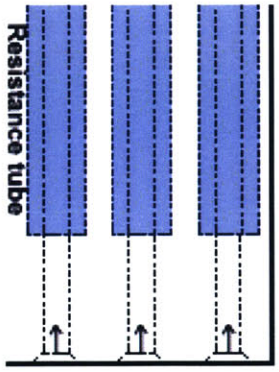

Figure 19: Design feature in resistance block that helps to guide test tubes into the resistance tubes. A conical entrance is molded into the bottom face of the resistance block and help guide test tubes from the test block in the direction of the arrows, until the tubes can mate with the resistance tubes (colored blue in this schematic).

The top of the resistance block will mate with a supporting piece of hardware that will provide the vacuum necessary to create the pressure drop to actuate the

blood flow. The tubes extend from the top surface of the block so that blood may flow out of the tubing and fall from the tubing end into a collection basin, from which the blood would be removed. This would help avoid any extra resistance due to blood pooling or clotting outside of, but above, the tube ends. Sections 3.2.5 and 3.2.6 explain the supporting structure of the test and resistance blocks, which greatly helps in the process of alignment of the tube ends.

3.2.3 BLOOD LOADER

The blood loader (Figure 20, Appendix B) is the first of the supporting pieces of hardware which are built to accommodate the test and resistance pieces. This polycarbonate piece enables the operator of the machine to take blood collected in a standard Vacutainer ® tube, connect it to the machine, and allow the supply of blood to feed the 24 channels of a test block when the vacuum has been applied. The blood loader has an 8×2 arrangement of wells, each of which mated to the bottom of a test block. The wells feature a 1mm step that matches the step cast into the bottom of the test block, which allows for a more secure airtight seal. This airtight seal would be very important, as any small leaks would cause unbalanced flows through the channels and could also inject air into the system, causing premature activation of thrombotic blood components.

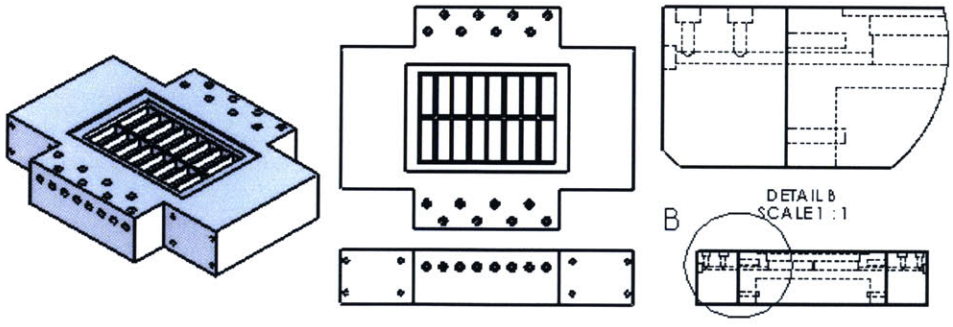

Figure 20: Schematic of the blood loader, viewed from various angles. (Right) A side view of the part showing hidden lines. Note that Detail B shows how channels connect the test block well to a port that connects to a Vacutainer.

Each one of the 16 wells of the blood loader feature a channel that connects the well to a supply of blood in a Vacutainer® (Figure 21). The connection to the Vacutainer is made through a needle fastened to a port of the channel. The blood loader must form a tight seal with the test block component which rests on it, but must also be quickly, safely, and easily removed from the test block during the testing process to perform the subsequent washing and assaying steps. To incorporate quicker transitions between testing stages, a site to secure a standard 384-well plate was machined into the blood loader.

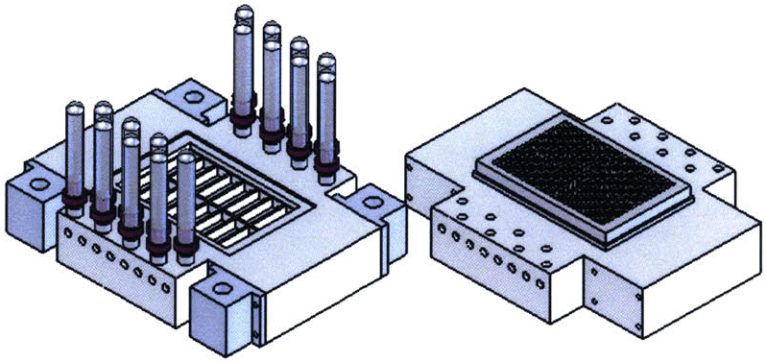

Figure 21: (Left) Blood hopper with attached Vacutainer tubes. (Right) Blood hopper with secured 384-well plate during assaying steps.

Finally, it was understood that not every test performed on this machine would involve 16 separate blood samples with their respective test blocks. Therefore the option to run a less than full load of test blocks during a particular test had to be made available. This would be completed by creating blank test blocks made of solid silicone rubber containing no glass tubes inside them. These blocks would allow no flow through their respective resistance tubes and wells in the blood loader. Therefore, vacuum pressure would only be applied to the channels of interest, allowing for testing of even just a single Vacutainer® collected sample.

3.2.4 VACUUM CONNECTION

The vacuum connection (Figure 22, Appendix B) is the second major piece of supporting hardware for the flow system. This polycarbonate component is designed to mate to the tops of both the resistance block and the 8×2 arrangement of test blocks, and provide the negative vacuum pressure to create a pressure gradient down the flow channels and actuate the flow of blood. As explained in the previous section, the flow of blood will begin from the enclosed Vacutainer® reservoir, and end in the vacuum chamber which encloses the protruding ends of the resistance tubes. The component also features side ports to allow for the pooled blood to be collected and discarded properly, and to allow for the injection of buffer into the vacuum chamber to assist in the removal of the blood.

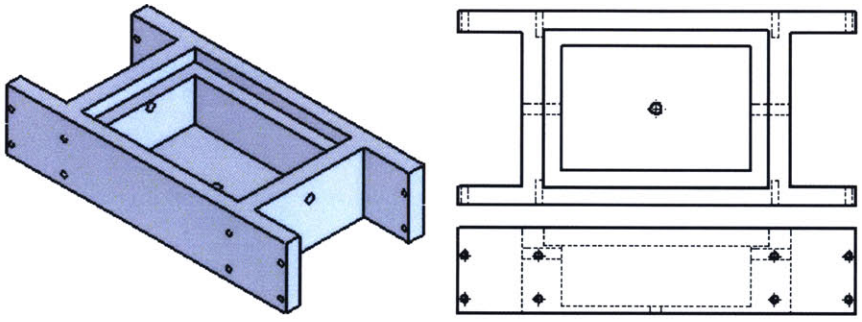

Figure 22: Schematic of the vacuum connection viewed from various angles. (Left) Note that the component is pictured upside-down in order to show its internal compartment. The part also features built-in mounting components which will be described in the following section. (Right) Top and side angle views of the component showing hidden lines. Note the side ports used to remove blood, and the port through the top used to provide the negative vacuum pressure.

The first iteration of the vacuum connection design featured a number of tapped holes in the top of the chamber interior which provided a stable base for a number of rods that would pass through and correctly align the test and resistance blocks. This idea was improved upon with a new structure and mounting system described in the next section. The top dimensions of the resistance block and the array of test blocks are identical to mate properly with the vacuum connection. The

vacuum connection also features a lip which fits over the top edge of the resistance and test blocks, to enhance the air-tight seal. The vacuum connection would be utilized during several phases of the testing process. During the blood run, the part would mate to the resistance block to actuate the blood flow, and safely collect the used blood. Next, during the tube buffer wash, the vacuum connection is mated to the top of the test block array to actuate the flow of buffer, and safely discard all the fluid. Finally, during the assaying phase, the component will remain connected to the test block array to suck the cell lysing solution into the channels and then to expel the solution into their respective wells in a 384-well plate.

3.2.5 COMPLETE APPARATUS

The complete testing apparatus (Figure 23) was built around the test and resistance blocks to facilitate the loading of blood, the buffer washing process, and the assaying of the biological signal held within the test tubes. The vertical layout of the apparatus takes advantage of gravitational effect on the fluids used in the system, such as the gravitational pressure head in a column of fluid, and the auto-leveling of a fluidic surface, that are extremely helpful in the controlled loading of fluid into the device. The machine's layout also allows for quick and easy transitions between phases of the testing process by simply sliding one component out of the system, and sliding another one in its place. The problems associated with proper alignment of components is

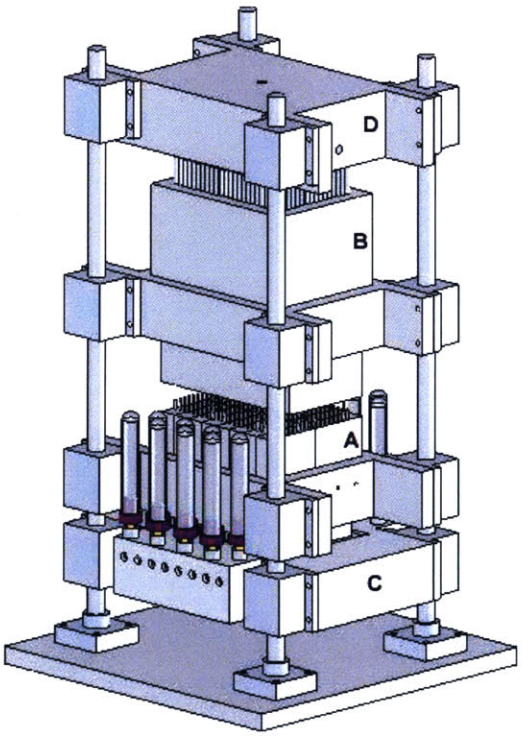

Figure 23: Picture of the complete apparatus containing the array of 16 test blocks (A), resistance block(B), blood loader (C), and the vacuum connection (D) as well as all mounting components.

solved with the use of four 0.5" precision hardened guide rails paired with precision linear ball bearings on all the components.

The test blocks and resistance block are each mounted on a set of precision linear ball bearings by means of a mounting sleeve mated with the structural step designed into the rubber body of the test and resistance blocks. During the blood run phase of testing, components A, B, C, and D are all mated (Figure 23). In addition, the top of the vacuum connection is attached to an electronic pressure regulator to provide the necessary pressure head to actuate the flow. The sides of the vacuum connection are attached to two syringe pumps, one of which infuses the vacuum cavity with buffer to wash out the blood, the other pump collects the pooled blood over the period of the run in a syringe for easy disposal. The next test phase, the buffer wash, involves removal of component B from the system, the disconnection of components A and C, and the connection of component A to D. An open top container full of a Tyrodes buffer with added MgCl (10 mMol) and HEPES (0.75 mMol) is placed under component A, and the vacuum pressure is applied once again to allow for buffer to run through the channels at a specified shear rate for a specified time period. The final test phase involves placing a 384-well plate in its designated spot on component C, filling its wells with a lysing solution, and bringing down components A and D to mate with the plate. A particular negative vacuum pressure will then be applied such that the lysing solution may rise to the tops of the channels without spilling over, and the fluid is incubated for a prescribed amount of time. Finally, the fluid is expelled from the channels back into their respective wells, and the solution is assayed colorimetrically.

3.2.6 SCALED DOWN FLOW MODEL

After designing the high-throughput flow model, it was decided that validation of a variety of the mechanics, designs, and processes would be necessary before manufacturing the full-scale 384-channel flow model (Figure 24, Figure 25, Appendix B). To perform the validation testing a 24-channel system was developed

by scaling down many of the components of the 384-channel system. A single test block with up to 24 channels would be tested with the help of a scaled-down resistance block, and reduced size versions of the vacuum connection and blood loader components.

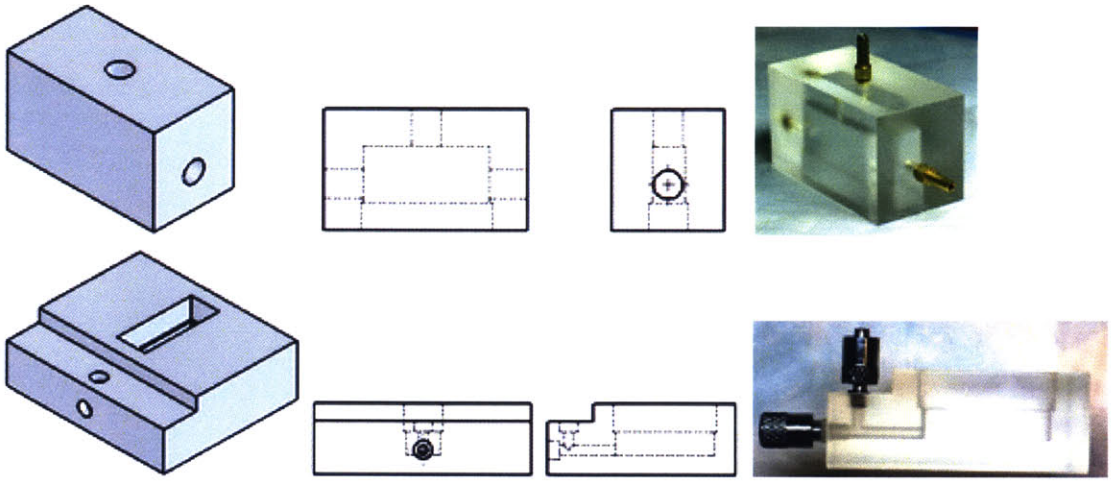

Figure 24: (Left) Schematic views of the vacuum connection (top) and the blood loader (bottom) for the 24-channel, single test block flow model. (Right) Photographs of the manufactured components. Note the extra views from different angles showing hidden lines to the right of the three-dimensional part views.

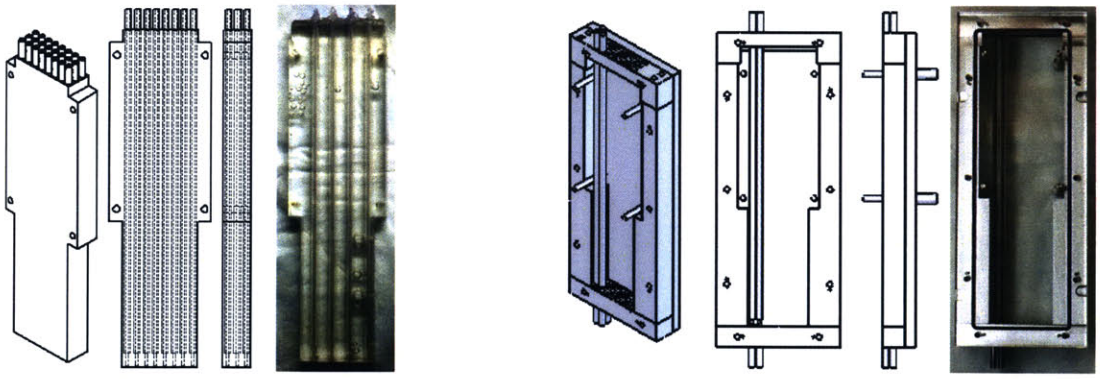

Figure 25: (Left) Schematic of the individual resistance block which is mated to a single test block with up to 24 flow channels. Three views from different angles are shown, the front and side view show the hidden lines. (Right) The mold used to create the individual resistance block. Three views from different angles are shown.

The reduced vacuum connection features an interior lip to form a tight seal around the top of both the individual test block and the individual resistance block.

The vacuum connection also contains a port to connect to a regulated wall vacuum source, as well as a pair of side ports that connect to syringe pumps to help remove blood or buffer that pools in the chamber during a test run. The blood loader features dimensions and an internal lip that allows for a secure air-tight seal with the bottom of the test block. A channel that leads up to the blood loading well (as shown in Figure 24) carries blood from a Vacutainer® reservoir, through a needle, to the glass channels. The individual resistance block is the test mule for a new way of casting the test and resistance blocks. Instead of casting the fragile glass tubes directly into the rubber, an extremely time-consuming process for even a skilled operator, PTFE tubes are cast into the rubber. Once the block is removed from the mold, the glass tubes are passed into the PTFE tubes, and secured in place with a small amount of epoxy. In addition, the resistance block features a conical entrance into the tubes from the bottom end of the block, which facilitates the mating of the test and resistance blocks.

A mounting system was designed for these components, and a vertical organization similar to that of the full-scale system was developed (Figure 26).

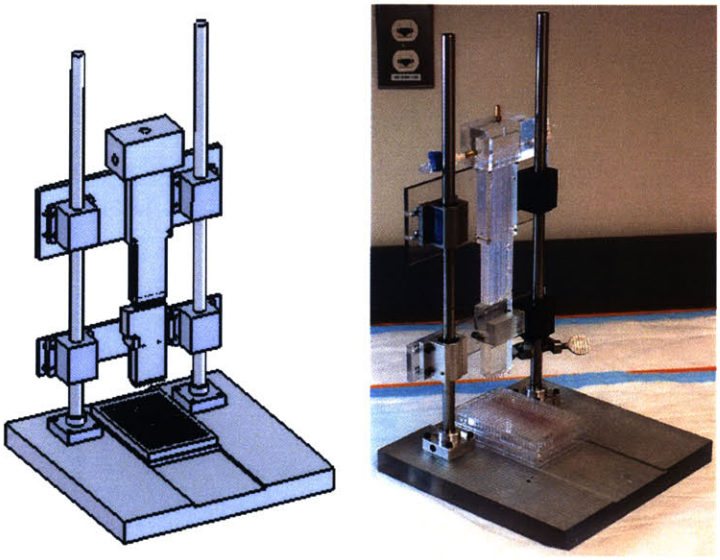

Figure 26: (Left) Schematic of the 24-channel, single test block testing setup. Note that a 384-well plate is below the test block, although the blood loader may also be placed below the test block. (Right) Photograph of manufactured test setup.

Validation testing upon this 24-channel setup should provide several advantages over immediately proceeding to the full-scale 384-channel testing. First, the high cost of manufacturing prototype equipment suggests that all potential design issues should be discovered and solved with the use of smaller scale equipment which maintains most or all of the problems and drawbacks of the full-scale system. Second, a close focus over individual components and even the features of individual components will improve our ability to track down the sources of problems to fix them more effectively. Finally, initial blood testing on this system will allow us to calibrate the thrombotic fingerprint signal to provide the most important portion of the data by scaling our investigational resolution around the parametric regions that provide the most interesting data. The next chapter will describe the theory, design, and procedural validation testing performed on the 24-channel setup in greater detail.

The system described allows a steady Poiseuille flow to be produced in the flow channels. The manner in which the flow is actuated is atraumatic, allowing for delicate processes like such as thrombosis to be studied in a low noise setting, even at high shear rates. The system minimizes the entire fluid contact surface between the sample blood reservoir and the used blood collection area. Also, the flow model design helps to streamline the testing process while maintaining hygienic conditions and ensuring user safety, to support the high-throughput nature of the study driven by the model. By readily allowing changes in flow shear rates, wall conditions, and blood pro/anti-thrombotic conditions, the system allows for the thorough, multi-parametric investigation of the biological and hemodynamic processes of thrombosis.

While the current embodiment has stood a great deal of validation testing (as will be explained in the next chapter) before finalizing the design to perform clinical testing, a number of potential system extensions and modifications have been

brought to light, and may be instituted in the future. These potential extensions of the system's applicability include the addition of pulsatile flow actuation, as well as mechanization and automation of many of the tests processes. Each of these modifications would require reconsidering the current embodiment's design, and would most likely be undertaken only after the current embodiment has reached the level of reliable clinical testing.

CHAPTER 4: FLOW SYSTEM CHARACTERIZATION TESTING – INITIAL VALIDATION OF HIGH-THROUGHPUT LINEAR FLOW MODEL

4.1 BIOLOGICAL CHARACTERIZATION

Following theoretical component design, we performed an initial assessment of the model's ability to study vascular thrombosis. The first testing was performed on a 12-channel model which investigated simple parametric variation along Virchow's Triad and the resulting thrombotic signal. Next, validation of the use of capillary tubes to acquire a strong and repeatable biological signal was performed.

4.1.1 COLLAGEN COATING CAPILLARY TUBES

As explained in Chapter 3, each channel of the flow model contains a test section that captures the thrombotic signal, and the resistance section, which modulates the shear rate experienced in each test section. The coating of the test section, which constitutes the reactive segment of the channel, fulfills the wall conditions axis of Virchow's Triad. The subendothelium is composed of a number of cell components, as well as structural and enzymatic proteins, which all play an essential role in maintaining vessel health and repair processes like thrombosis. Coating of the test section with one of more of these reactive species simulates blood flow past the exposed subendothelium after a vascular injury has occurred. Some of the proposed coatings for the test section include collagen, fibrinogen, von Willebrand Factor, tissue factor, or any combination of these components. Since the resistance tubes are to remain unreactive with the blood, they will be coated with albumin. The quality and strength of the signal derived from the testing sections is

directly related to the homogeneity and manner in which these components coat the inner surface of the capillary tubes.

The test tubes are coated by drawing up the proteins in solution into the tubes. Here, the solution is incubated inside the tube for a period of time, to allow for the protein to bind to the glass surface due to a difference in electric charge. Once the surface is completely coated with a homogenous layer of protein, the solution is removed from the tube, and the tube is washed with a PBS buffer for 5 minutes at 1000 s^{-1} shear rate to remove any loosely bound protein or debris. Before finalizing this process, it was necessary to determine that our incubation time would allow the protein solution to complete the coating process, whether the resulting coat was a homogenous single layer of protein, and whether the post incubation wash damaged the layer in any way. Also, the ability to remove protein from the test tube surface needed to be investigated as future design iterations would involve the reuse of a number of components, especially the test blocks.

4.1.2 VALIDATION OF THE COLLAGEN COATING PROCESS

4.1.2.1 QUALITATIVE VALIDATION OF COLLAGEN COATING HOMOGENEITY

The first step in validating the collagen coating process investigated the amount of incubation time necessary to lay a homogenous layer of collagen on the interior of the test tubes. To determine this, a bovine Achilles tendon collagen II solution was drawn up into test tubes and incubated for either 2, 4, or 20 hours, and then washed out with PBS at 1000 s^{-1} for 5 minutes. The tubes were then immuno-labeled with a α-bovine collagen II primary antibody and a rabbit α-goat FITC secondary, and imaged with fluorescence microscopy at several points down its length (Figure 27).

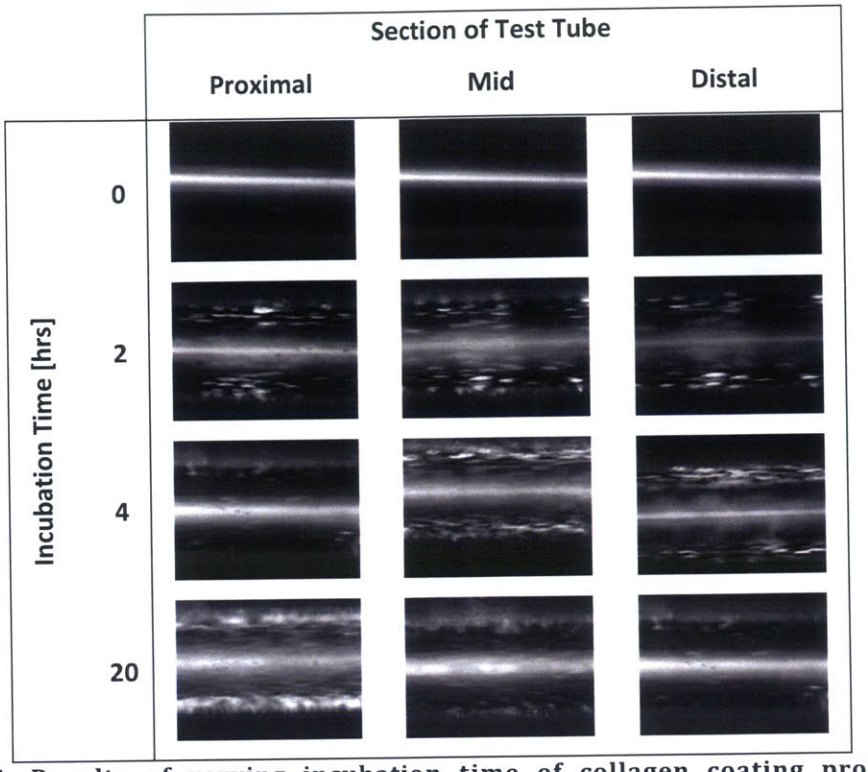

Figure 27: Results of varying incubation time of collagen coating process. 10x magnification. 0 hours of incubation indicates the negative control which is a blank tube with no collagen coating.

The results of varying the collagen solution incubation time qualitatively indicate that a homogenous coat of collagen is laid down the length of the tube. An increase in collagen content, or the thickness of the collagen layer is noted as the incubation time increases, especially after 20 hours. This effect was likely caused by drying out the solution over the period of incubation. This drying would cause excessive deposition and layering of the collagen inside the tube, providing a thick protein layer that may block the lumen of the tube. Therefore, the test would have to be run again without allowing the solution in the tubes to dry out.

The test was repeated with precautions taken to avoid evaporation of the solution. Two potential solutions were explored: plugging up the tube ends, and submerging the tubes. Half of the tubes had their open end plugged up with a putty after drawing up the collagen solution. Plugging up the end with putty prevented the escape of the collagen solution from the tube lumen during incubation. The other

half of the tubes were completely submerged in the collagen solution inside a beaker, which would ensure that there would always be solution inside the tube and that it would not dry out. The incubation times, wash process, and immuno-labeling and imaging were repeated (Figure 28).

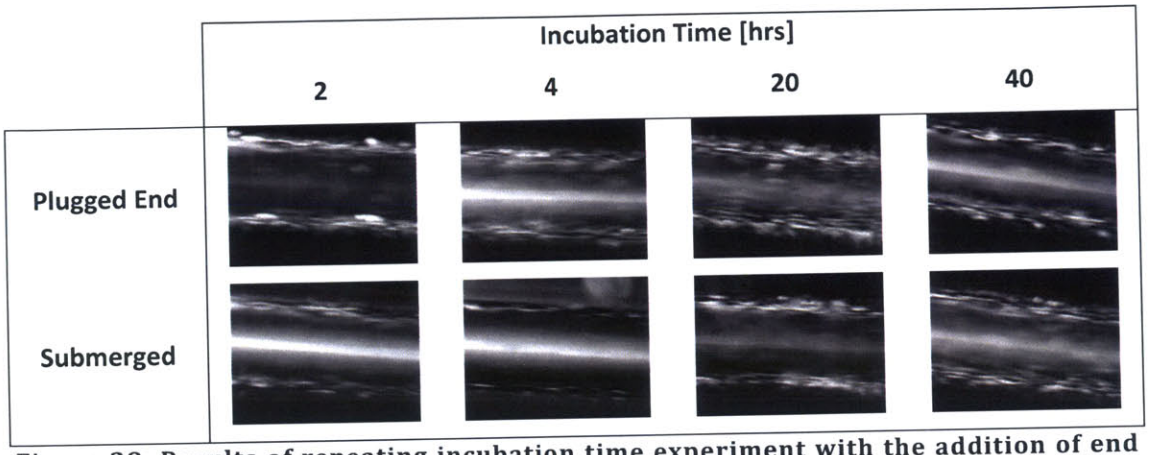

Figure 28: Results of repeating incubation time experiment with the addition of end plugging and tube submerging to avoid solution evaporation.

The results of this new incubation time test reveal that solution evaporation was indeed the reason for the thick collagen layers after long incubation times. At 2 hours and beyond the collagen layers are qualitatively equal in density. It was also found that the tubes with their ends plugged up with putty resulted in much more homogenous distributions of collagen coating compared to the tubes that were submerged in collagen solution. This may be due to air bubbles becoming entrapped in the tubes after submerging. This test qualitatively revealed that the collagen coating process is saturated by 2 hours of incubation time. To ensure that increasing the incubation did not result in a thickened collagen layer, a quantitative test would be required.

4.1.2.2 QUANTITATIVE VALIDATION OF COLLAGEN COATING HOMOGENEITY

The final test in ensuring that a saturation point was reached during the collagen incubation process was a quantitative measure of the amount of collagen coating the tube. A procedure involving the picro-Sirius red staining of the collagen

coat, followed by a colorimetric assay was adopted [56]. For the test, test tube segments were coated with collagen by drawing in the collagen solution, then plugging up the end and incubating for 2, 10, or 24 hours. The tubes were washed with PBS, then the collagen was fixed, incubated with picro-Sirius red dye, hydrolyzed with NaOH, and expelled into the wells of a 384-well plate. The wells were read by a spectrophotometer at a wavelength setting of 650 nm, (Figure 29).

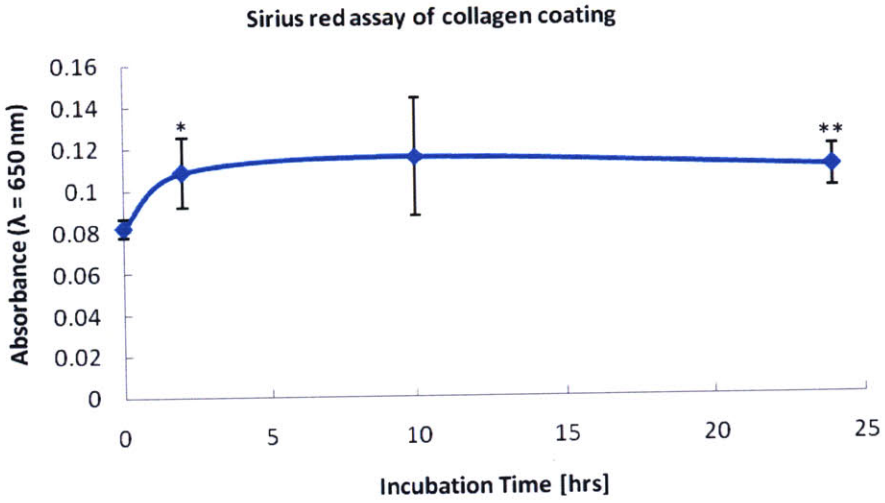

Figure 29: Results of the absorbance measurements of Sirius red staining of the collagen content of tubes incubated for different amounts of time (n=3). 0 incubation time represents the negative control which is tubes that were not coated with collagen. (* = p<0.1 and ** = p<0.05, with respect to negative control data.)

The results of this test show that the 2 hour incubated test samples provided a 25% increase in absorbance. On the other hand, after 2 hours of incubation, little to no difference is noted in the absorbance, and therefore, the amount of collagen contained in the tubes. In addition, the standard error in the data for each incubation time group is on the same order as the standard error for the negative control group, further indicating little variation from the collagen coating saturation point. Therefore, two hours of incubation with collagen solution will suffice to reach a collagen coat saturation point.

4.1.2.3 VERIFICATION OF CELL ADHESION TO COLLAGEN COAT & TUBE CLEANING

After determining that the test tube collagen coat was homogenous, it was necessary to verify the nature of cell binding to the collagen. The main questions to be answered involved whether the binding of blood components to the collagen was homogenous and determining whether the buffer flush step was too aggressive and would wash away portions of the thrombotic signal bound to the tube. In addition, it was important to determine whether blood components and collagen may be removed by a cleaning process so that tubes may be reused in the future.

Freshly drawn and untreated blood was run through collagen coated tubes for 2 minutes at a 1000 s^{-1} shear rate to allow for the buildup of thrombotic burden. The tubes were then flushed with Tyrodes buffer in the normal manner, a lysing solution was applied, and an α-actin FITC immuno-label was applied to the tube lumens. The tubes were then imaged through fluorescence microscopy. The actin contained in the cells bound to the collagen would tag the cell remnants left bound to the collagen in the tube, and provide a good indication of the density of cells bound to the tube wall. The results of actin immuno-labeling compared against a negative control are shown in Figure 30.

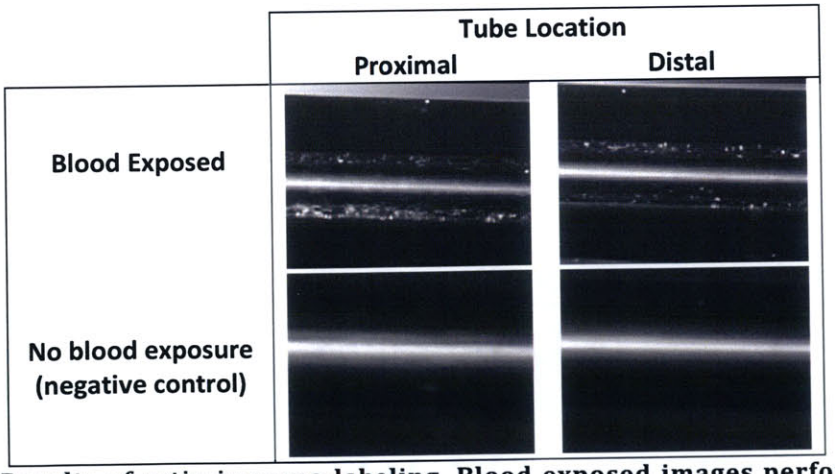

Figure 30: Results of actin immuno-labeling. Blood exposed images performed at 5x magnification, no blood exposure images performed at 10x magnification.

The results show a qualitatively homogenous distribution of immuno-labeled actin across the length of the test tube. In addition, since the application of the antibody was performed after the Tyrodes buffer wash was performed, the images also show that the bound cell components were resilient against the stress placed on them from the wash.

To further investigate the strength of the bound blood components, we considered the effect of cleaning the tubes with a variety of harsh conditions. The goal of these tests is to potentially allow for the reuse of the test block components of the flow model. As testing with this system continues to evolve, the need for test blocks (costly in both manual labor time and materials) will only grow unless a method of reusing the blocks is developed. Cleaning strategies that are capable of removing bound cell components as well as cleaving and/or hydrolyzing the collagen coating were investigated.

A variety of aggressive cleaning agents, such as collagenase, urea, and HCl, were first employed to remove the collagen coating. This test utilized tubes coated with collagen incubated for 2 hours. After the normal buffer wash procedure, collagenase (1mg/mL solution), 2M urea, or 6.5M HCl solution was drawn up into the tubes and incubated at 37°C for 60 minutes. The cleaning agent was then removed and the tubes were washed out with a 2% Sodium Dodecyl Sulfate (SDS) solution followed by deionized water at 1000 s^{-1} for 5 minutes. The tubes were then immuno-labeled with α-goat collagen II antibody and a FITC α-mouse secondary and imaged with a fluorescence microscope (Figure 31).

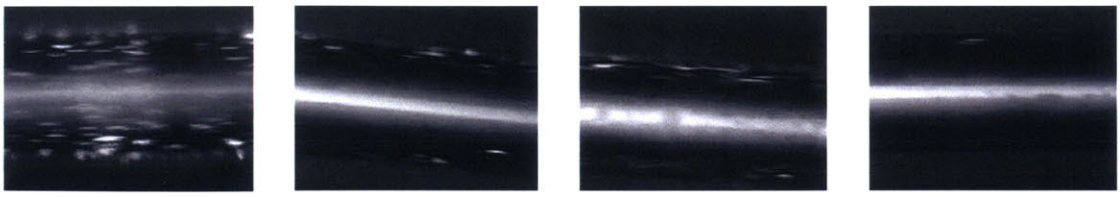

Figure 31: Results of collagen removal testing. Images were taken at 10x magnification. Each of the tubes were coated with collagen for 2 hours. Collagenase, urea, and HCl were then drawn into the tubes and incubated for 60 minutes followed by an 2% SDS and DI-H_2O wash. Qualitative results show that HCL provided the most effective collagen removal.

The results of the collagen removal testing indicate that incubation of 6.5M HCL in the tube provided better cleaning results than incubation with collagenase or urea. The results with HCL were not perfect, and the results are also not capable of determining whether the incubation with HCL actually caused the collagen to deform, as opposed to simply hydrolyzing and hindering the antibody's ability to bind to the protein, giving us a false negative result. To further investigate this cleaning process newly collagen coated tubes were exposed to blood and the HCL incubation process was repeated.

In this follow-up test, collagen coated tubes exposed to a 1000 s^{-1} blood flow for 2 minutes were immuno-labeled with an α-actin FITC antibody, and incubated with 6.5M HCl, followed up by a wash with 2% SDS, then a wash with an aggressive cleaning buffer formulated to remove cell components and hydrolyze bound collagen (100mM tris base, 3% SDS, 2% Triton-X, 2M NaCl, 6M Guanidine HCl). Finally, the tubes were immuno-labeled once more. The image results pre and post the second labeling are shown in Figure 32.

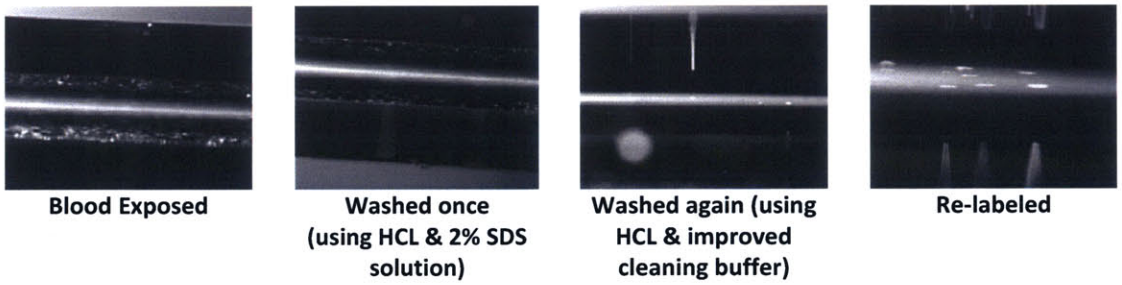

Figure 32: Results of repeating HCl incubation cleaning and staining for actin bound to collagen coat. Images were all taken at 5x magnification, except for "Re-labeled" image which was taken at 10x magnification.

The results of the HCl cleaning of tubes indicate that the 6.5M solution of HCl removes a large part of the bound cell components, but use of the improved cleaning buffer provides much more encouraging results than washing solely with the 2% SDS solution. Re-labeling the bound actin may have brought out slightly more

previously unmarked actin strands, but the actin content of the tube is significantly less than that of the blood exposed tubes.

This testing will have to be developed further to ensure substantial removal of all cellular debris and collagen such that it will not interfere with the reapplication of collagen and the reuse of the tubes in the flow model. Perhaps slight modification of the HCl incubation or buffer washing procedures will provide the desired results. The only way to finalize the efficacy of the washing process will be through repeated blood testing on the 384- or 24-channel flow model, to monitor for the possibility of cell remnants disturbing the results of subsequent tests. Final validation of the tube cleaning process will greatly increase the cost effectiveness of the device by decreasing many of the variable costs of testing such as the manual labor and the materials used to manufacture the test blocks.

4.1.3 12 CHANNEL FLOW MODEL

The preliminary biological characterization of the flow model of thrombosis was performed on a bench top prototype of the multichannel system (Figure 33). The system featured 6 to 12 individual flow channels of identical inner diameter to those used in the 384-channel and 24-channel concepts. The flow through the channels was actuated by means of a syringe pump properly set to achieve the desired flow rate in all the channels, connected in a parallel fashion.

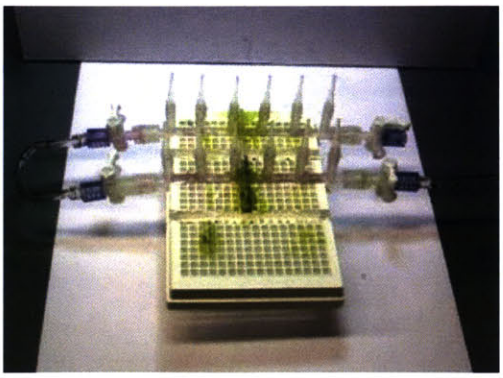

Figure 33: Initial 6 to 12 channel flow system powered by syringe pump.

This set up is capable of testing a single shear rate at a time, through a set of 6 to 12 glass tubes of equal dimensions, each with interior wall coating as prescribed. The blood supplied to the system came from a single source; therefore a single blood treatment condition could be tested at a time. An important limitation to note about this machine was its use of volumetric flow rate control as opposed to pressure control. Therefore, an assumption is made that the current through each branch of the circuit will remain the same during the test. In reality, the flow in each branch of a current controlled system is highly subject to changes in the currents in every other flow branch. So if any single branch experienced reduced flow rates due to a blockage, all the other branches would experience a commensurate increase in blood flow given that the blood now has fewer branches through which to travel. As a result, during the testing process, it was vital to note if any tubes became blocked off, so that they may be cleared or so the resulting shear rate in all of the other tubes could be calculated.

This model would allow for a number of preliminary tests to validate the efficacy of the assay system in combination with the test tubes used in the final 384-channel flow model. Primarily, this model would test with tubes identical to those of the final model, utilizing flow shear rates and blood run times similar to those intended for the full-scale machine, and the identical test process would be used on this system. The testing goals comprised resolving differences in thrombotic outcomes between test subjects, differing shear rates, blood treatments, and ensuring sufficient precision between tests with identical input parameters.

4.1.3.1 METHODS AND RESULTS

DETERMINING MINIMUM SAMPLE SIZE

The first biological validation system testing involved determining the minimum sample size necessary to provide reliable results through precision. In addition, we investigated the effect of varying blood condition. Two test samples from the same blood draw, one treated with 1.5μL/mL PPACK (an anti-platelet

drug), the other treated with 8.0µL/mL PPACK were run through the tubes for 2 minutes at a shear rate of 1000 s^{-1}. The tubes were then washed with Tyrodes buffer for 5 minutes at a shear rate of 1000 s^{-1}, and assayed for thrombosis products (Figure 34).

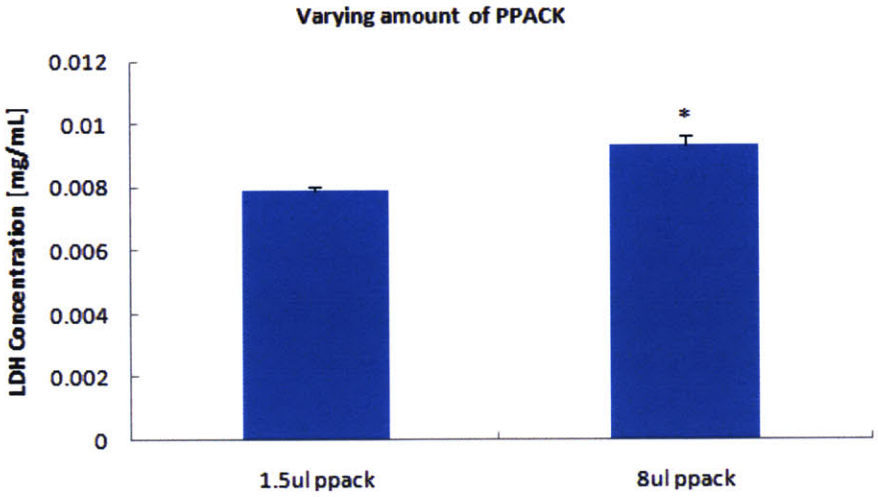

Figure 34: Results of varying PPACK levels show increased thrombotic activity at higher blood PPACK levels (n=3). The purpose of the test was to determine minimum number of test repeats necessary to ensure reliable results. An n = 3 proved to have low error. (*= $p<0.05$, with respect to 1.5µL PPACK data.)

The results of this test provided unexpected results in that the blood sample with a greater amount of PPACK provided a higher signal than the sample with less drug added. The results were speculated to have been due to the relatively greater role of platelet activity (as opposed to coagulation) in thrombogenesis at higher shear rates. The 1.5µL and 8.0µL PPACK tests both had n = 3, and resulted in a standard error of 1.3% and 2.9%, respectively. Although unexpected, the results of this test indicate that using 3 repeats of each condition would be sufficient to provide reliable results during validation testing.

EFFECT OF RUN DURATION ON SIGNAL

The next test re-examined the anti-coagulant blood treatment, while varying the blood run duration. A single blood draw was split into two groups and treated in

the same manner as the previous test (1.5µL or 8.0µL PPACK). In addition, the 2 blood treatment groups were further split into two groups: the first where the blood was run through the tubes for 1 minute, while the other group allowed blood to run for 2 minutes. All blood samples were run at a 1000 s^{-1} shear rate through collagen coated tubes, washed for 5 minutes at 1000s^{-1}, and assayed normally (Figure 35).

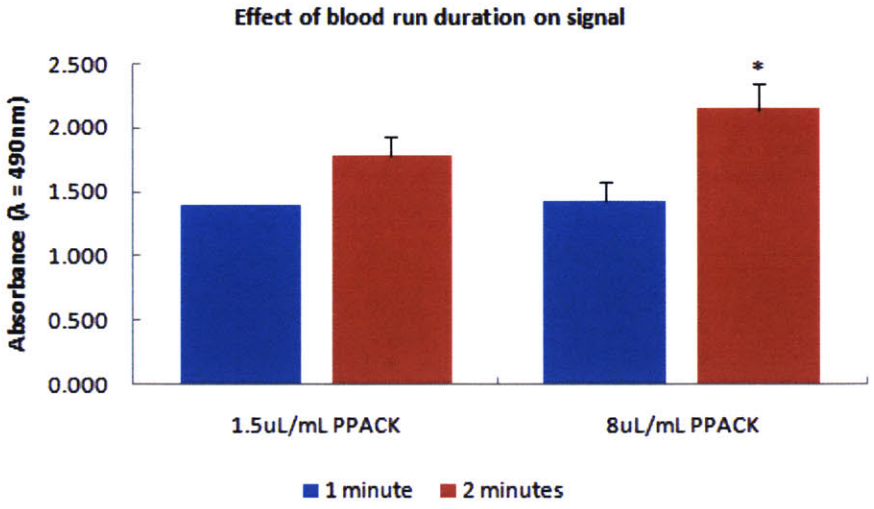

Figure 35: Results of varying test run duration (n=1 for 1 minute, 1.5µL PPACK data; n=4 for all other data groups). Longer run times provided higher signals in the 2 minute data, as expected. Unexpectedly, increased levels of PPACK in the blood increased the thrombotic activity in the 2 minute run data. (*= p<0.05, with respect to 2 minute, 1.5µL PPACK data.)

Once again, the results showed higher levels of thrombotic activity in the 8µL/mL PPACK exposed samples, but only in the 2 minute run data. Unfortunately a test problem provided an n=1 for the 1 minute, 1.5 µL/mL PPACK data group. On the other hand, the results of varying the test run duration indicate, as expected, that a longer run time produced a greater amount of thrombotic burden in the tubes. Doubling the run time in the 1.5µL and 8.0µL PPACK groups provided a 27% and 50% increase in thrombotic signal, respectively. The results of this test indicate the strong dependence between run time and signal, which will prove useful in order to calibrate the thrombotic fingerprint to best resolve detail.

EFFECT OF SHEAR RATE ON SIGNAL

The flow condition axis of Virchow's Triad was next to be investigated. A single draw of blood was treated with 6μL/mL of PPACK and was run for 2 minutes at $100s^{-1}$ or $1000s^{-1}$ shear rate through collagen coated tubes. The tubes were then washed out with buffer for 5 minutes at $1000s^{-1}$ and assayed. The same test was run again the next day, using fresh blood from the same volunteer, in order to investigate the variation in results on a day to day basis (Figure 36).

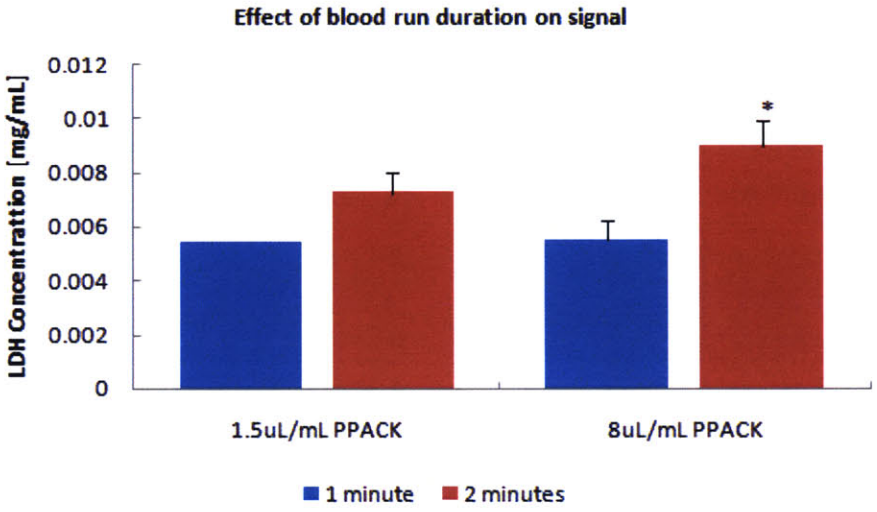

Figure 36: Results of varying blood shear rates and repeating the same test the next day (n=6 for Day 1 data sets, n=4 for Day 2 data sets). (*= $p<0.05$, with respect to Day 1, 100 s^{-1} data; ** = $p<0.05$, with respect to Day 2, 100 s^{-1} data.)

The increase in thrombotic signal came as an expected result of the increased shear rate causing the heightened levels of platelet excitation and activation. This result confirms the relevancy of our process' outcomes by matching the results of shear rate variation that have been acquired from previous models. In addition, the results of the tests show the amount of day to day variation innate to the blood and the thrombotic components and processes within it. The results of this test indicate that legitimate comparisons between test results could only be made from blood samples derived from a single draw and tested concurrently. Therefore, this will have to become the standard of our testing and data acquisition processes. This

further supports the need for the embodiment of our concept to test a large number of samples in parallel without requiring prohibitively large blood samples, to form relevant comparisons and resulting deductions from our data.

EFFECT OF VARYING BOTH SHEAR RATE BLOOD CONDITION ON SIGNAL

Due to the interesting results derived from adding PPACK to blood samples and comparing against untreated samples, more tests were performed to determine the nature of the interaction between the PPACK treatment and the shear rate. The tests involved addition of 8μL/mL of PPACK to a blood sample and comparing against a negative control of untreated blood from the same draw. The samples were tested at 1000 s^{-1} for 2 minutes, and were washed at 1000 s^{-1} for 5 minutes. Another test was performed with blood from the same volunteer, and treated in the same manner except that the flow conditions were set at 50 s^{-1}. The results are shown in Figure 37.

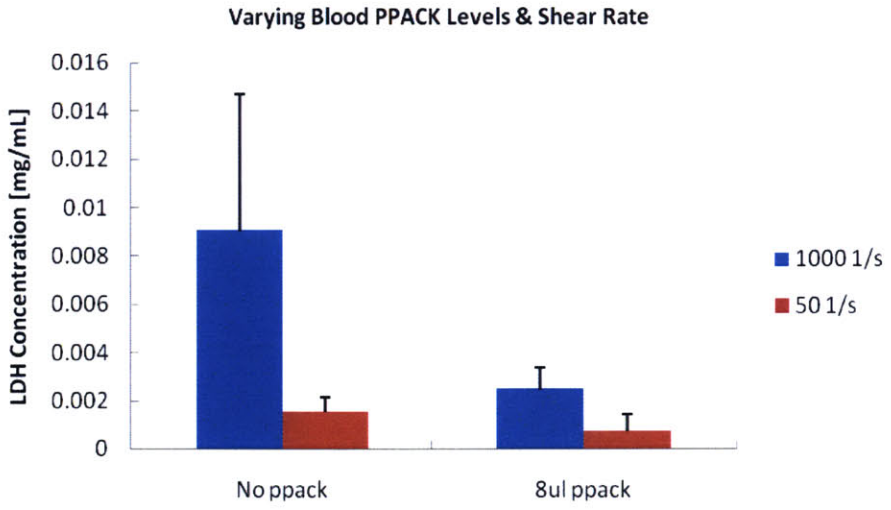

Figure 37: Results of varying blood PPACK content along with shear rate (n=3).

The results of these tests show a reduction in thrombotic signal as the PPACK is added to the blood sample. Therefore, another blood sample, treated in the same manner, was run at 50 s^{-1} to examine the shear dependent effects of the drug on the

blood (Figure 37). Thrombotic activity decreased due to the decrease in shear rate: -75% for the no PPACK group and -52% for the 8μL/mL PPACK group. This result confirms the positive shear dependent result from the previous test. In addition, the PPACK treatment caused a -62% and -28% change in signal for the 1000 s^{-1} and 50 s^{-1} groups, respectively. PPACK seems to have a greater effect in the higher shear rates, which happens to be the realm where platelet activation plays a greater part in thrombosis. In the lower shear realms, the coagulation cascade plays a bigger role in the process; therefore a drug that affects platelet activity will have less effect in these flow conditions.

4.1.3.2 12 CHANNEL TESTING SUMMARY

These preliminary validation tests run on the 12-channel device helped to finalize the run, wash, and assay portions of the test protocol. The conditions run during the tests provided evidence that our flow model and test procedure provided sufficient parametric control and assay resolution over the process of thrombosis in order to continue with the mechanical characterization of the higher-throughput model concepts.

4.2 MECHANICAL CHARACTERIZATION OF THE FLOW SYSTEM

The mechanical characterization of the flow model involved three goals: mathematical determination of the fluid flow and shear rate through an individual channel at a variety of applied vacuum pressures, determination of the effect of the collagen wall coating on flow characteristics, and mechanical characterization of the 24-channel flow model.

4.2.1 VACUUM PRESSURE VS. FLUID SHEAR RATE

4.2.1.1 FLUID THEORY VS. EXPERIMENTAL RESULTS

The first aim sought to establish the mathematical relationship between the vacuum pressure applied to the system and the shear rate experienced in the tubes. Initial tests were performed on a single test tube of dimensions equal to those of the test tubes utilized in the flow model (10 cm length, 0.3 mm ID, 1.27 mm OD). A specific and constant negative vacuum pressure was applied to one end, while the other was open to fluid. The resulting volumetric fluid flow was combined with the pressure differential reading to back calculate the fluid shear rate at the tube wall using the following equation:

$$\left.\frac{\delta V_z}{\delta r}\right|_{r=\frac{D}{2}} = \frac{32 \cdot Q}{\pi D^3} \quad \text{Eq. 12}$$

The test compared water against a 2:3 by volume solution of water and glycerol which replicates the viscosity of blood at the shear rates we intend to test, which is about 3-4 times the viscosity of water. In addition, the results (Figure 38) are compared against the fluid mechanical theoretical data.

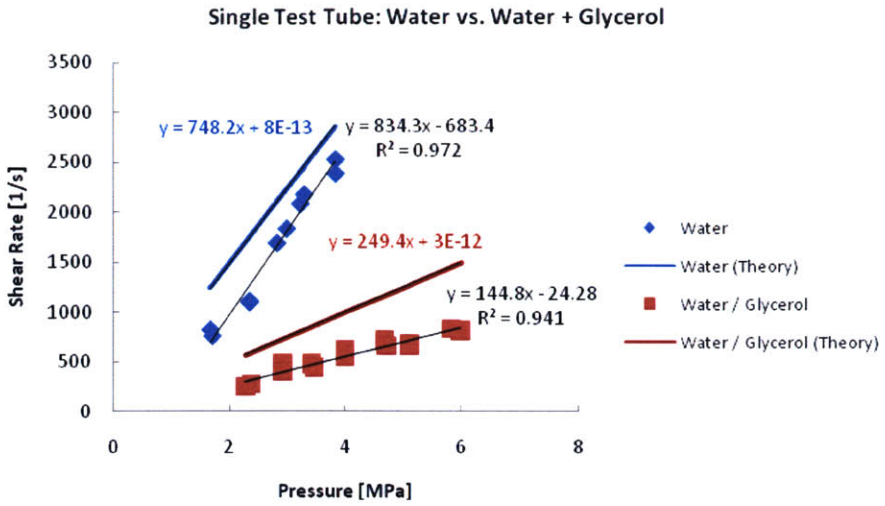

Data Set	Slope [s^{-1}/MPa]	Error from Theory	R^2
Water (Theory)	748.2	-	-
Water	834.3	11.5%	0.972
Water / Glycerol (Theory)	249.4	-	-
Water / Glycerol	144.8	- 41%	0.941

Figure 38: Test results for single test tube flow characterization. The test results for water and the water/glycerol solution are compared against theoretical data for the respective conditions.

The results of this first flow test provided evidence that our experimental calculations of flow resistance (slope of trend line) are off by 11.5% and -41% for the water and water + glycerol theoretical data sets, respectively. It is interesting to note that the water provided less error and provided a higher slope than theory, while the water + glycerol solution provided a slope lower than theory. Fortunately, the strong linear grouping of the data suggests a high level of repeatability and predictability in the flow system. The vertical displacement between the experimental and theoretical data sets is due to systemic pressure losses from imperfect seals, and must simply be compensated for by using the linear regression of the experimental data as opposed to the theoretical formula.

Once the flow characteristics of a single test tube was established, the combination of a single test tube and a resistance tube could be tested. The tests run on the single test tube flow were repeated on combinations of the test tube with

resistance tubes varying in inner diameter. A negative vacuum pressure was applied to one end of the tubing and the other end was exposed to a container with either water (Figure 39) or the 2:3 mixture of glycerol and water (Figure 40). The applied pressure and resulting volumetric flow rate were recorded and used to calculate the shear rate experienced by the inner wall of the test tube.

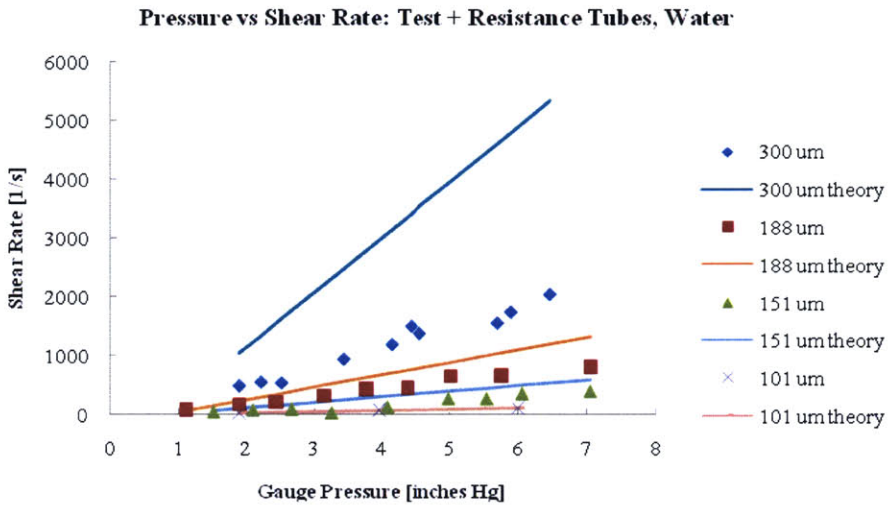

Data Set	Slope [s^{-1}/MPa]	Error from Theory	R^2 (Linear Trend line)
300 µm (theory)	940.6	-	-
300 µm	336.4	64.24%	0.965
188 µm (theory)	211.2	-	-
188 µm	127.6	39.58%	0.982
151 µm (theory)	92.4	-	-
151 µm	69.13	25.18%	0.891
101 µm (theory)	19.04	-	-
101 µm	18.45	3.10%	0.964

Figure 39: Results of pressure vs. shear rate testing with the use of the test and resistance tubing. The theoretical and experimental results for resistance tubing of each ID are shown. (Trend lines for experimental data are not shown for purposes of image clarity.)

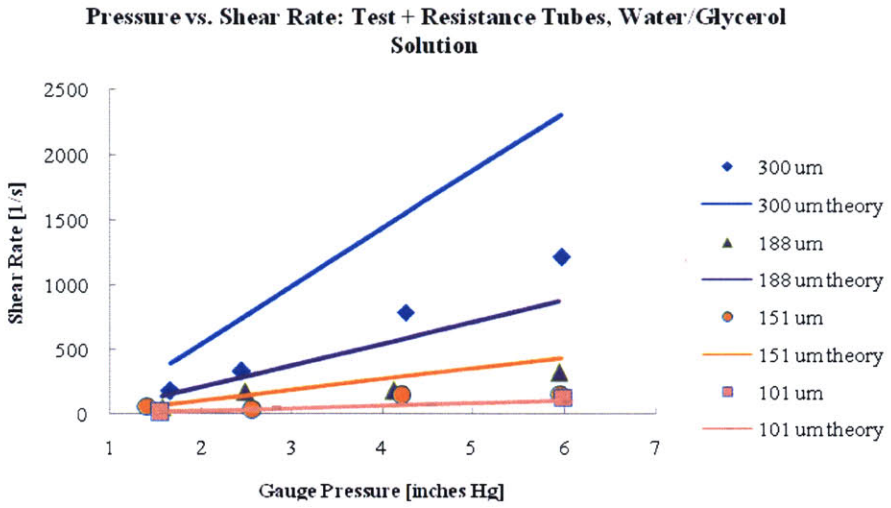

Data Set	Slope [s^{-1}/MPa]	Error from Theory	R^2 (Linear Trend line)
300 µm (theory)	445.5	-	-
300 µm	243.1	45.43%	0.998
188 µm (theory)	169	-	-
188 µm	54.04	68.02%	0.898
151 µm (theory)	83.3	-	-
151 µm	26.72	67.92%	0.723
101 µm (theory)	18.63	-	-
101 µm	26.24	-40.85%	1

Figure 40: Results of pressure vs. shear rate testing with the use of the test and resistance tubing in combination with the 3:2 water/glycerol solution to simulate the viscosity of blood. The theoretical and experimental results for resistance tubing of each ID are shown. (Linear trend lines are not shown for purposes of image clarity.)

The R^2 values of the linear trend lines on flow test results (Figure 39 and Figure 40) indicate a strongly linear correlation between the applied vacuum gauge pressure and the resulting test tube shear rate. The vertical shift between the experimental and theoretical results is due to losses of pressure throughout the flow system, such as imperfect seals between components, which are not accounted for in the mathematics of the theory. The slopes of the theoretical and experimental data encounter a significant amount of error when compared; indicating that the theory does not completely encompass the flow resistances encountered in the flow channels. Potential sources of this resistance calculation error may be the coupling devices used to link together the test and resistance sections of tubing. Fortunately,

the output parameters of this flow system, as observed through the R^2 value, are highly predictable, therefore flow conditions would be easy to control during blood testing. Since the tubes that were tested were bare-walled, and the thickness of the collagen coat was unknown, the effect of the collagen coat on the flow had to be determined.

4.2.1.2 EFFECT OF COLLAGEN COAT ON FLUID FLOW

The next step involved determining whether coating the interior wall of the test tube with a protein such as collagen builds up a layer thick enough to affect the fluid flow. The protocol of the previous single-tube test was repeated with two collagen coated test tubes (Figure 41).

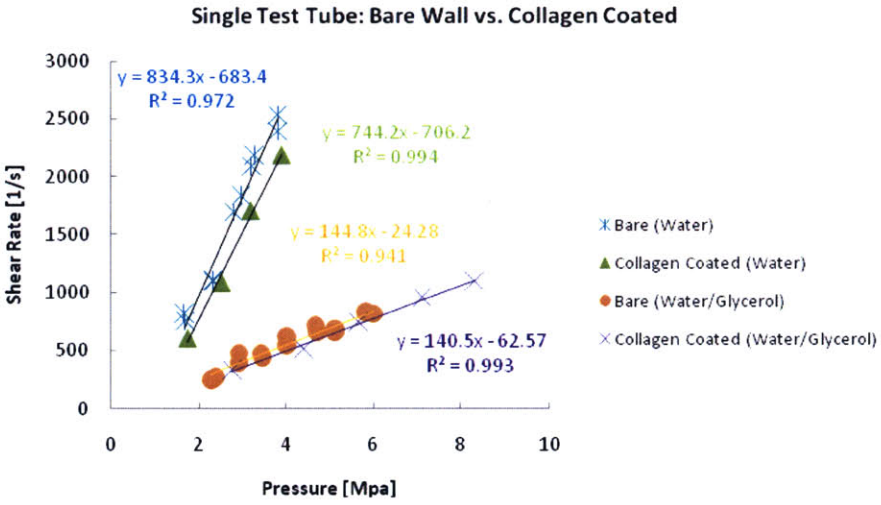

Data Set	Slope [s^{-1}/MPa]	Error from Bare Wall Tube	R^2 (Linear Trend line)
Bare (Water)	834.3	-	0.972
Collagen Coated (Water)	744.2	-10.80%	0.994
Bare (Water / Glycerol)	144.8	-	0.941
Collagen Coated (Water / Glycerol)	140.5	-2.97%	0.993

Figure 41: Results of bare wall vs. collagen coated test tube flow testing.

The results indicate a very small difference in the slopes of the bare-walled vs. collagen-coated data series, reaching a maximum of a -10.8% difference in measured shear rate of water at a 4 MPa pressure. This slope shift in the data should prove to have little effect on the results of blood tests, as is evident in the water/glycerol results, where there is only a -2% difference in slopes. Therefore, collagen coating the tubes does not provide a large difference in the inner diameter of the test tubes, and the flow effects remain negligible. The high R^2 values indicate a strongly linear data set, and therefore output flow parameters are highly predictable.

4.2.2 24 CHANNEL FLOW CHARACTERIZATION

The final flow characterization test was performed on the 24-channel flow setup without the resistance block attachment. A block with 24 bare walled tubes was compared against a block with 24 collagen coated tubes. The volumetric flow rate of both water (Figure 42) and the water/glycerol solution (Figure 43) was measured while maintaining a constant pressure head.

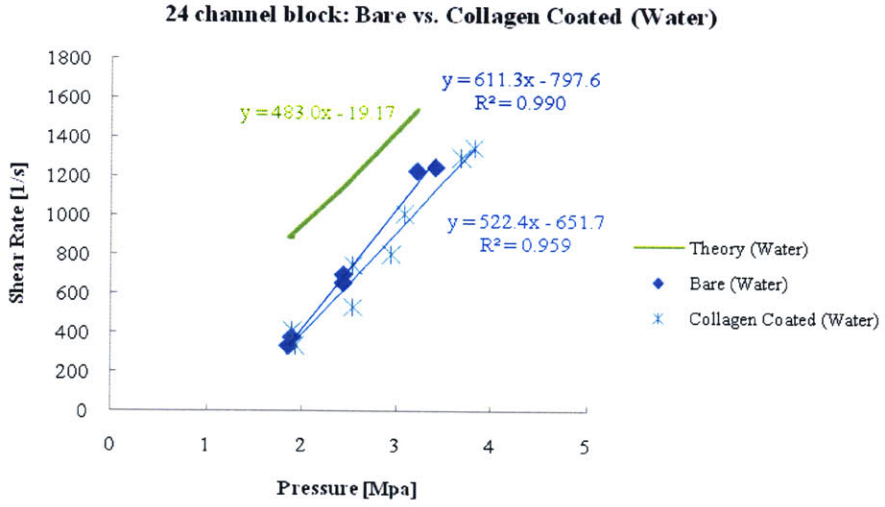

Figure 42: Results of flow testing on the 24-channel block running water through bare-walled and collagen-coated wall tubing.

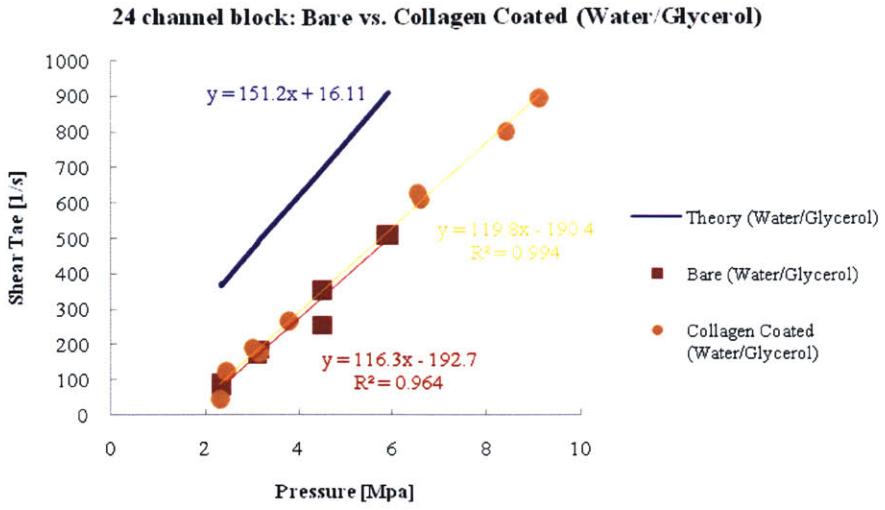

Data Set	Slope [s^{-1}/MPa]	Error from Theory	R^2 (Linear Trend line)
Theory (Water)	483	-	-
Bare (Water)	611.3	26.56%	0.99
Collagen Coated (Water)	522.3	8.14%	0.959
Theory (Water / Glycerol)	151.2	-	-
Bare (Water / Glycerol)	116.3	-23.08%	0.994
Collagen Coated (Water / Glycerol)	119.8	3.01%	0.964

Figure 43: Results of flow testing on the 24-channel block running the water/glycerol solution through bare-walled and collagen-coated tubing.

The 24-channel flow test results indicate a very predictable flow system based on the very tight linear data trends as observed by the R^2 values. Little difference is noted between the results for the bare-walled and collagen-coated tubes. Specifically, the error from theory in the slopes of the trend lines of the collagen coated tubes for the water/glycerol results were 8.14% and 3%, respectively, which cause little deviation in results over the range of pressures at which we test. The data suggests that collagen coating actually gives results closer to theory, and furthermore, that the addition of glycerol to the water brought the experimental results even closer to theory. On the other hand, it is also important to note that the vertical shift between the theoretical and experimental data is greater in these tests as compared to the single channel tests. This is due to the increased losses in the system pressure head due to imperfect mating between the test block

and vacuum connection, and between the test block and blood loader components. Finally, the resulting equations from the linear regression:

$$y = 522.4x - 651.7 \quad \text{Eq. 13}$$

$$y = 119.8x - 190.4 \quad \text{Eq. 14}$$

can be used to determine the vacuum setting necessary to achieve the desired flow shear rates through a 24-channel test block.

CHAPTER 5: DEVICE APPLICATION - DEVELOPMENT OF THE THROMBOTIC FINGERPRINT

Once the initial development and conceptual validation of the device was completed, it was possible to move on to the application of the device by means of the 24-channel system, to begin elucidation of the thrombotic fingerprint. The development of the thrombotic fingerprint began with optimization of the testing and assaying procedures to reduce noise and improve repeatability of the results. Next, the 24 channel system was utilized to begin testing for baseline fingerprint characteristics that will form the foundation of fully developed and detailed thrombotic fingerprints. Finally, the plans for future investigations to extend the reach and depth of the thrombotic fingerprint were laid out.

5.1 PROCEDURE OPTIMIZATION

5.1.1 DAY TO DAY VARIATION

The thrombotic propensity of an individual's blood is dependent on the integration of a large number of factors, some of which may vary on a daily, or even shorter, basis. These factors may be environmental, nutritional, or even psychological in nature. Due to this uncertainty, it was determined that preliminary applications of the flow model would require comparisons on results to be performed on a single day's blood samples. In addition, result variation may be simply due to the manner in which the blood was drawn and handled thereafter, necessitating comparisons to be made only between the test results derived from a single sample draw. This precaution would instill a much greater confidence in our preliminary results, as we are trying to form a basic understanding of the

parametric dependence of the thrombotic fingerprint. It is expected that as testing progresses, it will be possible to compare blood samples taken at different times as the thrombotic fingerprint will be better developed and the limits to an individual's variation will be understood.

5.1.2 MACHINE AND PROCESS NOISE

The processing of the test samples encounters a number of variable steps that may add or reduce the noise encountered in the results. These steps include the rate and extent of the Tyrodes buffer washing step, the use of a 5% Triton-X solution as a cell lysing agent, as well as the manner in which the colorimetric assay is applied and measured.

5.1.2.1 BUFFER WASHING

The buffer washing step immediately follows the blood test run, and involves passing a saline buffer through the channels of the flow system at a uniform shear rate. Initial tests utilized PBS as the buffer, but it was soon found that this solution was too harsh on the bound thrombotic products contained in the tube. The solution was then changed to a Tyrodes buffer with added MgCl (0.75 mMol) and HEPES (10 mMol), which helps protect the ionic environment needed by the platelets to remain strongly bound to the channel wall. The thrombotic signal from testing with Tyrodes was a stronger and more consistent thrombotic signal. The other variables involved with the wash step include the flow shear rate and the wash time length. The initial parameters chosen were a buffer wash of 5 minutes at a shear rate of 1000 s^{-1}, derived from the protocol created by Kolandaivelu [18]. After performing the cell debris and collagen removal testing explained in Chapter 4, it was qualitatively determined that the bound thrombotic components were resilient against a wide range of shear rates and wash times. Therefore, we believe that the wash

parameters chosen are sufficient to uniformly remove loosely bound blood components while not upsetting the true thrombotic signal.

Finally, depending on the flow rate, wall, and blood conditions of a test, blood in some channels would completely clot and prevent further flow through it. During the wash phase it would be possible to break off the clot and reopen the channel to a flow. If the clot remained, it would be blown out in a subsequent step, when a high pressure air flow was passed through the channels to remove any remaining fluid to allow for the assaying of the results. Initially, the hope was to remove the loosely bound clot and maintain the components more strongly bound to the channel wall. Results soon showed a great deal of result variation from the clotted channels, indicating that blowing out the clot with buffer or air produced an all or nothing effect on the thrombotic signal. Specifically, the signal would be polarized: it would either be higher than all other channel signals, or the signal strength would be on the same order as the negative control. The conclusion derived from these observations was that channels that became clotted over the period of a test would have to be discounted, as their results did not provide significant insight into the thrombotic fingerprint.

5.1.2.2 CELL LYSING

According to the original protocol by Kolandaivelu [18], from which we based our protocol, a 5% solution of Triton-X was used to lyse the cells bound onto the model's reactive surface, to release LDH into the surrounding medium and perform the assay. As Triton-X is a surfactant, it may permeate cellular membranes and burst the cell, it also has a soapy nature which readily forms bubbles following a process that may agitate and introduce air into the solution. During the lysing step of the assay process, the Triton-X solution is drawn up into the channels from individual wells on a 384-well plate. After a period of incubation (normally 30 minutes), the solution with all contained cellular elements is expelled back into the well. This step proved to be problematic during initial testing, as bubbles would

readily form at the channel tip feeding into the well plate and the expelled solution frequently overflowed from the wells, mixing with the surrounding expelled solution. De-ionized water was proposed as a lysing agent to replace the Triton-X solution. A serial dilution of blood in Tyrodes buffer was performed on a 96-well plate, then the samples were lysed with 5% Triton-X solution or de-ionized water, and an LDH color assay solution was added (Figure 44).

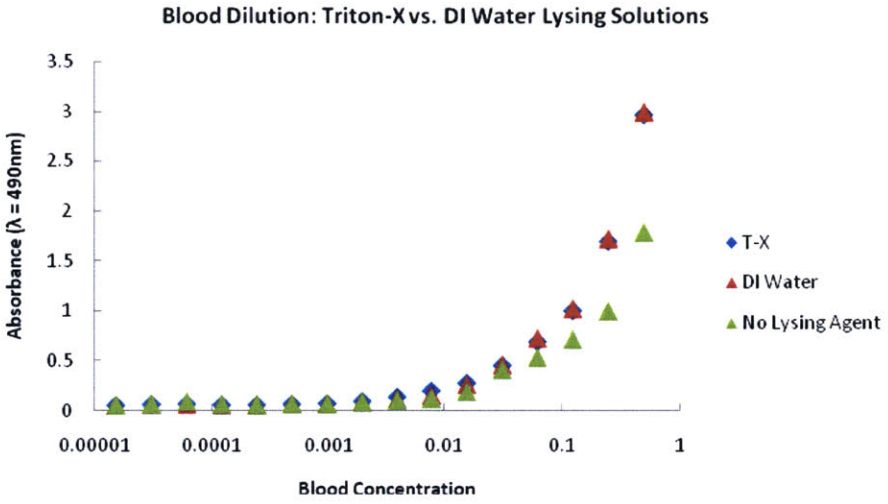

Figure 44: Results of lysing a variety of blood dilutions with a 5% Triton-x solution (T-X) and de-ionized water (DI) plotted in a semi-log manner.

There is little to no difference in the LDH signal from the samples lysed with Triton-X and those lysed with de-ionized water. Both the Triton-X and de-ionized water treated samples provided absorbances higher than the samples with no added lysing agent. A reason for the relatively high values of the samples with no lysing agent is the fact that whole blood was diluted for this test as opposed to solely platelets. The whole blood adds a red color to the solution, even before addition of the LDH substrate, due to the red blood cells and the iron of the hemoglobin. The results indicate that Triton-X and DI water are equally good as lysing agents. The benefit of the de-ionized water is its ability to be drawn into the channels and expelled back into the wells without forming bubbles that may mix with the samples

in other wells. For these reasons, de-ionized water was finally chosen as the lysing agent for the subsequent experiments performed on the 24-channel system.

5.1.2.3 COLORIMETRIC ASSAY

The final step to retrieve the test results involves adding a cytotoxicity assay (LDH substrate) solution to the samples. The assay changes the color of the sample to different intensities of the color red, which is then analyzed for light absorbance at 490 nm wavelength in a spectrophotometer. Optimization of this step involved three aims: determining the effect of dye on the absorbance reading, determining the effect of LDH substrate incubation time on the results, and correlating sample absorbance readings to measurements of LDH content in a sample.

Performing the lysing step during assay proved to be a challenge due to the clarity of the lysing solution in the thin tubes making the process very difficult to visualize. To ease the difficulty of this step, India Ink was added to the lysing solution (de-ionized water) to improve the visibility of the solution when drawing it up into the channels. During this step it is very important to ensure that none of the lysing solution overfills the channels and flows out through the top, as this would cause you to lose some of the signal contained in the solution of that channel. The increased visibility of the fluid allowed the user to maintain the lysing solution drawn up at a safe level. Since the India Ink is of a purple/blue color, it was hypothesized that it would have little effect on the spectrophotometer reading, since it was performed at the 490 nm wavelength absorbance setting, specific to the red color generated by the LDH substrate. To test the effect of the ink, a serial dilution of blood in Tyrodes buffer was lysed with either dyed or un-dyed lysing solution, and then the LDH substrate was added. In addition to the effect of dye, the test also investigated the effect of LDH substrate incubation time on the strength of the absorbance signal (Figure 45).

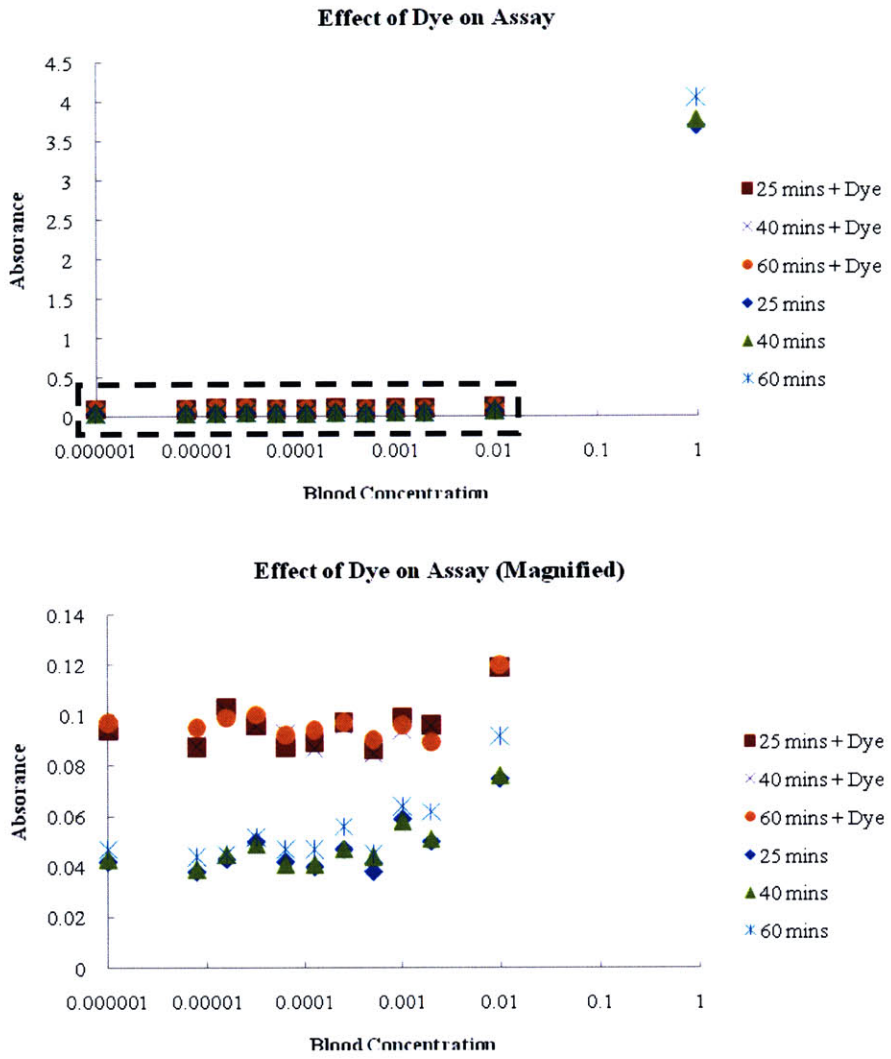

Figure 45: Plotted results of effect of dye on serial dilution of blood. Samples had no dye added to them unless stated. (Top) All results plotted. (Bottom) Magnified view of the data points in the dashed sqaure in the top plot (up to 0.01 concentration of blood).

The vertical shift in absorbance due to the dye added to the lysing solution is not simply constant, but rather, decreases as the blood concentration increases. This result indicated that the ink was not pure enough in color to use for this test and either another ink that wouldn't interfere with the absorbance reading would have to be used, or the lysing solution would have to remain clear and more care would have to be taken when drawing up the solution. A substitute ink has not yet been

employed, so more care has been taken to draw up the fluid, which has proven to work satisfactorily.

In addition, the plot also indicates very little difference in the results of incubating the samples with the LDH substrate for a variety of time. This allows for a more loose control over the time spent in this step, although it is always favorable to keep a record of the incubation time, and to try to keep it constant across all tests. Finally, the dilution experiment indicated that we were only beginning to enter the sensitive region of the LDH substrate, as the majority of our results remained on a relatively flat region (about 0.1 absorbance reading), while the 100% blood sample provided a much higher signal (about 4.0 absorbance reading). The sensitive region of the assay should fall between these two points, as should the results of our blood testing; therefore a dilution of LDH with greater resolution would be needed.

In order to covert the absorbance result into a measurement of the LDH content of a sample, an LDH calibration curve was created by performing a serial dilution of LDH in Tyrodes buffer, adding the LDH substrate, and reading the 490 nm wavelength absorbance result on a spectrophotometer (Figure 46).

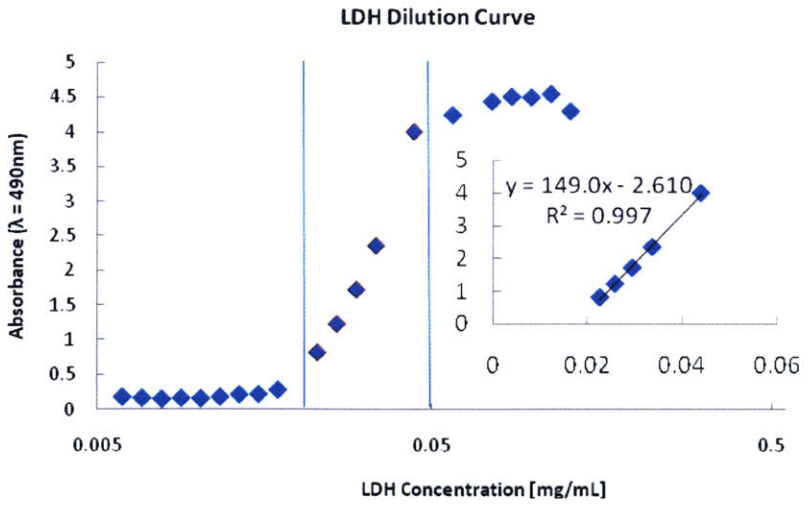

Figure 46: LDH standard calibration curve plotted on semi-log axes. The area between the two vertical lines depicts the cytotoxicity kit's region of sensitivity. This region is characterized by an absorbance reading that is linearly proportional to the LDH concentration of a sample. The inset plot shows the linear regression and equation used to convert between absorbance readings and LDH concentrations.

Note that these results were read on a different spectrophotometer than the one used to acquire the results shown in Figure 45. Therefore the absorbance measurement scales may not match up.

The results of the LDH dilution indicate a region of absorbance linearity between LDH concentrations of 0.2% and 1.0%. Outside of this region, the assay kit cannot be considered linear, and therefore results outside the region of sensitivity cannot be compared to results inside the region.

At this point, preliminary application testing on the 24-channel device could commence testing parametric variation to establish the rough characteristics of the thrombotic fingerprint.

5.2 CHARACTERIZATION OF THE THROMBOTIC FINGERPRINT

The validation testing afforded us the necessary confidence in our system and procedure to enter the early stages of blood testing with the use of the 24-channel device. In a manner very similar to that employed during the initial 12-channel biological validation, a set of preliminary tests for the 24-channel device were devised. The first set of tests performed on the 24-channel system were planned to establish the thrombotic fingerprint foundation, or baseline results, by exploring its inherent precision, signal variation from one test to another, and finally the effect of manipulating the testing parameters on the thrombotic signal.

5.2.1 SYSTEM PRECISION

The first blood tests were performed on a single test block with 12 or 24 collagen-coated channels. Fresh, untreated blood was drawn from a volunteer and run through the channels of the test block at a shear rate of 1000 s^{-1} for 2 minutes. The runs were followed by a Tyrodes buffer wash at 1000s^{-1} for 5 minutes, and assaying of the results. These tests allowed us to investigate the variation inherent to blood, the system, and the pre- and post-blood run process steps. Analysis of this

type allowed the testing process to be tweaked to provide a tighter, more reliable, set of results over time. Once the system variability was brought to a level low enough to ensure clarity of results, baseline blood tests were performed.

5.2.1.1 INTRA-INDIVIDUAL VARIATION

The first goal of the baseline blood tests was to establish the amount of test variation that may be expected from a single volunteer's blood test results from one day to the next. Blood was collected from two individuals each day for two days, run through the flow model at a shear rate of 1000 s^{-1} for 2 minutes, and washed and assayed as normal (Figure 47 and Figure 48).

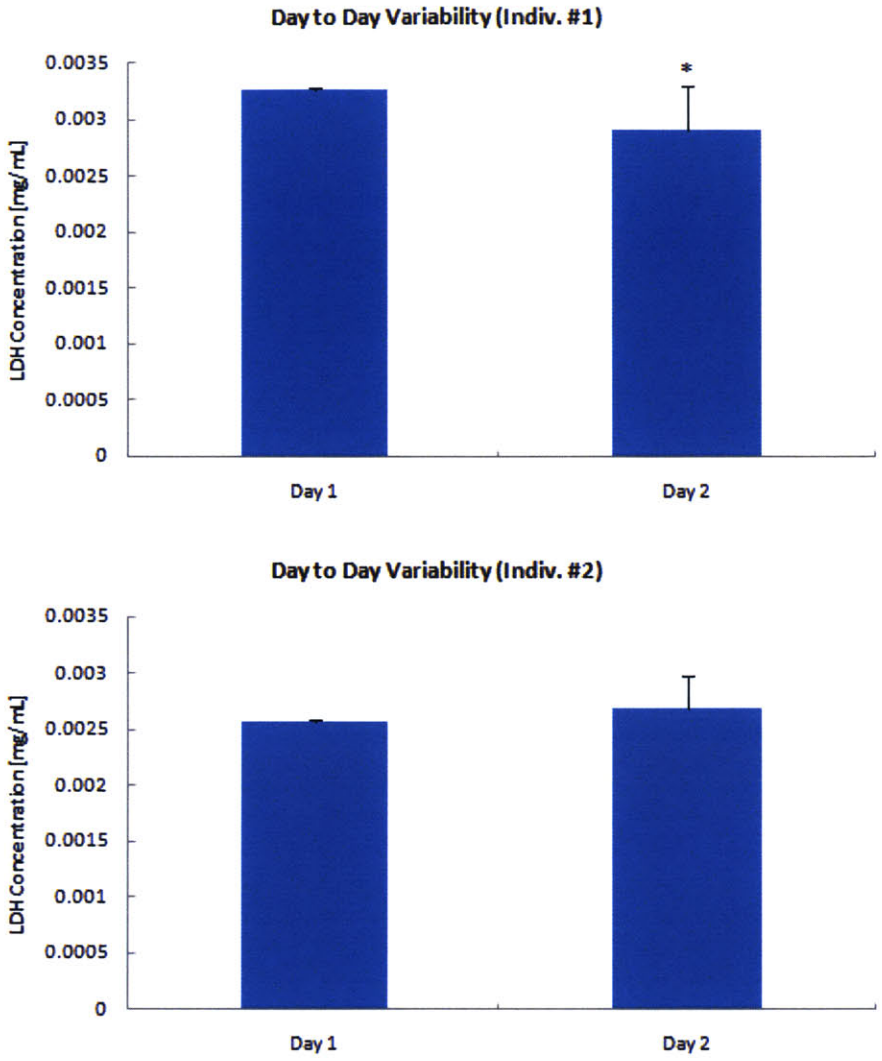

Figure 47: Average absorbance result of the consecutive day testing for the 2 individuals (data for individual 1 has n=9; data for individual 2 has n=14). (*= $p<0.05$, with respect to Individual 1, Day 1 data)

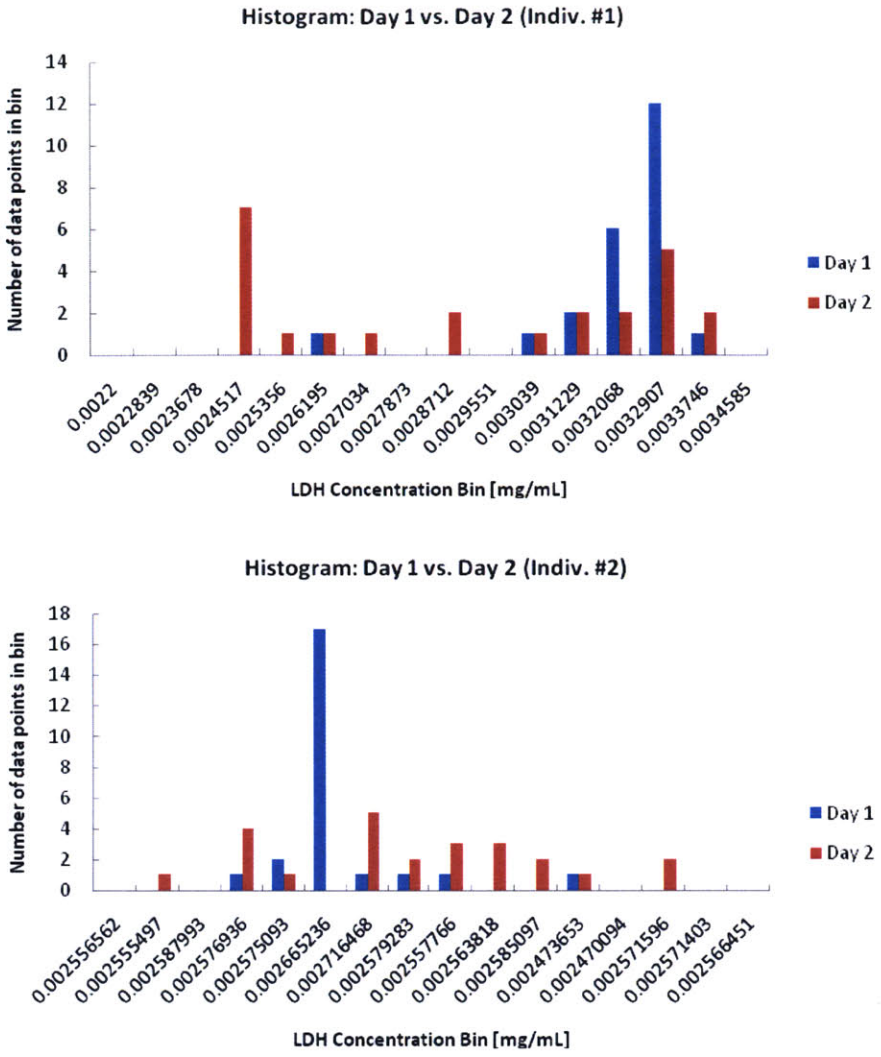

Figure 48: Histograms of the results from the consecutive day blood tests. The x-axes on both histograms are the same so that the horizontal shift of data distributions can be observed between the two individuals (data for individual 1 has n=9; data for individual 2 has n=14).

The results from the consecutive days of blood tests indicate the highly volatile thrombotic nature of blood. Provided that all testing conditions were equivalent, the differing environmental, dietary, physiological, and psychological conditions individuals encounter on a daily basis provided a -33% change in thrombotic activity for individual #1, and a 22% increase for individual #2 after just a single day of delay time between tests. The data spread shown in the histograms (Figure 48) indicate that the two days' data sets cover fairly similar ranges, while

distributing their point density differently in this spread. This result may be explained by one of two reasons. Since the data spread from the second day for both individuals seem to be equally spread out with no significant peaks, a protocol error may have occurred on the tests of this day, injecting a great deal of variability in the day's data. On the other hand, this data may provide evidence that the day to day variation is occurring within a larger envelope of physiologic limits specific to the individual.

5.2.1.2 INTER- INDIVIDUAL VARIATION

The consecutive day tests on the two individuals also provided data which roughly showed the extent to which the current system can resolve between the blood characteristics of two different individuals. A histogram showing the difference in results between individuals #1 and #2 (Figure 49).

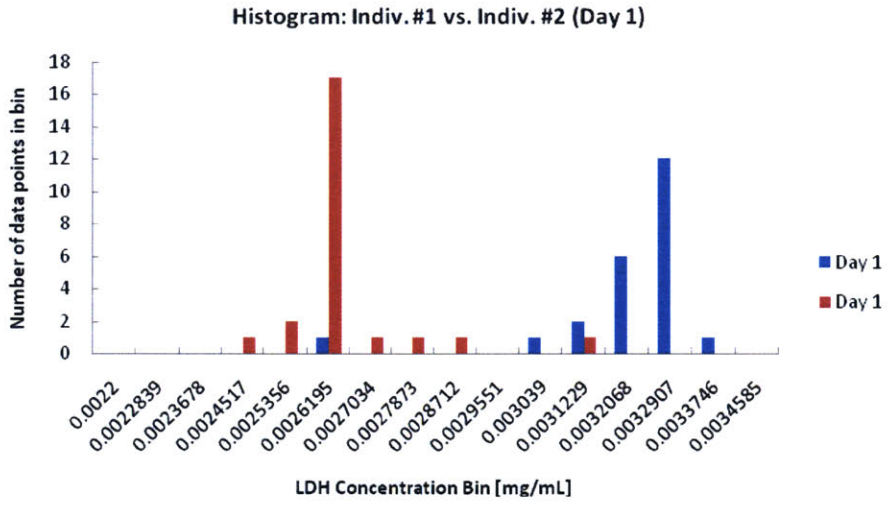

Figure 49: Histogram of the day 1 blood test results of individuals #1 and #2.

The cross-individual results show a clear separation between the two individuals' results distributions. As expected, each individual maintains a personal fingerprint of their thrombotic capabilities, therefore the results (Figure 49) were

encouraging in that our model was capable of clearly discerning basic differences between individuals. The next steps would involve manipulation of a single variable at a time to further influence the results and compare the outcome to some of the well understood principles of platelet activity.

5.2.2 SINGLE PARAMETER VARIATION

Once an understanding of the natural distribution of the thrombotic signal as well as the level of inter-test variability was established, the primary foundation of the fingerprint could be continued to be laid through parametric manipulation. By varying a single parameter at a time, we could acquire a general understanding of our system's ability to illustrate the better understood concepts of the biology of thrombosis.

5.2.2.1 FLOW CONDITION MODULATION: SHEAR RATE EFFECTS ON THROMBOTIC SIGNAL

The first test featuring parametric manipulation involved comparing the effects of low shear flow conditions to those resulting from relatively high flow conditions. Untreated fresh blood from a single draw was aliquoted into two groups and used during two consecutive flow tests. The two tests were run through collagen coated tubes for 2 minutes at either a shear rate of 500 s^{-1} or 3200 s^{-1}. The tests were followed by a normal wash procedure (Tyrodes buffer + MgCl + HEPES for 5 minutes at 1000 s^{-1}) and assayed (Figure 50).

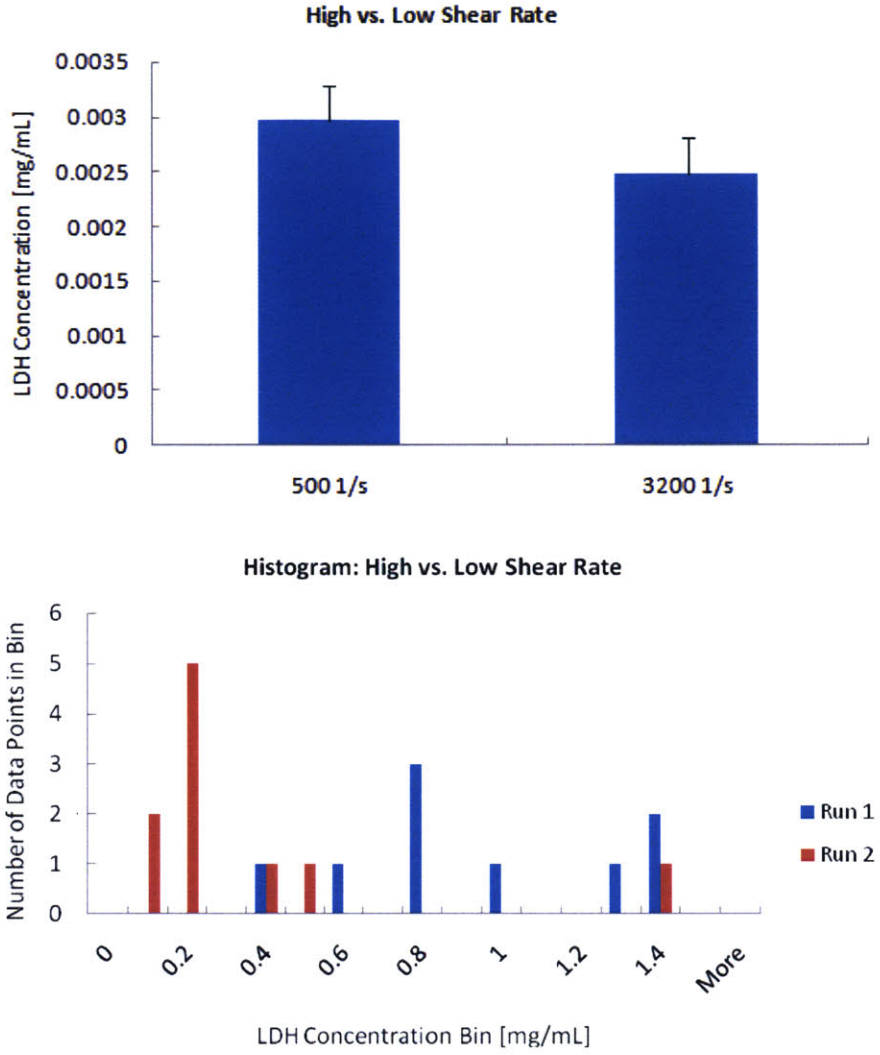

Figure 50: Results of high vs. low shear rate testing. (Top) Average absorbance measurement of data set compared against blank wells with no blood content. (Bottom) Histogram of results to show the distribution of the data (the 500 s^{-1} data has n = 8, and the 3200 s^{-1} data has n = 7).

The results of the high vs. low shear rate testing provided an unexpected outcome in that the 500 s^{-1} shear rate actually provided a stronger thrombotic signal than the 3200 s^{-1} shear rate group, even though the opposite result was expected. The tight grouping of data for each flow condition, the clear group separation shown in the histogram, combined with the number of samples for each test instills confidence in these results as opposed to writing them off as random fluctuations due to experimental noise. Note the extremely low signal of the 3200 s^{-1} test results,

due to experimental noise. Note the extremely low signal of the 3200 s^{-1} test results, which approaches the level of the negative control blanks that contain no products of thrombosis. This brought us to postulate our first hypothesis about this phenomena, which was that at this elevated shear rate, the thrombogenesis occurring on the collagen coated walls of the tubing was simply not robust enough to withstand the hydrodynamic forces of the high-shear-rate blood flow. Therefore, much of the thrombotic burden may not have built up on itself, but rather was washed away by the stream.

The second hypothesis put forth questioned the effect of the low shear rate on thrombosis. At low shear rates, the coagulation cascade comprises the majority of the blood's thrombotic effort as can be seen in deep vein thrombosis cases. On the other hand, at high shear rates platelet activity takes over the clotting process. The tests run at 500 s^{-1} may have emulated low flow, even stasis conditions, which may have more strongly supported the coagulation reactions than the 3200 s^{-1} condition may have supported platelet activity and binding. To study the low shear conditions, the blood condition parameter had to be manipulated and tested.

5.2.2.2 BLOOD CONDITION MODULATION: EFFECT OF ANTICOAGULANT ON THROMBOTIC SIGNAL

To investigate the hypothesis that the low-shear conditions brought about the high signal due to high coagulation activity, the use of anticoagulant was proposed. Treating a blood sample with an anticoagulant drug such as Heparin will inhibit the coagulation cascade which is prevalent at low shear rates and during stasis conditions. The resulting thrombotic signal will then mostly, if not completely, be a result of the binding of activated platelets. Blood from a single draw from the same volunteer that provided the sample for the high vs. low shear rate testing, was broken into two groups. One group was treated with Heparin while the other remained untreated. The two blood samples were then concurrently run though test

block with collagen coated tubes at a 500 s^{-1} shear rate, followed by the normal wash and assay steps (Figure 51).

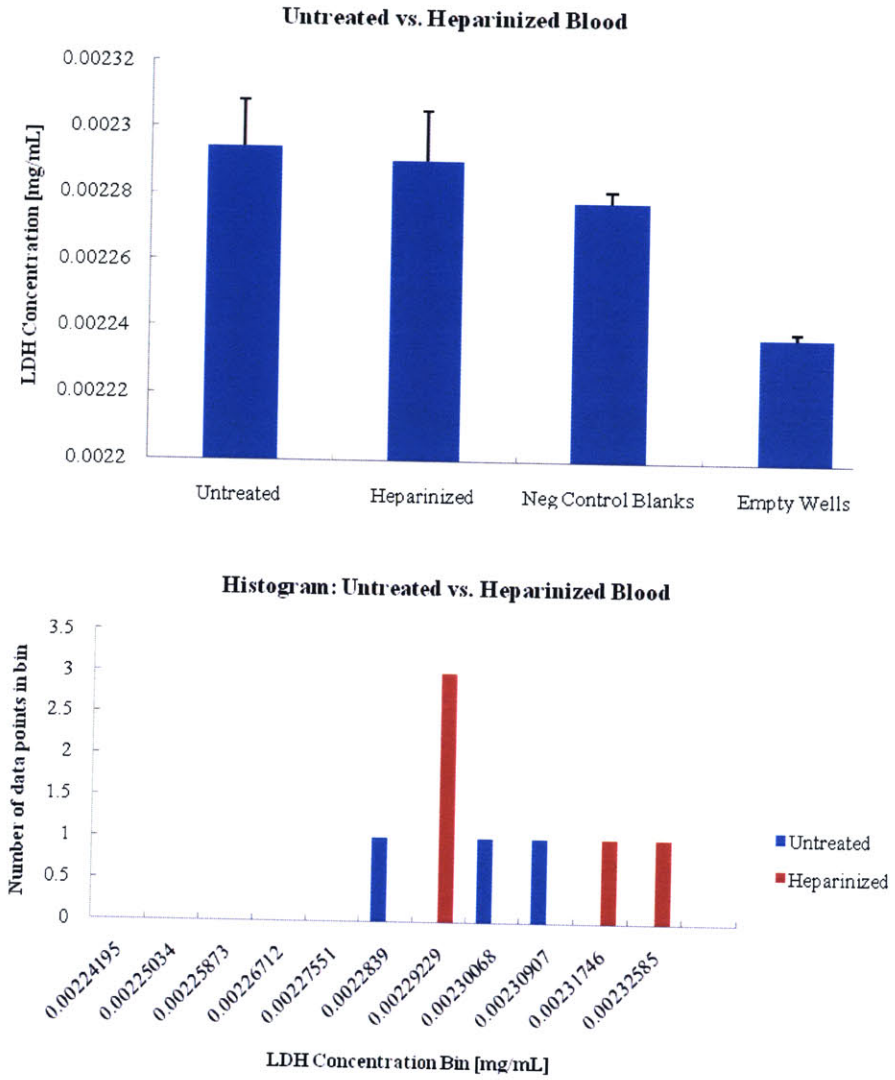

Figure 51: Results of untreated vs. heparinized blood testing. (Top) Average absorbance readings from the untreated and heparinized groups. Results are also compared against samples negative control blanks, which contain no blood content, as well as empty wells, which contain no fluid. (Bottom) A histogram of the results to show the distribution of results (untreated results have n = 3, and heparinized results have n = 5).

The results shown in Figure 51 indicate a very small signal difference between the untreated and anticoagulated test groups, which are still higher than

the negative control signal. The histogram reveals that the majority of the heparinized signal resides among the untreated blood signal, essentially proving no difference in thrombotic signal strength. These results led to two possible conclusions: either the majority of thrombotic activity occurring at a 500 s^{-1} shear rate is due to the activation and binding of platelets and not the coagulation cascade, or some error in the test procedure caused a major loss of the signal. Due to the extremely large difference between the untreated blood signals at 500 s^{-1} from the high vs. low shear and untreated vs. treated blood tests (0.977 vs. 0.11), the result is most likely due to a preparation error with the tube collagen coating step. Therefore, the test will have to be repeated to provide more conclusive results.

The application of the flow model to the scenarios presented in the previous section represents the very first observations obtained from parametric variation of the thrombotic signal. The large amount of validation testing and resulting design modification on the device has eventually brought us to a point where precision optimization now allows us to place confidence in the blood test results. During this period we are shifting from device development to device application, therefore experimentation to characterize the thrombotic fingerprint is ongoing, and is subject to an investigatory plan laid out in the following chapter. The upcoming steps of the project will involve the parallel goals of characterization and optimization of the thrombotic signal, as well as system optimization to reduce costs and increase efficiency. These steps will help in reaching towards the future goal of high-volume testing to build a library of thrombotic fingerprint information.

CHAPTER 6: FUTURE DIRECTIONS

The immediate future of this device involves a focus shift from device development to that of device application. The conceptual framework for the creation of an individualized thrombotic fingerprint as well as a prototype of a device capable of generating this thrombotic fingerprint, have been established. The new goal is to now establish the collective set of run conditions that will define the thrombotic fingerprint and to eventually experimentally validate this model. Three milestones will have to be met to reach this new goal: manufacture of the high-throughput system for application testing, optimization of the thrombotic fingerprint, and establishing libraries of the thrombotic fingerprints.

6.1 MANUFACTURING HIGH-THROUGHPUT SYSTEMS FOR APPLICATION TESTING

The application testing phase of this project has begun, and it has become evident that first round testing may be performed on the 24-channel device, but effective application testing of the device will eventually require a large number of blood runs to be performed. This future direction necessitates the shift from the 24-channel device to the full-sized 384-channel flow model. As explained in Chapter 3, this device will incorporate a maximum of 16 test blocks with their associated resistance block, as well as the supporting hardware such as the full-sized vacuum connection and blood loader components. Specifically, the components necessary for four stand-alone full-sized systems are planned for manufacture, as well as more than 100 test blocks. This number of components will allow for streamline testing as devices are set up, tested, and cleaned. Following full-scale model completion, systemic troubleshooting will follow immediately with the understanding that many

of the design problems have been revealed and resolved with the use of the 24-channel device.

A secondary aim during the process of high-throughput model manufacture is a further enhancement of component manufacturability and process automation, while minimizing the operator effort during machine use. As the project moves forward, an ever-increasing number of test blocks will be needed, which raises concerns regarding the fixed versus variable costs items, as well as the cost of labor to manufacture all the test blocks. Attention will be paid to the man hours involved in the test block and resistance block mold setup, as well as the variable expense costs of items such as the glass capillary tubes used in the test blocks, which may become a limiting factor during testing. This variable cost will be tended to through the limited-reuse of glass channels (after establishing a satisfactory cleansing and sterilization formula), and through comparison shopping of the glass tubes such that they may be bought in bulk, at wholesale pricing. In addition, new design modification strategies to end the model's dependence on the glass tubing, are being taken into account. One strategy currently being explored is to cast flow channels directly into the silicone rubber of the test blocks, rather than use the implanted glass tubing. This modification could significantly improve ease of set up and cost during large scale production and testing. As a general rule, throughout all these stages of testing, attention will continue to be paid to keeping the machine compatible with future process changes, with the projected goal of full system automation.

6.2 PARAMETER SPACE DEFINITION AND OPTIMIZATION

The definition of the parameter space inspired by Virchow's triad will continue to be explored with use of both the 24-channel and 384-channel flow models. This testing is to be performed with the use of citrated whole blood obtained from the Red Cross and normal volunteers, and replenished with divalent

cations (calcium and magnesium) in order to capture a broad region of thrombotic information. After a sufficient amount of data has been collected, a critical part of development of the thrombotic fingerprint will be determination of a set of run conditions that define an appropriately large, while at the same time, appropriately detailed parameter space. In the field of finite-element analysis, a well-recognized problem is the designation of a geometric mesh that appropriately covers a designated area, some parts of which may undergo large amounts of change in a relatively small area, while other parts may remain relatively stationary. This problem is solved by utilizing a optimal gridwork that has a fine mesh size in regions of rapid change, while a mesh with larger, more widely spaced elements is used in regions of gradual change. The optimization of the thrombotic fingerprint parameter space will be executed in an analogous manner. The 384 run conditions will be tailored in a manner such that the outputted thrombotic fingerprint will cover the desired parametric space, while skewing run condition density to regions of high parameter dependence and interaction.

6.2.1 OPTIMIZING WALL CONDITION

The process of selecting the optimal wall conditions and flow rate will be accomplished by first testing a broad range of both conditions. The test tube walls will be coated with specified compositions of fibrinogen, collagen, cryoprecipitate, and thromboplastin. Fibrinogen and collagen will generate a baseline level of shear dependent wall reactivity, as fibrinogen supports low shear rate platelet/wall interactions, while collagen supports high shear binding in the presence of vWF. Specifically, tests featuring collagen, fibrinogen, and a 1:1 collagen: fibrinogen surface composition will be tested in conjunction with varying surface concentrations of cryoprecipitate and thromboplastin. To establish a wide range of wall reactivity, cryoprecipitate and thromboplastin will be considered in a variety of concentrations both individually and in combination.

6.2.2 OPTIMIZING FLOW RATE

Each of these surfaces will be considered at a low, low/moderate, moderate, and high shear rate (50 s^{-1}, 200 s^{-1}, 1000 s^{-1}, 4000 s^{-1}, respectively) to create dynamic flow interactions yielding a total of 192 wall/flow conditions, which comprises N=4 on two full 384-channel test runs. The data from this testing will be analyzed in a three-dimensional plot of surface thrombus formation as a function of wall surface composition and flow rate. Focus will be placed on regions of high parametric dependence, which are defined by local peaks and troughs in signal intensity. A priori determination of the location of these regions of interest is very difficult, therefore once initial fingerprints are obtained, smaller, more-focused studies will be performed to better characterize these regions using a higher density of local parameter variation, for example, an increased number of flow rates under a certain wall condition. Channel test conditions will then be skewed to better represent these areas of change, while making an effort to minimize the number of run conditions to adequately capture the parametric space.

6.2.3 OPTIMIZING BLOOD STATE

Once the thrombotic fingerprint has been optimized with respect to the wall and flow conditions, the blood state will be modified to further expand the thrombotic parameter space, and encompass the final axis of Virchow's Triad. In addition, the blood state testing will serve to validate the thrombotic fingerprint as a means of detecting thrombotic differences between blood samples. These experiments will initially consider the optimized set of wall and flow conditions that used whole blood samples, against low concentrations of known modifiers of platelet function (ADP, epinephrine) and coagulation (cephalexin, PPACK). To limit the amount of blood pre-activation, these samples will be drawn from healthy volunteers according to approved protocols. These blood conditions that either exhibit new peaks or troughs in surface thrombus formation, or augment the

parameter dependence, will be incorporated into the final fingerprint data set as enriched parameters. Finally, an iterative process will be utilized to determine the optimal use of the 384 conditions of the high-throughput flow model.

6.3 ESTABLISHING A LIBRARY OF THROMBOTIC FINGERPRINTS

Once the thrombotic fingerprint has been properly defined and optimized, the focus of the project will shift towards establishing a limited library of thrombotic fingerprints which can then be compared against standard clinical measures of thrombosis. This period of time will be spent accumulating data, searching for patterns, and generating hypotheses which can later be tested in a prospective manner and correlated with clinical outcomes. Animal subjects will be exposed to environmental stressors such as antithrombotic drugs commonly used in the clinical setting. In particular, a variety of concentrations of aspirin (a ubiquitous platelet inhibitor that decreases thromboxane production and platelet activation), plavix (a platelet inhibitor that inhibits ADP dependent platelet activation and which is commonly used in conjunction with aspirin to manage cardiac disease), and Coumadin (a widely used inhibitor of the coagulation cascade, more specifically, of the extrinsic pathway limb) alone, and in combination.

The thrombotic fingerprints of the animal models will then be collected and compared. The resulting data will serve to compare the effects of these well established medications on the thrombotic activity of the subject's blood. Although these medications have found widespread use in the clinical environment, it remains unclear what the optimal doses and durations of use should be, or if they should be used in conjunction with one another. This is especially relevant in the case of a given individual who, for example, may display drug resistance or be at a particular risk for major bleed. The process of animal model validation of the flow system may prove long and complicated, therefore a tentative animal testing plan

has been developed early and may be modified as the animal model validation stage approaches.

6.3.1 ANIMAL MODEL TESTING PLAN

Animal model testing will serve as the second to last major step in validation of this model, while the last step involves validation of the flow system with the help of healthy and diseased human subjects. During the animal testing phase, we will consider farm swine exposed to a variety of anti-thrombotic agents. Four swine will be maintained and exposed to aspirin, plavix, or coumadin alone or in combination. The fingerprints derived from the animals will be assessed using a 50mL blood sample under each "environmental state," in addition to the baseline control fingerprint which will be obtained from each pig prior to drug administration, as well as one week after completion of the experiment following cessation of all medication. An additional blood sample of 10mL will be drawn for each control and drug state to concurrently assess PT, aPTT, and platelet aggregation to ADP, thrombin, epinephrine, and collagen as standard clinical measures of thrombosis.

6.3.2 EXPOSURE TO A SINGLE ANTI-PLATELET AGENT: ASPIRIN

A single pig will be administered aspirin in a dose escalating, step-wise manner using doses that have previously tested in clinical trials, or are approximately that in widespread clinical use for anti-platelet or anti-inflammatory effect. Each dose will be given daily for one week to allow for the steady state inhibition to be achieved. Immediately prior to initiating the administration of the new dose, 60 mL of blood will be withdrawn, 50 mL of which will be run through the high-throughput flow model, while the remaining 10 mL of blood will be used for standardized thrombotic assessment.

6.3.3 EXPOSURE TO A SINGLE ANTI-COAGULANT AGENT: COUMADIN

A second porcine model will be exposed to coumadin titrated to a goal INR (International Normalized Ratio) of 1 to 4, ranging from a subtherapeutic to a supratherapeutic level for most current clinical applications. Daily INR levels will be monitored to ensure that the coumadin dose helps reach the required INR goal level; the thrombotic fingerprint will then be obtained in parallel to the standardized thrombotic assessment test results.

6.3.4 EXPOSURE TO COMBINED ANTI-COAGULANT AND ANTI-PLATELET AGENTS: ASPIRIN AND COUMADIN

A third pig will be used to probe the interaction between anti-platelet and anti-coagulant conditions, as a means of assessing how inhibition of each limb interacts to alter the thrombotic fingerprint. Four conditions will be considered: each a combination of high a low dose aspirin and coumadin (aspirin 25mg + INR 2 / aspirin 25mg + INR 4 / aspirin 300mg + INR 4 / aspirin 300mg + INR 2). During this process the aspirin will be administered daily for a week, at 25mg doses, along with coumadin, which will be titrated to an INR 2. Once this level is achieved, the thrombotic fingerprint data will be collected. Next, the INR will be titrated up to 4 by increasing the coumadin dose, and fingerprint data will once again be collected. Aspirin will then be increased to 300mg daily while the INR is maintained at 4, after waiting a week, a blood sample will be collected and analyzed. Finally, the coumadin dose will be reduced to allow the INR to fall back to 2, while a daily 300mg aspirin dose is maintained. At this point, the last thrombotic data set may be collected. This chronological organization of the procedure's environmental states will help to minimize the total experiment time.

6.3.5 EXPOSURE TO DUAL ANTI-PLATELET AGENTS: ASPIRIN AND PLAVIX

A fourth and final pig will be exposed to the condition of dual anti-platelet agents and the drugs' interactions will be monitored. The specimen will be given 75mg of aspirin daily for a single week followed by collection of the thrombotic fingerprint. The following week, no medication will be administered, and then once again placed on a daily 75mg dose of plavix for a single week and data will then be collected. The final environmental state will involve administration of a combination of 75mg of aspirin and 75mg of plavix. After a week of exposure to the drug combination, the final thrombotic results will be collected.

6.3.6 COMPILING THE THROMBOTIC FINGERPRINTS

The test plan provided above will allow for each swine to be maintained for no longer than 5-6 weeks. Once the data for each environmental state in each porcine model has been collected, inter-individual similarities and differences in the four study pigs will be determined by comparing against the pre-exposure control fingerprints. Next, the focus will be shifted to characterizing the effect of the altered blood state by delineating similarities in fingerprints obtained from a pig exposed to a given agent (aspirin or coumadin) from a drug concentration independent and dependent point of view. The similarities and differences between the fingerprint patterns of the two anti-platelet agents (aspirin and plavix), as well as the differences between anti-platelet and anti-coagulant exposure (aspirin and coumadin) will be examined.

The thrombosis model will be validated during this phase by verifying that the data output contains information that can be correlated with the output of any single traditional assay, for example, an elevated PT may correlate to characteristic, graded changes in the fingerprint. The test data will be analyzed to show the unique information provided by the model by characterizing the effects of multiple anti-thrombotic agents on the fingerprint, such as in the dual anti-platelet or combined anti-platelet/anti-coagulant therapy cases. Additional degrees of freedom will be investigated, such as additional independent outputs, beyond those offered by the

set of standardized clinical tests. This biologically relevant additional information will provide proof of the enhanced correlative power of our novel assay. Special attention will be paid to unexpected events, such as regions of the thrombotic fingerprint that experience rapid topological change, which may be representative of synergistic effects. An important secondary goal will involve gaining insight on how the fingerprints may be represented in the best and most constructive manner to allow for proper statistical comparison, which will be crucial to the system's projected application in a clinical setting.

6.4 THE PATH TO CLINICAL APPLICATION

Once the thrombotic fingerprint system has been optimized, tested, and correlative methods have been established, the system will be shifted towards clinical applicability as soon as possible. The fingerprint library derived from animal sources will continue to grow, incorporating environmentally and genetically variant fingerprints as part of the scientific foundation. The main goal, though, will be to apply the device to clinically relevant human test populations, such as in studies to characterize the effect of fingerprint distribution in normal and diseased populations. These studies will document the effects of drugs as well as known procoagulant determinants (e.g. factor V Leiden, prothrombin gene mutation, smoking, etc.) in these individuals. The effect of these environmental variations on the thrombotic fingerprint will be explored as well as the interactions between the variations.

The flow model will then have to be validated in a clinical setting, for example, by characterizing levels of aspirin dosage based on achieving a desired fingerprint pattern and following clinical outcomes. Another set of tests may examine select populations at increased risk of thrombosis (e.g. pancreatic cancer) and correlate the resulting fingerprint patterns with clinical outcomes. This information could then be used to carry out prospective clinical trials involving

prophylactic use of antithrombotic agents. One crucial aspect of the concept is that for any given scenario, we hypothesize that there will be a reduced number of run conditions which retain sufficient predictive power. The reduced set of run conditions, once determined for a given scenario, will greatly reduce the assay complexity and sample volumes, thereby greatly facilitating the transfer of the thrombosis model technology to the clinical environment.

6.5 POTENTIAL IMPACT

The availability of this thrombosis model will enable basic science research to more fully understand the complex thrombotic phenomena through investigation of different blood, vessel wall, and flow condition interactions, as well as the interactions of specific thrombotic activators and inhibitors. New patterns of phenotypic expression, such as that induced by subtle polymorphisms (e.g. platelet receptors), will be appreciated, allowing identification of new molecular pathways, as well recognizing the importance of established pathways. Through correlation with the clinical environment, the results will help to guide and focus research directives by delineating bench-top phenomena with high clinical impact from those without. Such a system could be used to drive the process of drug development, functioning as a screen for novel thrombotic modifiers. Therapeutic ratios and document toxicity may be determined prior to extensive clinical testing.

The clinical setting could greatly benefit from this technology: by grading a particular individual's risk, counseling and preventative measures can be focused. When needed, appropriate antithrombotic regimens can be selected and tailored to the individual by determining proper drug titrations and durations of exposure. Safe utilization of devices and implants which often require concurrent use of antithrombotic agents (for example drug eluting coronary stents and plavix, or valve replacement and coumadin), can be promoted. On a more fundamental level, the general strategy forms a paradigm for translating *in vitro* test results to *in vivo*

predictions. At the core of this new paradigm is the ability to blur the demarcation between the areas of research, clinic, and industry, greatly fostering "bench-to-bedside" translational efforts.

REFERENCES

1. Libby, P. and P. Theroux, eds. *Pathophysiology of coronary artery disease.* Circulation. Vol. 111. 2005. 3481-8.
2. Demer, L.L., *Vascular calcification and osteoporosis: inflammatory responses to oxidized lipids.* Int J Epidemiol, 2002. **31**(4): p. 737-41.
3. Clarkson, T.B., et al., *Remodeling of coronary arteries in human and nonhuman primates.* Jama, 1994. **271**(4): p. 289-94.
4. Glagov, S., et al., *Compensatory enlargement of human atherosclerotic coronary arteries.* N Engl J Med, 1987. **316**(22): p. 1371-5.
5. Schoenhagen, P., et al., *Extent and direction of arterial remodeling in stable versus unstable coronary syndromes: an intravascular ultrasound study.* Circulation, 2000. **101**(6): p. 598-603.
6. Bruschke, A.V., et al., *The dynamics of progression of coronary atherosclerosis studied in 168 medically treated patients who underwent coronary arteriography three times.* Am Heart J, 1989. **117**(2): p. 296-305.
7. Yokoya, K., et al., *Process of progression of coronary artery lesions from mild or moderate stenosis to moderate or severe stenosis: A study based on four serial coronary arteriograms per year.* Circulation, 1999. **100**(9): p. 903-9.
8. Beck, W.S., *Hematology.* 5th ed. 1991, Cambridge, Mass.: MIT Press. xvi, 667 p.
9. UpToDate. *Coagulation Cascade.* 2007 [cited; Available from: http://utdol.com/utd/content/image.do?imageKey=hema_pix/coagulat.htm.
10. Zwaal, R.F.A. and H.C. Hemker, *Blood coagulation.* New comprehensive biochemistry ; v. 13. 1986, Amsterdam ; New York
New York, NY, U.S.A.: Elsevier ;
Sole distributors for the U.S.A. and Canada, Elsevier Science Pub. Co. xii, 321 p.
11. Lilly, L.S. and Harvard Medical School., *Pathophysiology of heart disease : a collaborative project of medical students and faculty.* 3rd ed. 2003, Philadelphia: Lippincott Williams & Wilkins. xiii, 445 p.
12. Davies, M.J., *The pathophysiology of acute coronary syndromes.* Heart, 2000. **83**(3): p. 361-6.
13. Vaughan, D.E., *Plasminogen activator inhibitor-1 and the calculus of mortality after myocardial infarction.* Circulation, 2003. **108**(4): p. 376-7.
14. Dickson, B., *Venous thrombosis: on the history of Virchow's triad.* UTMJ, 2004(81): p. 166-171.
15. Lip, G.Y. and A.D. Blann, *Does hypertension confer a prothrombotic state? Virchow's triad revisited.* Circulation, 2000. **101**(3): p. 218-20.
16. Blann, A.D., *How a damaged blood vessel wall contibutes to thrombosis and hypertenasion.* Pathophysiol Haemost Thromb, 2003. **33**(5-6): p. 445-8.
17. Blann, A.D. and G.Y. Lip, *Virchow's triad revisited: the importance of soluble coagulation factors, the endothelium, and platelets.* Thromb Res, 2001. **101**(4): p. 321-7.

18. Kolandaivelu, K. and Harvard University--MIT Division of Health Sciences and Technology., *The development and application of an in vitro model of coronary lesion thrombosis.* 2005. p. 2 v. (205 leaves).
19. Badimon, L., et al., *Platelet thrombus formation on collagen type I. A model of deep vessel injury. Influence of blood rheology, von Willebrand factor, and blood coagulation.* Circulation, 1988. **78**(6): p. 1431-42.
20. Blackman, B.R., K.A. Barbee, and L.E. Thibault, *In vitro cell shearing device to investigate the dynamic response of cells in a controlled hydrodynamic environment.* Ann Biomed Eng, 2000. **28**(4): p. 363-72.
21. Cheng, G.C., et al., *Distribution of circumferential stress in ruptured and stable atherosclerotic lesions. A structural analysis with histopathological correlation.* Circulation, 1993. **87**(4): p. 1179-87.
22. Huang, H., et al., *The impact of calcification on the biomechanical stability of atherosclerotic plaques.* Circulation, 2001. **103**(8): p. 1051-6.
23. Lee, R.T. and R.D. Kamm, *Vascular mechanics for the cardiologist.* J Am Coll Cardiol, 1994. **23**(6): p. 1289-95.
24. Loree, H.M., et al., *Mechanical properties of model atherosclerotic lesion lipid pools.* Arterioscler Thromb, 1994. **14**(2): p. 230-4.
25. Chang, L.J. and J.M. Tarbell, *A numerical study of flow in curved tubes simulating coronary arteries.* J Biomech, 1988. **21**(11): p. 927-37.
26. Kolandaivelu, K. and E.R. Edelman, *Low background, pulsatile, in vitro flow circuit for modeling coronary implant thrombosis.* J Biomech Eng, 2002. **124**(6): p. 662-8.
27. Nosovitsky, V.A., et al., *Effects of curvature and stenosis-like narrowing on wall shear stress in a coronary artery model with phasic flow.* Comput Biomed Res, 1997. **30**(1): p. 61-82.
28. Perktold, K., R.M. Nerem, and R.O. Peter, *A numerical calculation of flow in a curved tube model of the left main coronary artery.* J Biomech, 1991. **24**(3-4): p. 175-89.
29. Lasclazo, J., Schafer, AJ, *Thrombosis and Hemorrhage.* 1994: Blackwell Scientific Publications.
30. Denis, C.V. and D.D. Wagner, *Insights from von Willebrand disease animal models.* Cell Mol Life Sci, 1999. **56**(11-12): p. 977-90.
31. Makkar, R.R., et al., *Effects of clopidogrel, aspirin and combined therapy in a porcine ex vivo model of high-shear induced stent thrombosis.* Eur Heart J, 1998. **19**(10): p. 1538-46.
32. Nichols, T.C., et al., *von Willebrand factor and occlusive arterial thrombosis. A study in normal and von Willebrand's disease pigs with diet-induced hypercholesterolemia and atherosclerosis.* Arteriosclerosis, 1990. **10**(3): p. 449-61.
33. Schmidt, B., *Experimental test systems for the assessment of the blood compatibility of materials used in extracorporeal circuits.* Nephrol Dial Transplant, 1994. **9 Suppl 2**: p. 77-82.
34. Engelberg, H., *Studies with the Chandler rotating loop. Evidence that thrombin generation is responsible for the formation of the artificial in vitro thrombi.* Thromb Diath Haemorrh, 1969. **22**(2): p. 344-50.

35. Gardner, R.A., *An examination of the fluid mechanics and thrombus formation time parameters in a Chandler rotating loop system.* J Lab Clin Med, 1974. **84**(4): p. 494-508.
36. Haycox, C.L. and B.D. Ratner, *In vitro platelet interactions in whole human blood exposed to biomaterial surfaces: insights on blood compatibility.* J Biomed Mater Res, 1993. **27**(9): p. 1181-93.
37. Beythien, C., W. Terres, and C.W. Hamm, *In vitro model to test the thrombogenicity of coronary stents.* Thromb Res, 1994. **75**(6): p. 581-90.
38. Gutensohn, K., et al., *Flow cytometric analysis of coronary stent-induced alterations of platelet antigens in an in vitro model.* Thromb Res, 1997. **86**(1): p. 49-56.
39. Eto, K., et al., *Two distinct mechanisms are involved in stent thrombosis under flow conditions.* Platelets, 2001. **12**(4): p. 228-35.
40. Goto, S. and S. Handa, *Coronary thrombosis. Effects of blood flow on the mechanism of thrombus formation.* Jpn Heart J, 1998. **39**(5): p. 579-96.
41. Grabowski, E.F., *Effects of contrast media on erythrocyte and platelet interactions with endothelial cell monolayers exposed to flowing blood.* Invest Radiol, 1988. **23 Suppl 2**: p. S351-8.
42. Savage, B., F. Almus-Jacobs, and Z.M. Ruggeri, *Specific synergy of multiple substrate-receptor interactions in platelet thrombus formation under flow.* Cell, 1998. **94**(5): p. 657-66.
43. Tsuji, S., et al., *Real-time analysis of mural thrombus formation in various platelet aggregation disorders: distinct shear-dependent roles of platelet receptors and adhesive proteins under flow.* Blood, 1999. **94**(3): p. 968-75.
44. Blackman, B.R., G. Garcia-Cardena, and M.A. Gimbrone, Jr., *A new in vitro model to evaluate differential responses of endothelial cells to simulated arterial shear stress waveforms.* J Biomech Eng, 2002. **124**(4): p. 397-407.
45. Bluestein, D., et al., *Steady flow in an aneurysm model: correlation between fluid dynamics and blood platelet deposition.* J Biomech Eng, 1996. **118**(3): p. 280-6.
46. Lyne, W., *Unsteady viscous flow in a curved pipe.* Journal of Fluid Mechanics, 1970. **45**(1): p. 13-31.
47. Basmadjian, D., *The effect of flow and mass transport in thrombogenesis.* Ann Biomed Eng, 1990. **18**(6): p. 685-709.
48. Turitto, V.T. and H.R. Baumgartner, *Platelet deposition on subendothelium exposed to flowing blood: mathematical analysis of physical parameters.* Trans Am Soc Artif Intern Organs, 1975. **21**: p. 593-601.
49. Moore, J.E., Jr., et al., *Preliminary analysis of the effects of blood vessel movement on blood flow patterns in the coronary arteries.* J Biomech Eng, 1994. **116**(3): p. 302-6.
50. Perktold, K., et al., *Validated computation of physiologic flow in a realistic coronary artery branch.* J Biomech, 1998. **31**(3): p. 217-28.
51. Wedemeyer, E.H., *The unsteady flow within a spinning cylinder.* Journal of Fluid Mechanics, 1964. **20**(3): p. 383-399.
52. Greenspan, H.P. and S. Weinbaum, *On a time dependent motion of a rotating fluid.* Journal of Fluid Mechanics, 1963. **17**: p. 385-404.

53. Watkins, W.B. and R.G. Hussey, *Spin-up from rest in a cylinder.* Physics of fluids., 1977. **20**(3): p. 1596-1604.
54. Weidman, P.D., *On the spin-up and spin-down of a rotating fluid. Part 1. Extending the Wedemeyer model.* Journal of Fluid Mechanics, 1976. **77**(4): p. 685-708.
55. Duck, P.W., *Spin-up of homogenous and stratified fluids.* Annual review of fluid mechanics., 2001. **33**: p. 231-263.
56. Tullberg-Reinert, H. and G. Jundt, *In situ measurement of collagen synthesis by human bone cells with a sirius red-based colorimetric microassay: effects of transforming growth factor beta2 and ascorbic acid 2-phosphate.* Histochem Cell Biol, 1999. **112**(4): p. 271-6.

APPENDIX A: MATLAB CODE TO CALCULATE INNER DIAMETERS OF RESISTANCE TUBING

```
%This section finds the required pressure head
%to get a shear rate of 4000 in the largest tube
%diameter (300 microns)

%Length of test section
L_test_cm = 10;
L_test = L_test_cm/100;

%Length of resistance section
L_resistance_cm = 15;
L_resistance = L_resistance_cm/100;

%Diameter of test section
D_test_microns = 300;
D_test = 300/10^6;

%Diameter of highest shear tube in microns
D_largest_microns = 300;
D_largest = D_largest_microns/10^6;

%Desired shear rate in largest tube (1/seconds)
shear = 4000;

%Viscosity at specified shear rate (kg/m*s)
viscosity = .004;

%Necessary pressure head (in Pa = N/m^2);
delta_P = (4*L_test*viscosity*shear)/D_largest +
(4*L_resistance*viscosity*shear)/D_largest;
delta_P_kpa = delta_P/10^3;
```

```
%Now the pressure drop has been set, so the
%diameter of the other tubes can be determined.

%Desired shear rates
shear = [50 100 200 500 750 1000 2000 4000];

%Diameter of resistance sections
```

```
D_res = ((4*viscosity*L_resistance.*D_test.^3.*shear)./(delta_P -

(4*viscosity.*L_test.*shear)./D_test)).^(1/4);
D_res = D_res';
D_res_microns = D_res*10^6;
```

%Plots of the flow profiles, first finding the effective pressure
%drop in each test tube

```
delta_P_test = delta_P - (2*viscosity*L_resistance*shear(:,1)*(D_test/2).^3)/(D_res

(1,:)/2).^4;

r = [-D_test_microns/2:.01:D_test_microns/2];

v_z = (1/(2*viscosity))*delta_P_test*(((D_test_microns/10^6)/2)^2-(r./10^6).^2);

plot(r,v_z);
hold

xlabel('Radius [microns]')
ylabel('V_z [m/s]')

for i = 2:length(D_res);

   delta_P_test = delta_P - (2*viscosity*L_resistance*shear(:,i)*(D_test/2).^3)/(D_res

(i,:)/2).^4;
   r = [-D_test_microns/2:.01:D_test_microns/2];
   v_z = (1/(2*viscosity))*delta_P_test*(((D_test_microns/10^6)/2)^2-(r./10^6).^2);
   plot(r,v_z);
end
```

%Shear rate plots

```
for i = 1:length(D_res);

   r2 = [0:.01:D_test_microns/2];
   y = -shear(:,i).*((r2-(D_test_microns/2))/10^6);
   plot(r2,y,'r');
end
```

%Reynold's Number Calculation (density in kg/m^3)

density = 1060;

Re = (density*shear*(D_test/2)^2)/(8*viscosity);

figure(2)
plot(shear, Re);
xlabel('Shear Rate');
ylabel('Re');

%This code finds out the resistance diameters necessary
%while factoring in the Fahraeus Effect

%This section finds the required pressure head
%to get a shear rate of 4000 in the largest tube
%diameter (300 microns)

%Length of test section
L_test_cm = 10;
L_test = L_test_cm/100;

%Length of resistance section
L_resistance_cm = 15;
L_resistance = L_resistance_cm/100;

%Diameter of test section
D_test_microns = 300;
D_test = 300/10^6;

%Diameter of highest shear tube in microns
D_largest_microns = 300;
D_largest = D_largest_microns/10^6;

%Desired shear rate in largest tube (1/seconds)
shear_test = 4000;

%Viscosity at specified shear rate (kg/m*s)

```
viscosity_test = .0007*log(D_largest)+.0104;

%Necessary pressure head (in Pa = N/m^2);
delta_P = (4*(L_test+L_resistance)*viscosity_test*shear_test)/D_largest;
delta_P_kpa = delta_P/10^3;
```

```
%Now the pressure drop has been set, so the
%diameter of the other tubes can be determined.

D_res_vector = [50*10^-6:1*10^-7:300*10^-6];

%Desired shear rates
shear_test = [4000];
shear_res = (D_test./D_res).^3.*shear_test;

%In order to find the necessary resistance tube diameter
%you must find an equal resistance tube viscosity from the Fahraeus correlation
%and from the pressure drop equation
%In order to find the required tube diameters, you must change the shear_test
%value and plot the viscosity_res1 and 2 functions and find their point of
intersection

%viscosity_res1 = .0007*log(D_res_vector)+.0104;

%viscosity_res2 = (D_res_vector./(4*L_resistance.*shear_res)).*(delta_P -

(4*L_test.*viscosity_test.*shear_test)./D_test);

%figure(3)
%plot(D_res,viscosity_res1);
%hold
%plot(D_res,viscosity_res2);
%xlabel('D_ res [meters]');
%ylabel('Viscosity [kg/m*s]');

%The final results from analyzing the graphs:

shear_test_final = [50,100,200,500,750,1000,2000,4000];
D_res_final = [8.3887*10^-5,1.0071*10^-4,1.2103*10^-4,1.5498*10^-4,1.7345*10^-
4,1.8828*10^-

4,2.3251*10^-4,3*10^-4]';

figure(4)
```

```
plot(shear_test_final,D_res_final);
xlabel('shear rate [1/s]')
ylabel('D res [m] (blue = Fahraeus compensation, red = no compensation)')
hold
plot(shear,D_res,'r')
```

Results before Fahraeus compensation:

Shear rate	Resistance Diameter (microns)
50	88.4
100	105.3
200	125.5
500	159.0
750	177.2
1000	191.7
2000	234.8
4000	300.0

Results after Fahraeus compensation:

Shear Rate	Resistance Diameter (microns)
50	83.9
100	100.7
200	121.0
500	155.0
750	173.5
1000	188.3
2000	232.5
4000	300.0

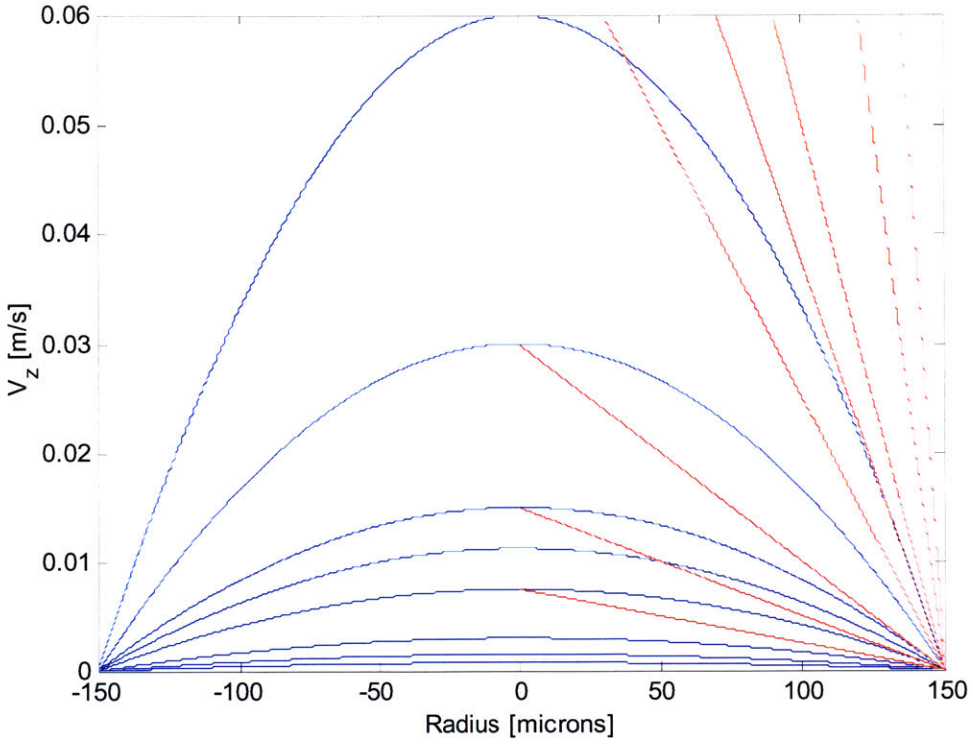
0.06
0.05
0.04
0.03
0.02
0.01
0
V_z [m/s]
-150
-100
-50
0
50
100
150
Radius [microns]

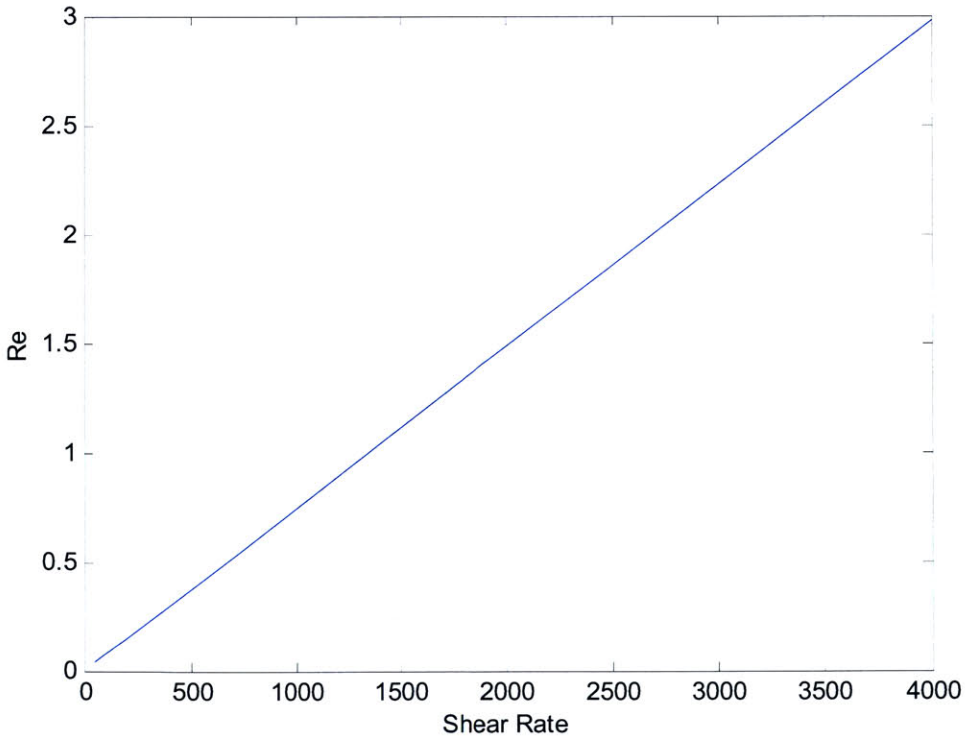
3
2.5
2
1.5
1
0.5
0
Re
0
500
1000
1500
2000
2500
3000
3500
4000
Shear Rate

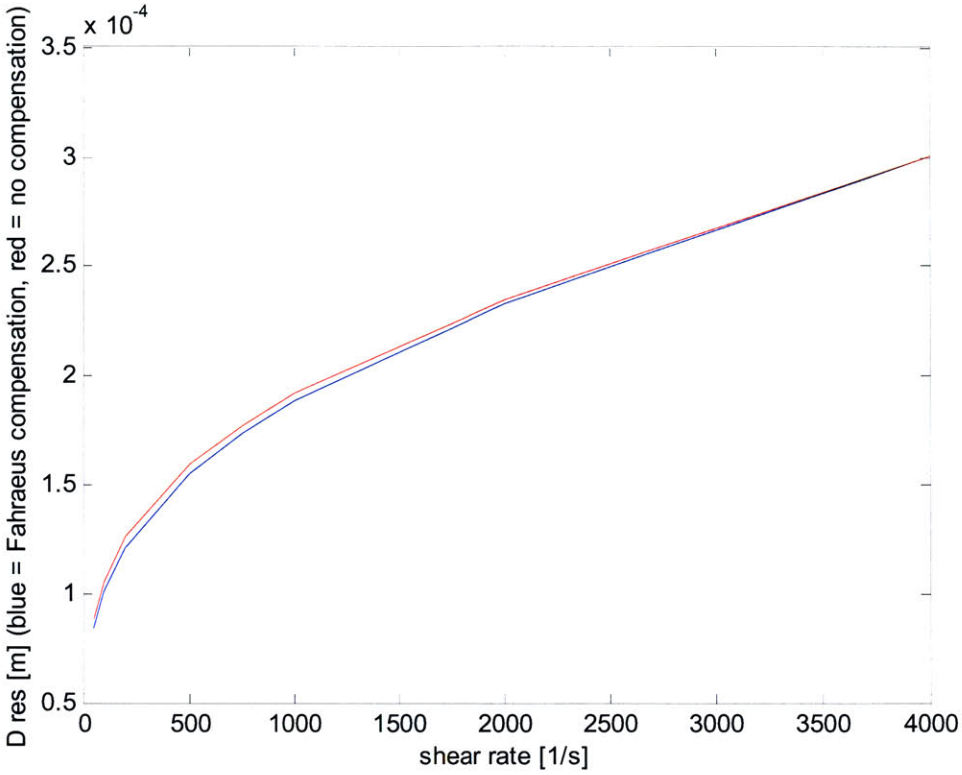
x 10^-4
3.5
3
2.5
2
1.5
1
0.5
D res [m] (blue = Fahraeus compensation, red = no compensation)
0
500
1000
1500
2000
2500
3000
3500
4000
shear rate [1/s]

APPENDIX B: PART SCHEMATICS

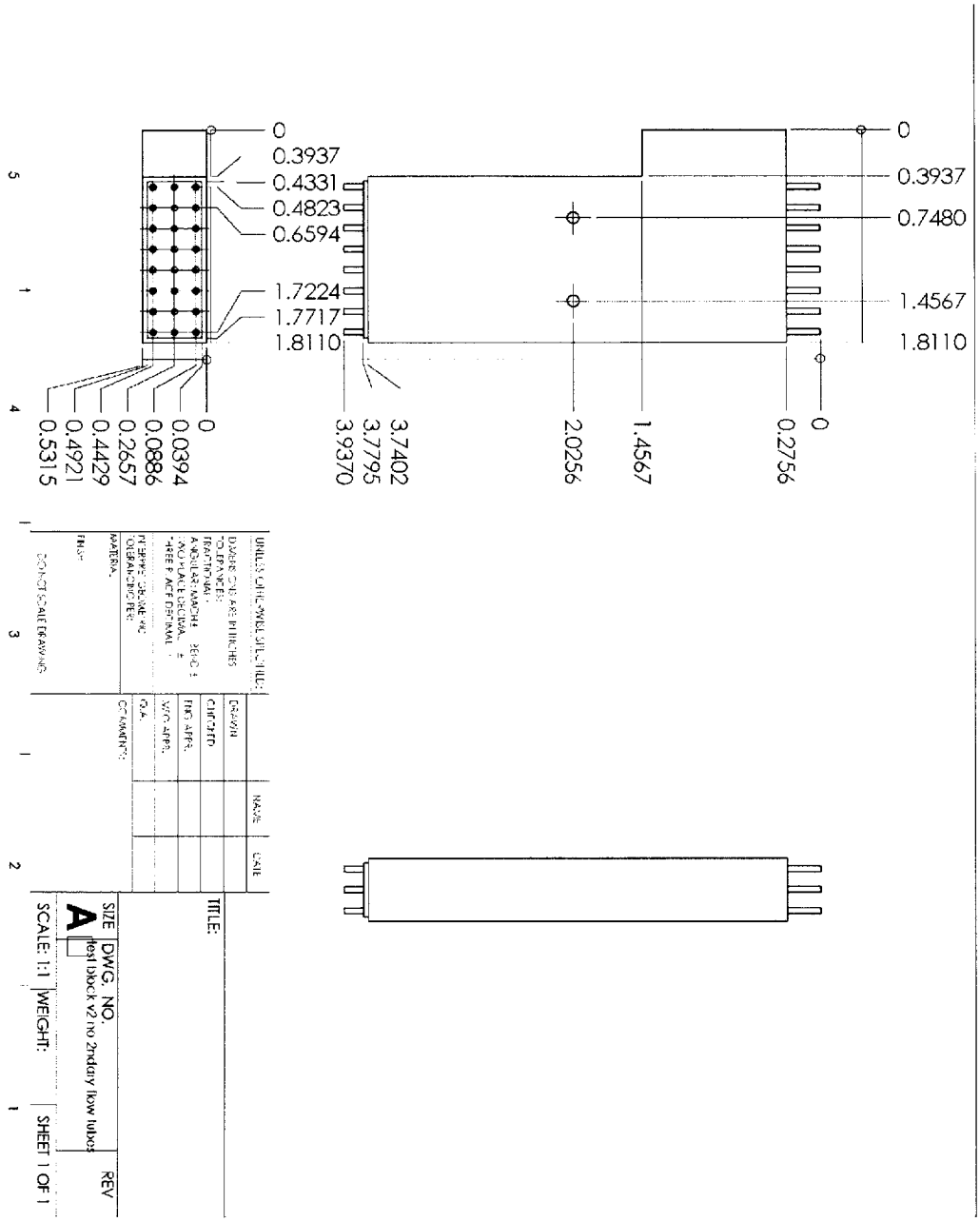

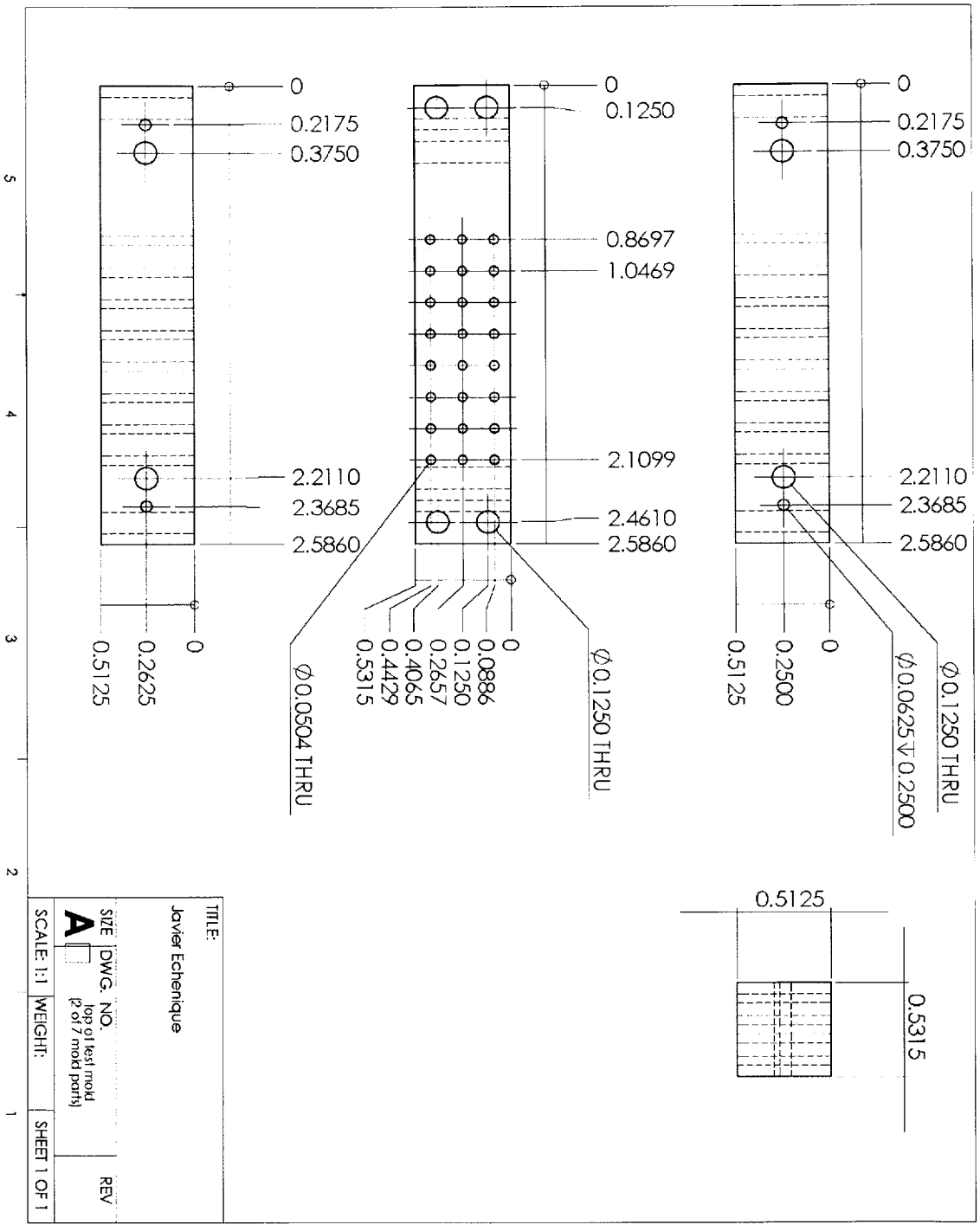
0
0.2175
0.3750
2.2110
2.3685
2.5860
0.5125
0.2625
0
0.0504 THRU
0
0.1250
0.8697
1.0469
2.1099
2.4610
2.5860
0.5315
0.4429
0.4065
0.2657
0.1250
0.0886
0
0.1250 THRU
0
0.2175
0.3750
2.2110
2.3685
2.5860
0.5125
0.2500
0
0.0625 ↧ 0.2500
0.1250 THRU
0.5125
0.5315
TITLE:
Javier Echenique
SIZE
A
DWG. NO.
top of test mold
(2 of 7 mold parts)
REV
SCALE: 1:1
WEIGHT:
SHEET 1 OF 1

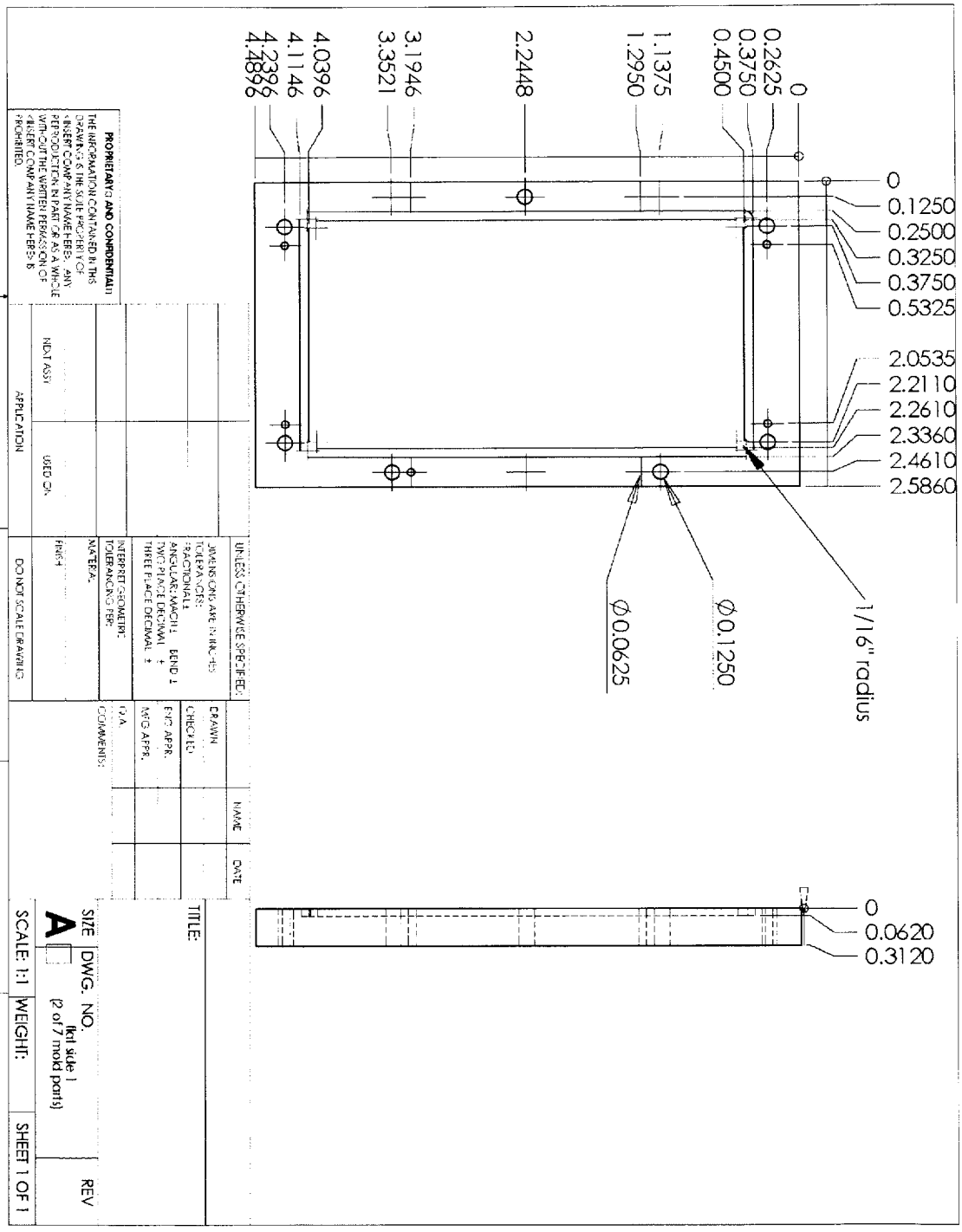
0
0.2625
0.3750
0.4500
1.1375
1.2950
2.2448
3.1946
3.3521
4.0396
4.1146
4.2396
4.4896
0
0.1250
0.2500
0.3250
0.3750
0.5325
2.0535
2.2110
2.2610
2.3360
2.4610
2.5860
Ø0.0625
Ø0.1250
1/16" radius
0
0.0620
0.3120
PROPRIETARY AND CONFIDENTIAL
THE INFORMATION CONTAINED IN THIS DRAWING IS THE SOLE PROPERTY OF <INSERT COMPANY NAME HERE>. ANY REPRODUCTION IN PART OR AS A WHOLE WITHOUT THE WRITTEN PERMISSION OF <INSERT COMPANY NAME HERE> IS PROHIBITED.
APPLICATION
NEXT ASSY
USED ON
DO NOT SCALE DRAWING
UNLESS OTHERWISE SPECIFIED:
DIMENSIONS ARE IN INCHES
TOLERANCES:
FRACTIONAL ±
ANGULAR: MACH ± BEND ±
TWO PLACE DECIMAL ±
THREE PLACE DECIMAL ±
INTERPRET GEOMETRIC TOLERANCING PER:
MATERIAL
FINISH
DRAWN
CHECKED
ENG APPR.
MFG APPR.
Q.A.
COMMENTS:
NAME
DATE
TITLE:
SIZE
A
DWG. NO.
(text side 1
(2 of 7 mold parts)
REV
SCALE: 1:1
WEIGHT:
SHEET 1 OF 1

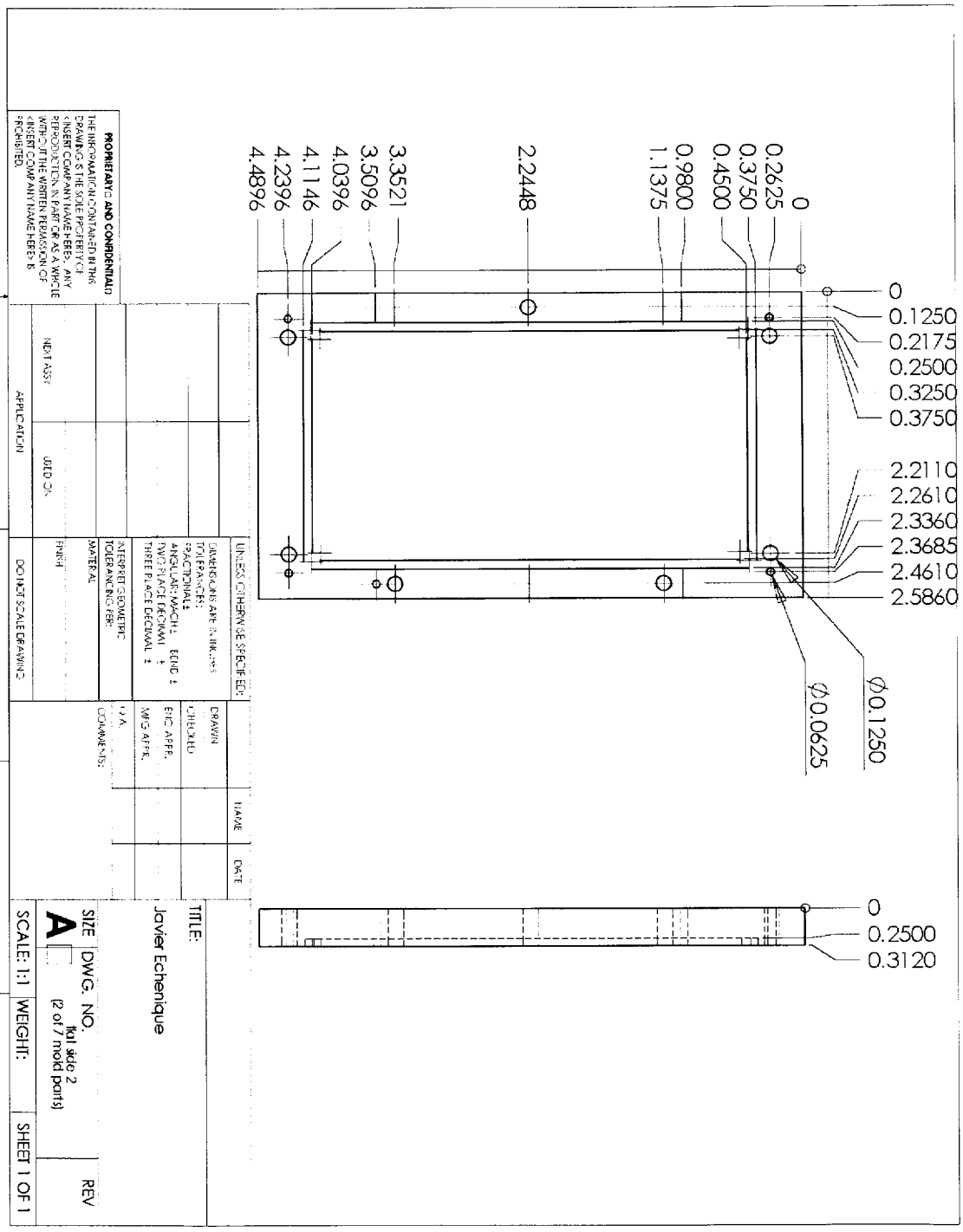
0
0.2625
0.3750
0.4500
0.9800
1.1375
2.2448
3.3521
3.5096
4.0396
4.1146
4.2396
4.4896
0
0.1250
0.2175
0.2500
0.3250
0.3750
2.2110
2.2610
2.3360
2.3685
2.4610
2.5860
ϕ0.1250
ϕ0.0625
0
0.2500
0.3120
PROPRIETARY AND CONFIDENTIAL
APPLICATION
NEXT ASSY
USED ON
UNLESS OTHERWISE SPECIFIED:
DRAWN
CHECKED
ENG APPR.
MFG APPR.
NAME
DATE
MATERIAL
FINISH
DO NOT SCALE DRAWING
TITLE:
Javier Echenique
SIZE
A
DWG. NO.
flat side 2
(2 of 7 mold parts)
REV
SCALE: 1:1
WEIGHT:
SHEET 1 OF 1

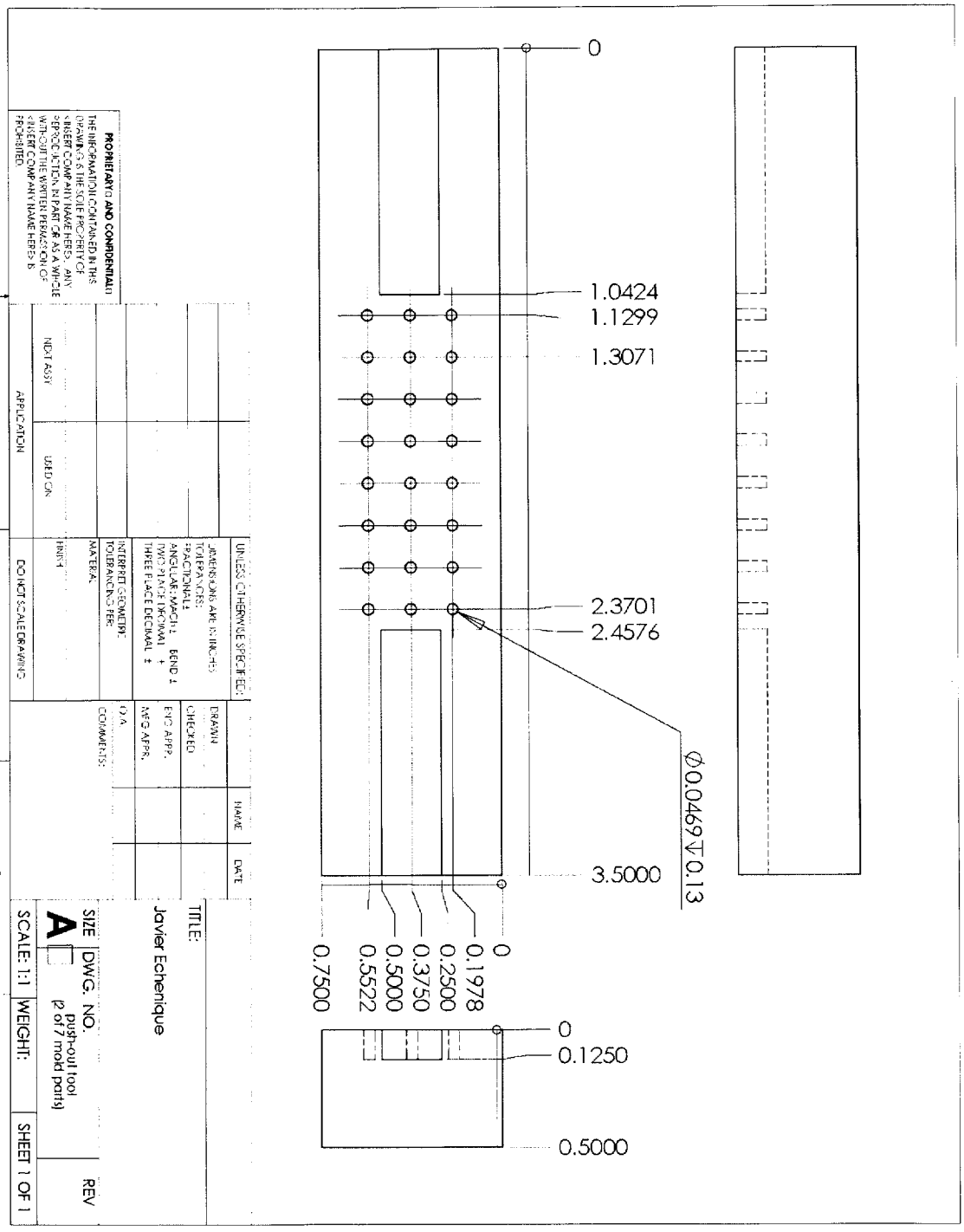
0
1.0424
1.1299
1.3071
2.3701
2.4576
Ø0.0469 T 0.13
3.5000
0
0.1978
0.2500
0.3750
0.5000
0.5522
0.7500
0
0.1250
0.5000
PROPRIETARY AND CONFIDENTIAL
UNLESS OTHERWISE SPECIFIED:
DRAWN
CHECKED
ENG APPR.
MFG APPR.
COMMENTS:
NAME
DATE
TITLE:
Javier Echenique
SIZE
A
DWG. NO.
push-out tool
(2 of 7 mold parts)
REV
SCALE: 1:1
WEIGHT:
SHEET 1 OF 1

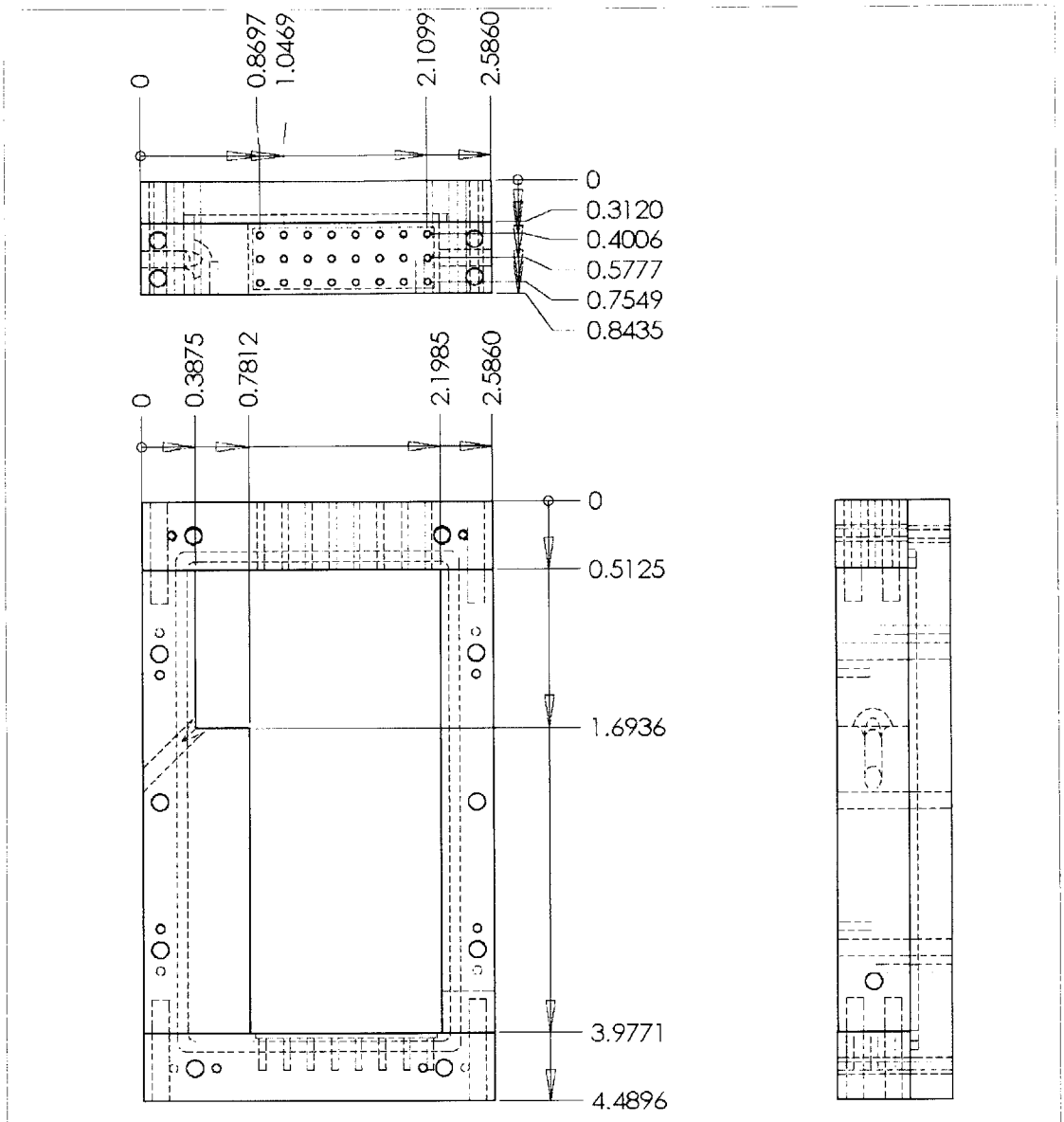

	DIMENSIONS ARE IN INCHES TOLERANCES: FRACTIONAL ± ANGULAR: MACH ± BEND ± TWO PLACE DECIMAL ± THREE PLACE DECIMAL ±		NAME	DATE
		DRAWN		
		CHECKED		
		ENG APPR.		
		MFG APPR.		
		Q.A.		
	MATERIAL	COMMENTS:		
NEXT ASSY	USED ON			
APPLICATION	DO NOT SCALE DRAWING			

SIZE	DWG. NO.	REV.
A	test block mold assembly	
SCALE: 1:1	WEIGHT:	SHEET 1 OF 1

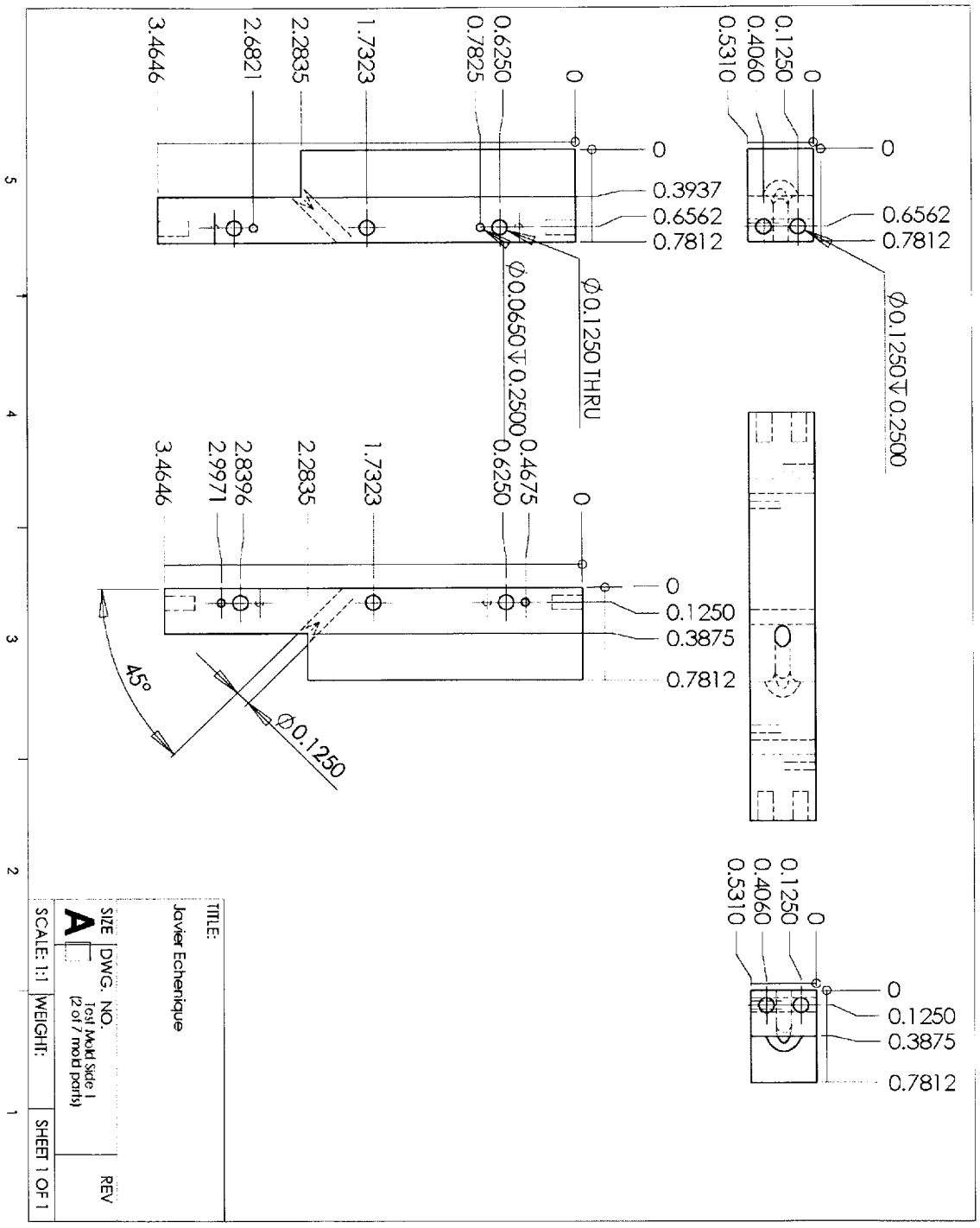
0.5310
0.4060
0.1250
0
0
0.6562
0.7812
Ø0.1250↧0.2500
3.4646
2.6821
2.2835
1.7323
0.7825
0.6250
0
0
0.3937
0.6562
0.7812
Ø0.1250 THRU
Ø0.0650↧0.2500
3.4646
2.9971
2.8396
2.2835
1.7323
0.6250
0.4675
0
0
0.1250
0.3875
0.7812
45°
Ø0.1250
0.5310
0.4060
0.1250
0
0
0.1250
0.3875
0.7812
TITLE:
Javier Echenique
SIZE
A
DWG. NO.
Test Mold Side 1
(2 of 7 mold parts)
REV
SCALE: 1:1
WEIGHT:
SHEET 1 OF 1

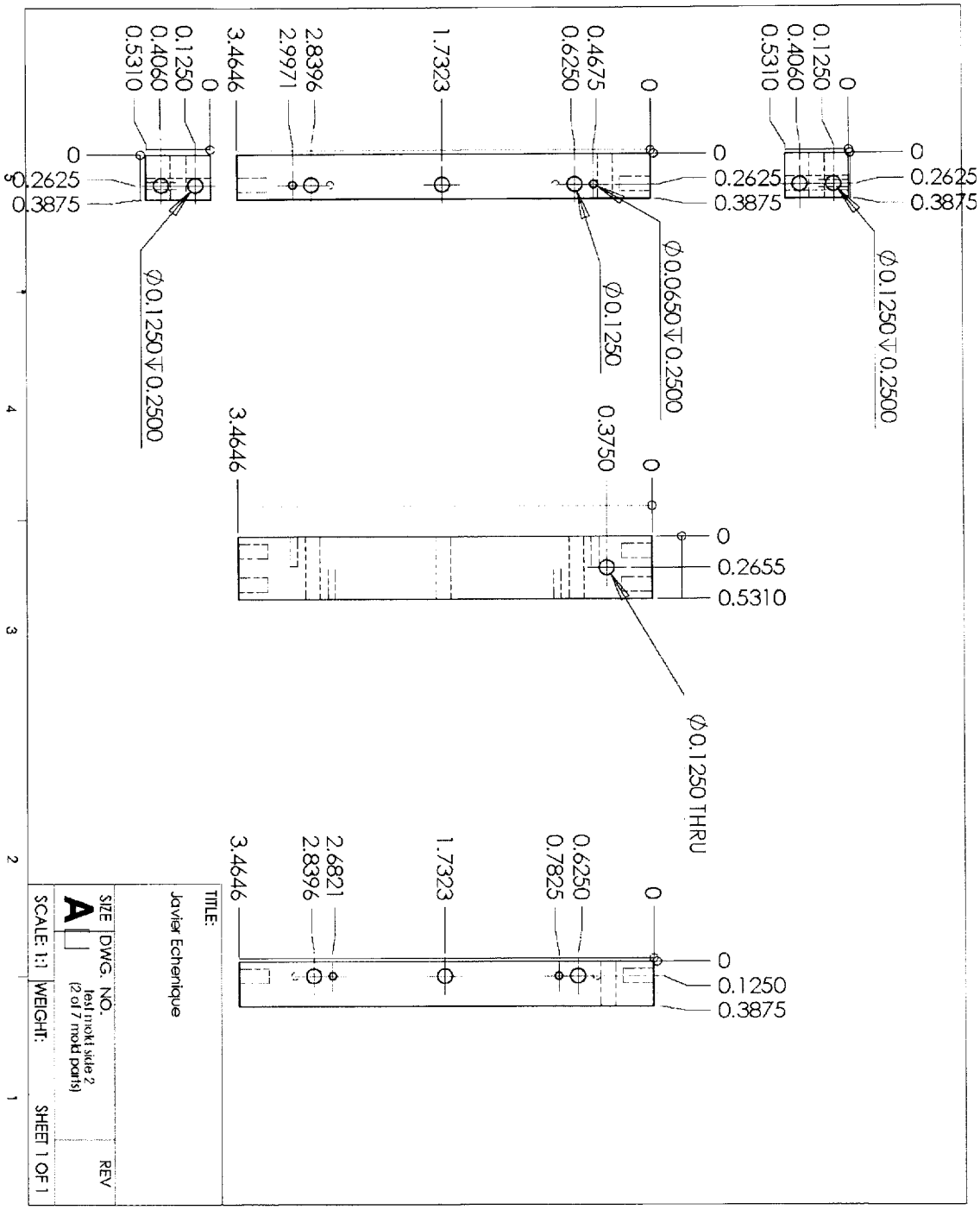
0.1250
0.4060
0.5310
0
0.2625
0.3875
Ø0.1250⌀0.2500
0.4675
0.6250
Ø0.0650⌀0.2500
Ø0.1250
1.7323
2.8396
2.9971
3.4646
0.3750
0.2655
Ø0.1250 THRU
0.6250
0.7825
2.6821
0.1250
TITLE:
Javier Echenique
SIZE
A
DWG. NO.
test mold side 2
(2 of 7 mold parts)
REV
SCALE: 1:1
WEIGHT:
SHEET 1 OF 1

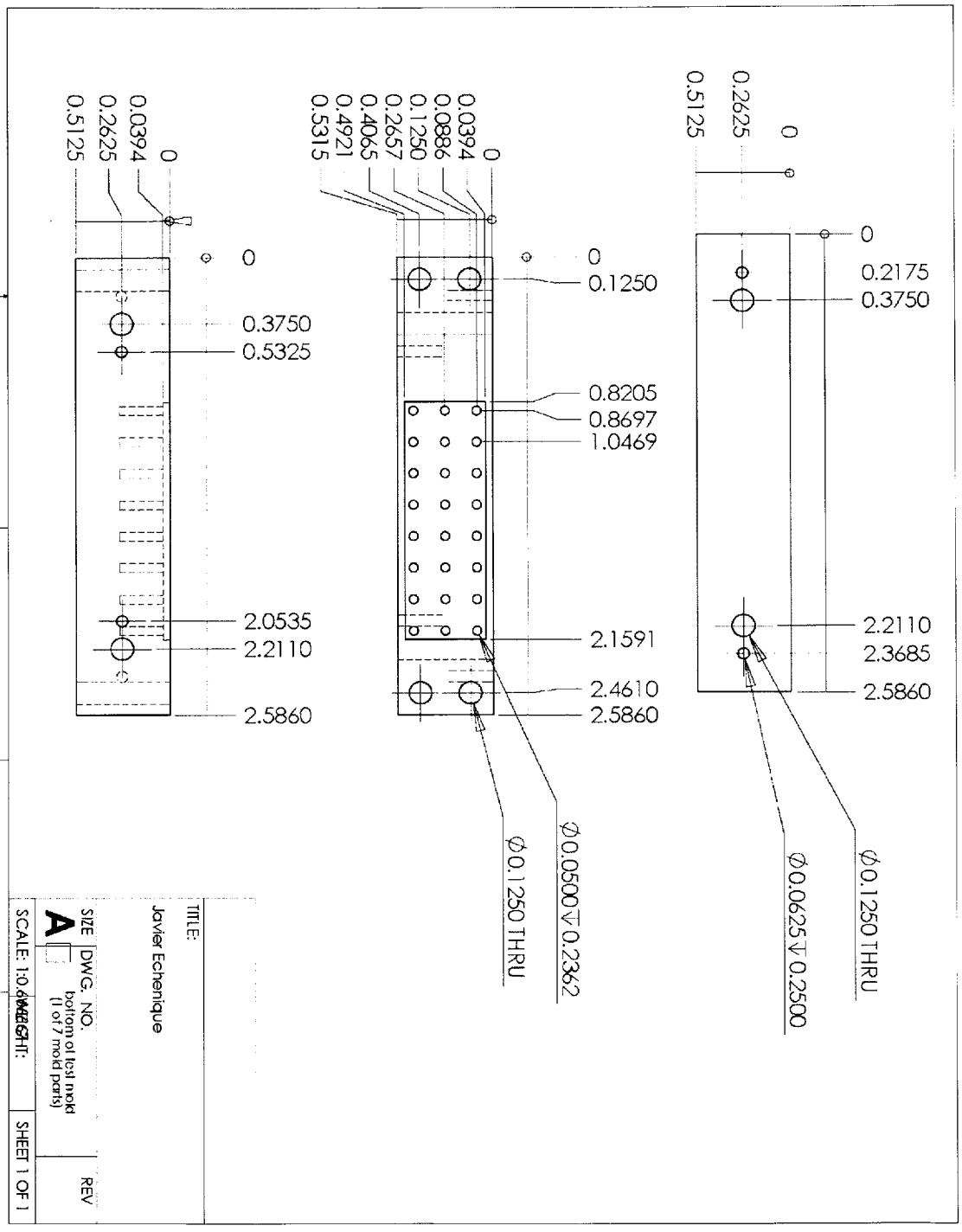
0.5125
0.2625
0
0
0.2175
0.3750
2.2110
2.3685
2.5860
Ø0.1250 THRU
Ø0.0625 ↧ 0.2500
0.5315
0.4921
0.4065
0.2657
0.1250
0.0886
0.0394
0
0
0.1250
0.8205
0.8697
1.0469
2.1591
2.4610
2.5860
Ø0.0500 ↧ 0.2362
Ø0.1250 THRU
0.5125
0.2625
0.0394
0
0
0.3750
0.5325
2.0535
2.2110
2.5860
TITLE:
Javier Echenique
SIZE
A
DWG. NO.
bottom of test mold
(1 of 7 mold parts)
REV
SCALE: 1:0.666667
SHEET 1 OF 1

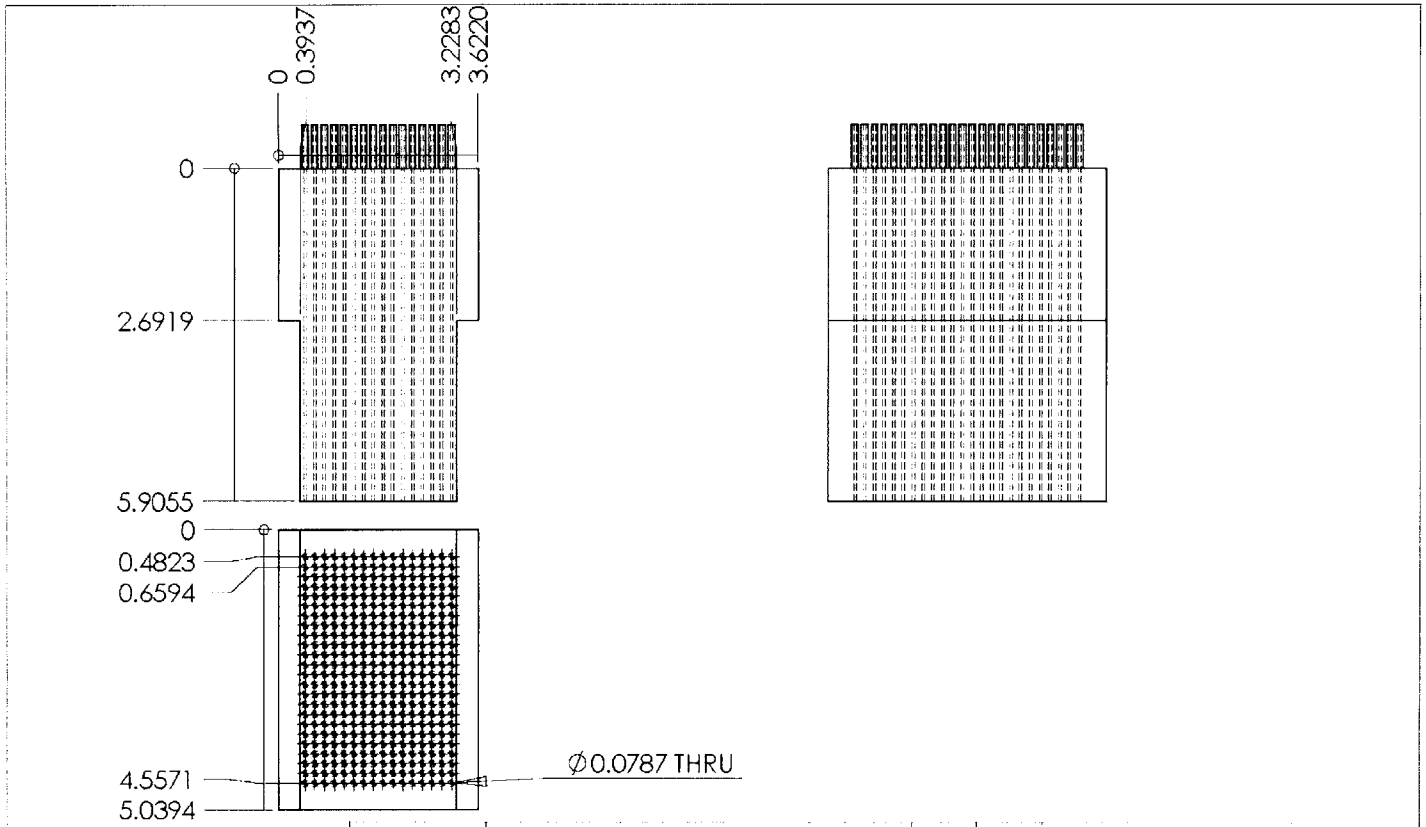

UNLESS OTHERWISE SPECIFIED:
DIMENSIONS ARE IN INCHES
TOLERANCES:
FRACTIONAL ±
ANGULAR: MACH ± BEND ±
TWO PLACE DECIMAL ±
THREE PLACE DECIMAL ±
INTERPRET GEOMETRIC TOLERANCING PER:
MATERIAL
FINISH
NEXT ASSY
USED ON
APPLICATION
DO NOT SCALE DRAWING

	NAME	DATE
DRAWN		
CHECKED		
ENG APPR.		
MFG APPR.		
Q.A.		
COMMENTS:		

TITLE:

SIZE A | DWG. NO. resistance block v2 | REV

SCALE: 1:5 | WEIGHT: | SHEET 1 OF 1

4 3 2 1

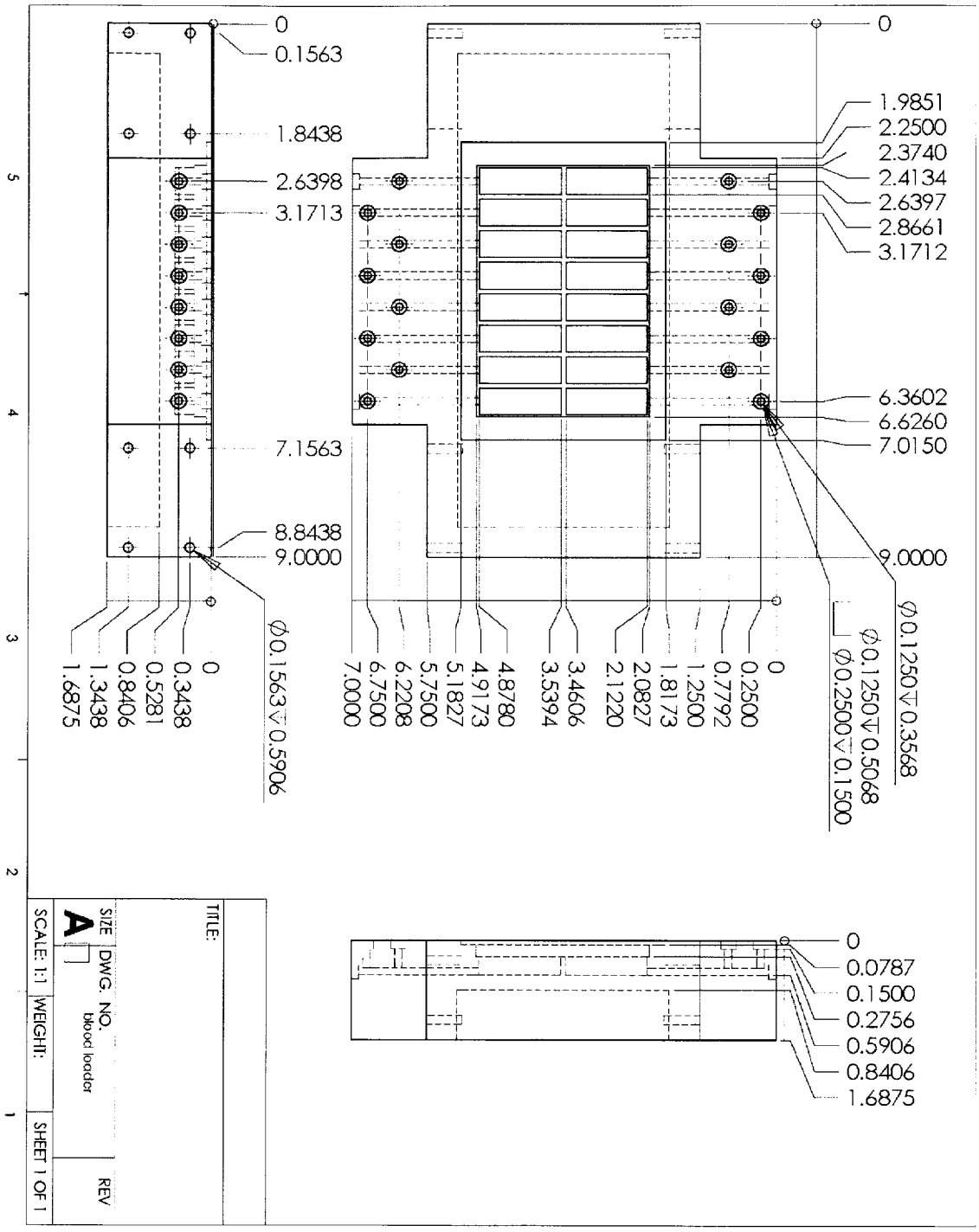
0
0.1563
1.8438
2.6398
3.1713
7.1563
8.8438
9.0000
Ø0.1563▽0.5906
1.6875
1.3438
0.8406
0.5281
0.3438
0
7.0000
6.7500
6.2208
5.7500
5.1827
4.9173
4.8780
3.5394
3.4606
2.1220
2.0827
1.8173
1.2500
0.7792
0.2500
0
1.9851
2.2500
2.3740
2.4134
2.6397
2.8661
3.1712
6.3602
6.6260
7.0150
9.0000
Ø0.1250▽0.3568
Ø0.1250▽0.5068
Ø0.2500▽0.1500
0
0.0787
0.1500
0.2756
0.5906
0.8406
1.6875
TITLE:
SIZE
A
DWG. NO.
blood loader
REV
SCALE: 1:1
WEIGHT:
SHEET 1 OF 1

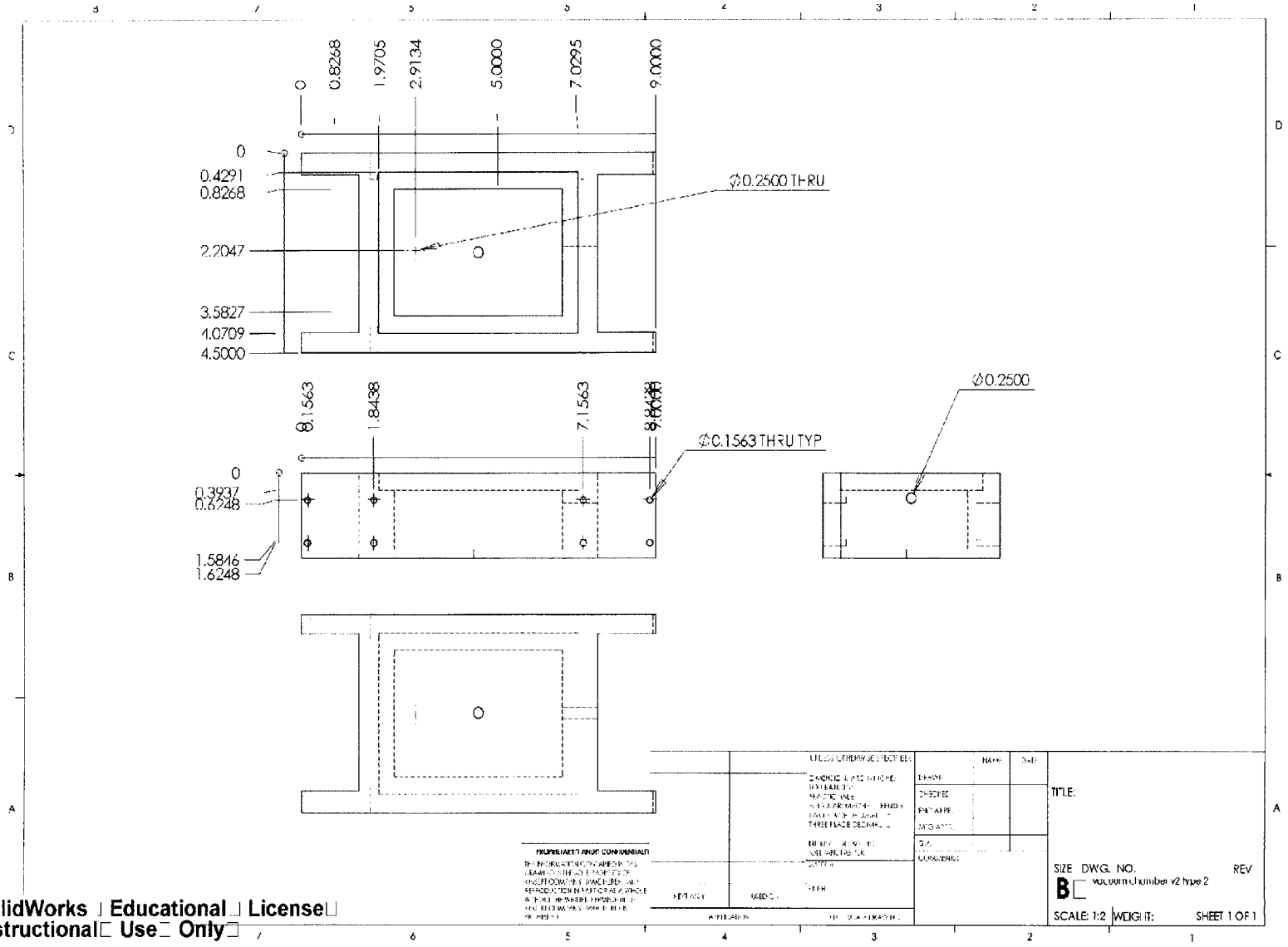

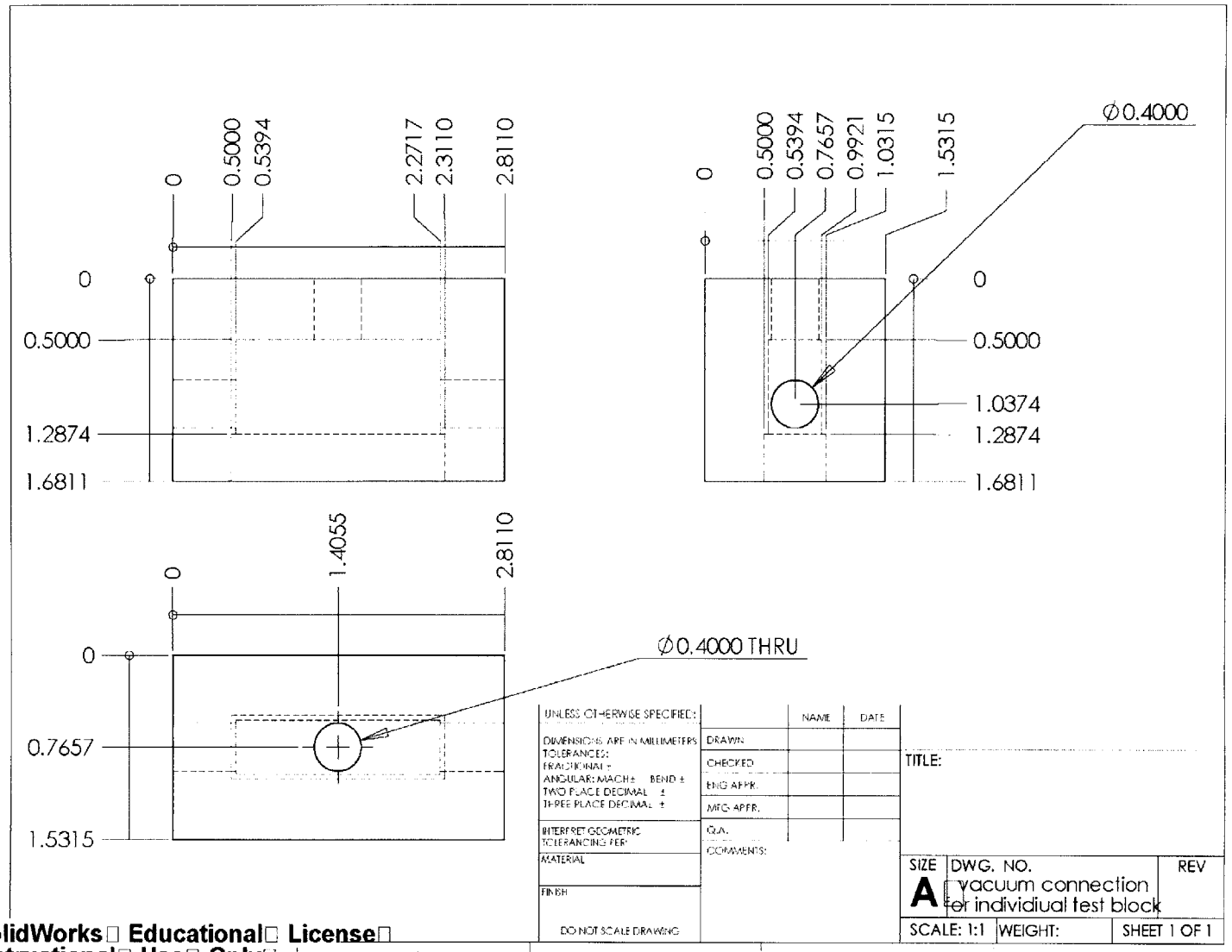

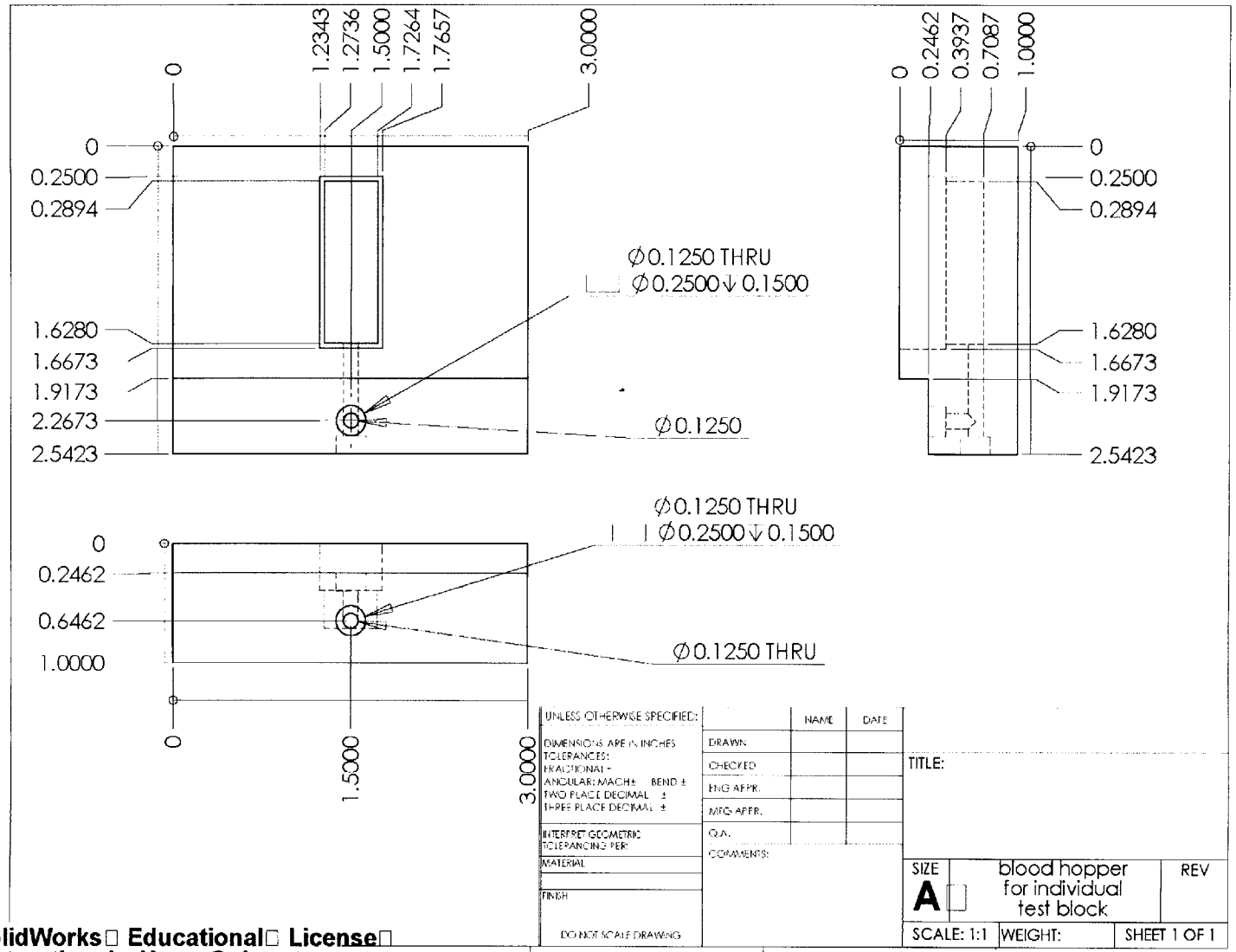

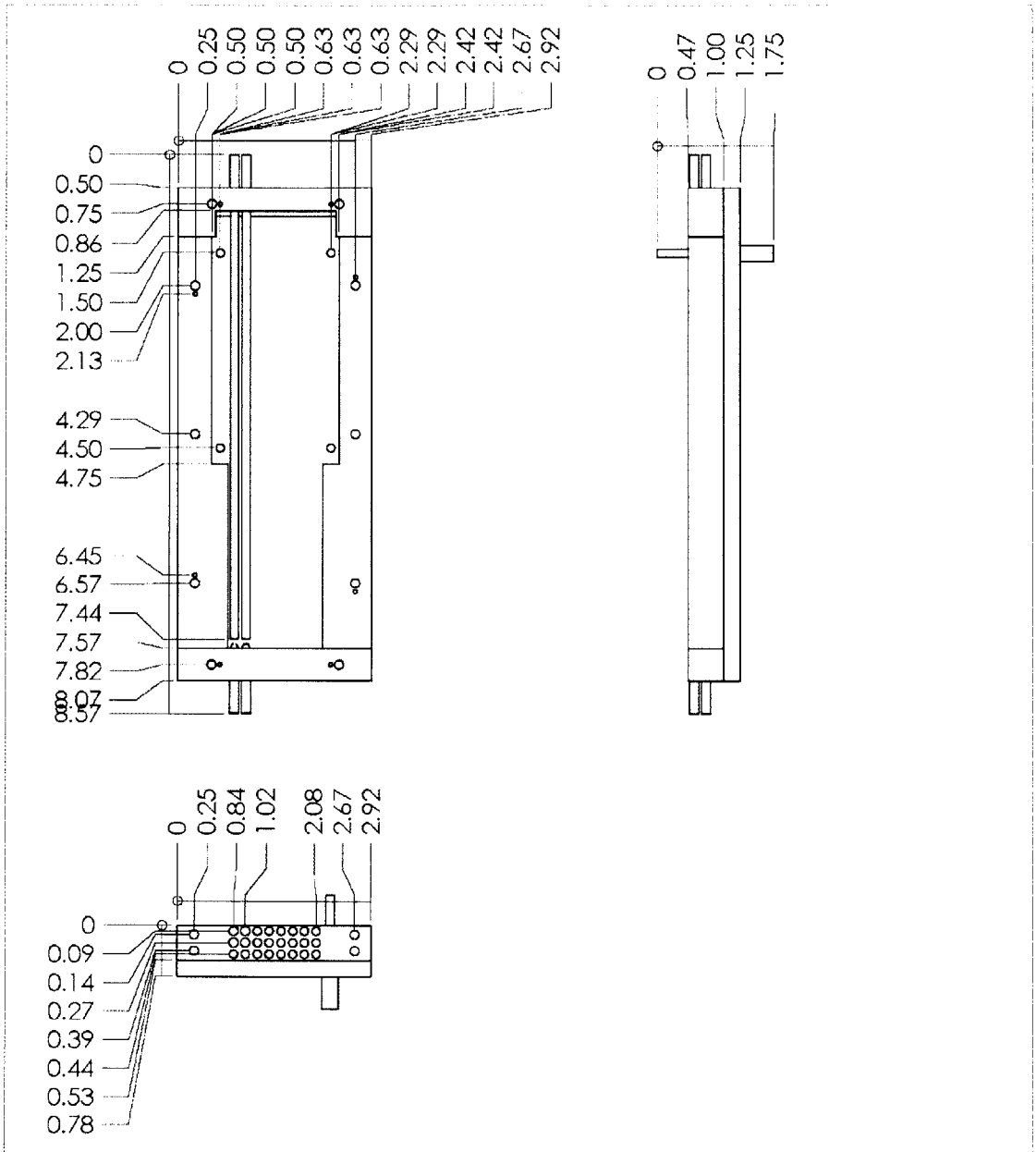
0 0.25 0.50 0.50 0.50 0.63 0.63 0.63 2.29 2.29 2.42 2.42 2.67 2.92
0 0.50 0.75 0.86 1.25 1.50 2.00 2.13 4.29 4.50 4.75 6.45 6.57 7.44 7.57 7.82 8.07 8.57
0 0.47 1.00 1.25 1.75
0 0.25 0.84 1.02 2.08 2.67 2.92
0 0.09 0.14 0.27 0.39 0.44 0.53 0.78
DIMENSIONS ARE IN INCHES
TOLERANCES:
FRACTIONAL ±
ANGULAR: MACH ± BEND ±
TWO PLACE DECIMAL ±
THREE PLACE DECIMAL ±
MATERIAL
FINISH
NEXT ASSY
USED ON
APPLICATION
DO NOT SCALE DRAWING
NAME
DATE
DRAWN
CHECKED
ENG APPR.
MFG APPR.
Q.A.
COMMENTS:
PROPRIETARY AND CONFIDENTIAL
THE INFORMATION CONTAINED IN THIS DRAWING IS THE SOLE PROPERTY OF <INSERT COMPANY NAME HERE>. ANY REPRODUCTION IN PART OR AS A WHOLE WITHOUT THE WRITTEN PERMISSION OF <INSERT COMPANY NAME HERE> IS PROHIBITED.
SIZE
DWG. NO.
REV.
A
individual resistance block mold assembly
SCALE:1:1
WEIGHT:
SHEET 1 OF 1

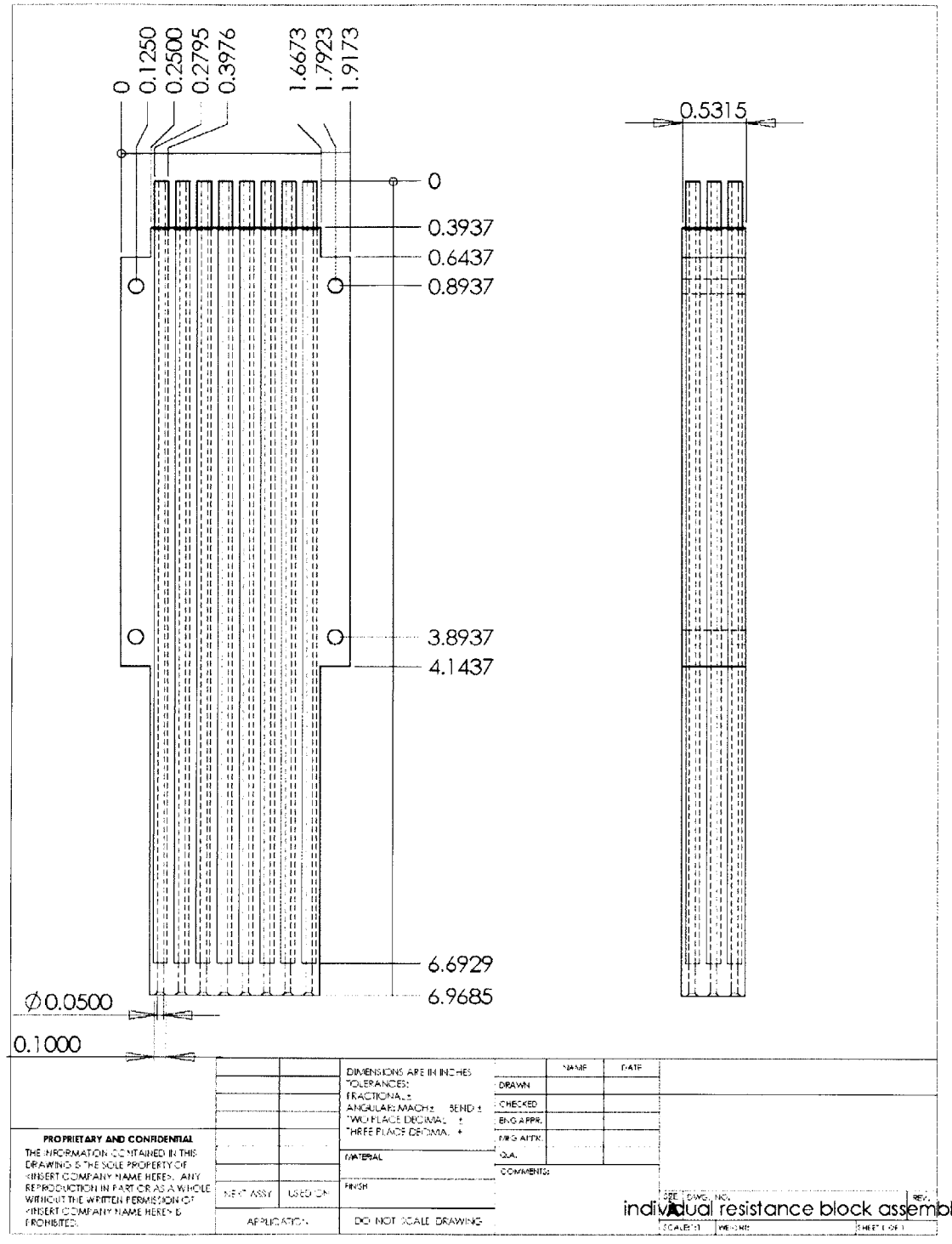
0
0.1250
0.2500
0.2795
0.3976
1.6673
1.7923
1.9173
0.5315
0
0.3937
0.6437
0.8937
3.8937
4.1437
6.6929
6.9685
∅0.0500
0.1000
DIMENSIONS ARE IN INCHES
TOLERANCES:
FRACTIONAL ±
ANGULAR: MACH ± BEND ±
TWO PLACE DECIMAL ±
THREE PLACE DECIMAL ±
MATERIAL
FINISH
DO NOT SCALE DRAWING
NAME
DATE
DRAWN
CHECKED
ENG APPR.
MFG APPR.
Q.A.
COMMENTS:
PROPRIETARY AND CONFIDENTIAL
THE INFORMATION CONTAINED IN THIS DRAWING IS THE SOLE PROPERTY OF <INSERT COMPANY NAME HERE>. ANY REPRODUCTION IN PART OR AS A WHOLE WITHOUT THE WRITTEN PERMISSION OF <INSERT COMPANY NAME HERE> IS PROHIBITED.
NEXT ASSY
USED ON
APPLICATION
SIZE
DWG. NO.
REV.
SCALE: 1
WEIGHT:
SHEET 1 OF 1
individual resistance block assembly